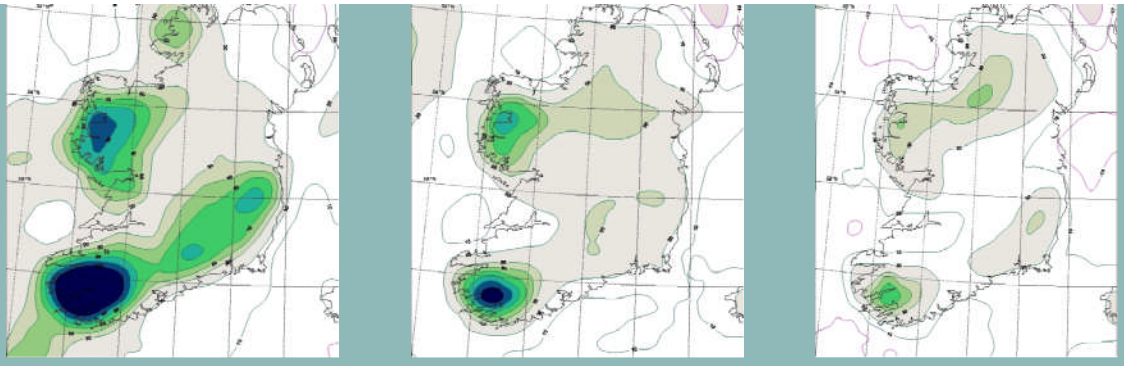

c4i

Community Climate Change Consortium for Ireland

2004 Annual Report

C4I

Community Climate Change Consortium for Ireland

2004 Annual Report

Ray Mc Grath, Elisa Nishimura, Paul Nolan, J. Venkata Ratnam,Tido Semmler, Conor Sweeney, Shiyu Wang

C4I
Met Éireann, Glasnevin Hill, Dublin 9, Ireland
Telephone: +353 1 8065 520
Email: C4I@met.ie

Acknowledgements

C4I is supported and funded by the Environmental Protection Agency (under the National Development Plan), Met Éireann, Sustainable Energy Ireland, and the Higher Education Authority.

This work was carried out in collaboration with the CosmoGrid Project, funded under the Programme for Research in Third Level Institutions (PRTLI) administered by the Irish Higher Education Authority under the National Development Plan and with partial support from the European Regional Development Fund.

Support from Met Éireann staff, particularly those in the IT and Climate and Observations Divisions, is also acknowledged.

C4I is registered as a Special Project with the European Centre for Medium-Range Weather Forecasts.

Table of Contents

Glossary

CosmoGrid	Network of distributed computing resources in Ireland (see www.CosmoGrid.ie).
ECHAM4	European Centre Hamburg Model Version 4. Global climate model developed at the Max-Planck Institute for Meteorology in Hamburg, Germany.
ECMWF	European Centre for Medium-Range Weather Forecasting
ERA-40	Re-analysis project of the European Centre for Medium-Range Weather Forecasting; archive of re-analysis data.
GCM	General Circulation Model.
HBV	Hydrological discharge model.
HOAPS	Hamburg Ocean Atmosphere Parameters and Fluxes from Satellite Data. A satellite-derived global climatology of freshwater flux (see www.hoaps.zmaw.de), produced by the Meteorological Institute of the University of Hamburg and the Max-Planck Institute for Meteorology in Hamburg.
IPCC	Intergovernmental Panel on Climate Change.
RCA	Rossby Centre Atmospheric model. Regional climate model developed at the Rossby Centre, the climate research unit at SMHI, Norrköping, Sweden.
RCM	Regional Climate Model.
SMHI	Swedish Meteorological and Hydrological Institute.
SRES	Special Report on Emissions Scenarios. The ECHAM4/OPYC3 simulation uses the SRES-B2 scenario, a scenario of moderately increasing greenhouse gas concentrations, for the period 1990-2100. For further details see www.grida.no/climate/ipcc/emission/095.htm.
SST	Sea Surface Temperature.
T159	Refers to the resolution of the global ERA-40 data in spherical harmonic format. Triangular truncation at wave number 159 corresponds to grid point resolutions of approximately 1.125 degrees. ECHAM4 data have a native horizontal resolution of approximately 2.8 degrees (T42).

UKCIP	UK Climate Impacts Programme. Resource provides gridded observation data for elements such as temperature and precipitation.

1 Executive summary

The main achievement over the past 12 months has been the completion of a simulation of the future Irish climate (2021-2060) using a regional climate model.

The results show a general warming in the future period with mean monthly temperatures increasing typically between 1.25 and 1.5 degrees Celsius. The largest increases are seen in the south-east and east, with the greatest warming occurring in July. For precipitation the most significant changes occur in the months of June and December; June values show a decrease of about 10% compared with the current climate, noticeably in the southern half of the country; December values show increases ranging between 10% in the south-east and 25% in the north-west. There is also some evidence of an increase in the frequency of extreme precipitation events (20 mm or more per day) in the north-west.

In a practical application of this new dataset a hydrological model was used to assess the impact of climate change on river discharge and local flooding in the Suir catchment area. The increase in winter precipitation was found to produce a significant increase in the more intense discharge episodes, raising the risk of future flooding in the area.

In the future scenario the frequency of intense cyclones over the North Atlantic area in the vicinity of Ireland is increased by about 15% compared with the current climate. This is probably related to the general rise in sea surface temperatures. A 16-year sensitivity experiment provides further support and suggests that a warming Atlantic will lead to more hurricanes, the remnants of which may impact on European coastal areas.

As part of the climate model validation work a 40-year simulation of the past climate (1961-2000) was also completed. The output data complement the archive of existing climate observations and, together with the data for the future climate, greatly enhances the scope for climate research in Ireland.

The simulation of the future climate is driven at the boundaries by the output of a single general circulation model (ECHAM4) with future greenhouse gas concentrations following the SRES-B2 scenario (i.e. moderately increasing concentrations). This is a first step in a more ambitious program to run an ensemble of simulations, using different global driving data to quantify the uncertainty in the climate projections.

2 Technical summary

2.1 Simulations

Considerable progress was made during 2004. A 40-year simulation of the past climate (1961-2000) was run to verify that the RCA model is capable of capturing the essential features of the Irish climate at the scale of the model configuration (0.12 degree horizontal grid). This produced an extensive dataset of surface and upper-air weather parameters (around 260 GB in size) for comparison against available observations. Sample verification results are discussed in section 3 while section 4 provides an in-depth analysis of the changing precipitation patterns over the 40 years.

In general, the performance of the model is quite good; some weather parameters show systematic errors relative to the observations but these may also be related to deficiencies in the ERA-40 re-analysis data used to drive the RCA. Interestingly, the verification run also highlights the "global dimming" effect seen in the long-term decrease of solar radiation in the Valentia observations. Unfortunately, the model does not capture this trend, possibly because of a static representation of the effects of aerosols in the model. The simulation output is a valuable resource that complements existing observations.

The highlight of the year's work was undoubtedly the simulation of the future climate (2021-2060). As a first step in a planned ensemble sequence of simulations, data from the Max Planck Institute ECHAM4/OPYC3 coupled atmosphere-ocean general circulation model were used to drive the RCA. This transient simulation, extending from 1860 to 2100, used observed GHG concentrations up to 1990 and the "SRES-B2" scenario for the future (i.e. moderately increasing GHG concentrations). Evaluation of the climate change requires a reference simulation and this was run for the period 1961-2000, again driven by ECHAM4 data. The results are discussed in section 5. Basically, the simulation shows a general warming in the future period with mean monthly temperatures increasing typically between 1.25 and 1.5 degrees Celsius. The largest increases are seen in the south-east and east, with the greatest warming occurring in July. For precipitation the most significant changes occur in the months of June and December; June values show a decrease of about 10% compared with the current climate, noticeably in the southern half of the country; December values show increases ranging between 10% in the south-east and 25% in the north-west. There is also some evidence of an increase in the frequency of extreme precipitation events (20 mm or more per day) in the north-west.

2.2 Case studies and climate research

The results of a case study in which the HBV hydrological model was used to simulate river discharge in the Suir catchment area are discussed in section 6. The increase in winter precipitation was found to

produce a significant increase in the more intense river discharge episodes, raising the risk of future flooding in the area.

Section 7 analyses the frequency and intensity of cyclones, and their movement, comparing statistics from the ERA-40 re-analysis data with those from the past simulation. In the future simulation the frequency of intense cyclones over the North Atlantic area in the vicinity of Ireland is found to be increased by about 15% compared with the current climate. This is also supported by the results of a 16-year sensitivity study (section 8) that examines the influence of sea surface temperature on the climate. Increasing the sea surface temperature by a flat 1 degree Celsius compared to a reference simulation produced three hurricanes that were absent from the reference run.

Is the downscaling sensitive to the resolution of the GCM driving data? Section 9 describes the results of a simulation experiment to shed some light on this important issue.

Section 10 examines the use of radiosonde observations for detecting climate change in the upper atmosphere. The temporal and spatial drift of the observations are usually ignored in compiling statistics; this study takes a closer look at this practice using simulated observations to quantify the errors.

2.3 Computing resources

The main climate simulations were run on the ECMWF High Performance Computing Facility while the UCD IBM computer was used to run the 16-year sensitivity simulation (described in section 8). Work on a Grid-capable version of the climate model was completed and the software fully tested on a simulated Grid; the computational scientist assigned to this task in UCD completed his contract and left the Project in December. Climate simulations will be run on the CosmoGrid system once access issues are resolved.

Plans for ensemble simulations and very high resolution downscaling experiments will require enhanced computer resources well in excess of our ECMWF allocation. The recent acquisition of a computer cluster by UCD and the proposal for a High End Computing Centre in Ireland are welcome developments that may open up new resources for C4I.

2.4 Cooperations and links

- A researcher from NUI Galway began work on porting an aerosol and chemical transport model into the RCA climate model.

- Cooperation with the Coastal and Marine Resources Centre (CMRC) in University College Cork has been initiated. CMRC will use the simulated future 10-metre winds to evaluate climate change in the sea state in coastal areas.

- Links with the ICARUS group in Maynooth continue; C4I has benefited in resolving problems in defining catchment areas for flooding assessment (section 6).

- In cooperation with the Rossby Centre C4I optimised the new version (RCA3) of the climate model by implementing an efficient MPI decomposition strategy.

- Cooperation with the Spanish Meteorological Institute (Instituto Nacional de Meteorología) continues; C4I has shared its RCA model expertise with INM to aid them in running their own climate simulations.

- Links with UCD have been strengthened with the recently established Research Centre in Meteorology and Climatology in the Faculty of Science at UCD.

- C4I initiated contact with the EU-sponsored ENSEMBLES project with a view to becoming a partner. Initial response has been positive.

2.5 Conferences/Meetings attendance

- RIA Agmet meeting (26 February).

- 2nd COSMOS Workshop (8-9 March) in Lueneburg, Germany.

- Visit to Armagh Observatory (5 April) – presentation on C4I work.

- EGEE/CosmoGrid Meeting (18-22 April).

- EPA: "Bridging the Gap" Conference (28-30 April), Dublin.

- Visit to Rossby Centre (6 May and 6 October), Norrköping, Sweden.

- IPCC Uncertainty and Risk Workshop (11-13 May), Maynooth.

- European Workshop on Flood Forecasting and Warning (22-23 June), Helsinki, Finland

- PRUDENCE Meeting (6-9 September), Madrid, Spain.

- European Meteorological Society, 4th Annual Meeting (26-30 September), Nice, France.

- 11th Workshop on the use of High performance computing in Meteorology (27-28 October), Reading, UK.

- Visit to CMRC (12 November), Cork.

Staff attended the following training courses:

- ECMWF: Use and interpretation of ECMWF Products (15-19 March), Reading, UK.
- ECMWF: Parameterization of diabatic processes (22 March – 1 April), Reading, UK.
- 3rd NCCR Climate Summer School (29 August – 3 September), Ticino, Switzerland

On 9 December C4I held a 1-day meeting in UCD to present results and advertise the work of the project.

2.6 Publications

Two papers have been submitted for publication in peer-reviewed journals:

Semmler T., McGrath R., Nolan P., Sweeney C., Wang S., 2005: Influence of an increased sea surface temperature on North Atlantic cyclones.

Wang S., McGrath R., Semmler T., Sweeney C., 2005: Validation of simulated precipitation patterns over Ireland for the period 1961-2000.

3 Simulation of past climate

The regional climate model has been validated by performing a 40-year simulation of the Irish climate (1961-2000), driven by ERA-40 re-analysis data, and the output compared against a wide range of observational data. Results confirm that the model is able to capture the essential features of the Irish climate. While there is evidence of systematic errors in the simulation of some weather elements, they are not regarded as serious enough to compromise the ability of the model to simulate the future climate. Some of the errors revealed in the validation run may be related to errors in the ERA-40 driving data.

3.1 Introduction

The regional climate model used by C4I is the RCA climate model, adapted from the model developed by the Rossby Centre climate modelling research unit at SMHI, Sweden (Rummukainen *et al.* 2001). Earlier work with the model (C4I Annual Report 2003) showed that while the dynamical downscaling is sensitive to the domain size and orientation for specific weather events, for climate evaluation the sensitivity was marginal for the range of domains used in the original assessment work. Accordingly, the choice of domain for validating the model and for generating future climate scenarios was based primarily on two factors: computational economy, and the desirability of having the lateral boundary zones away from areas of steep orography while sufficiently far away from Ireland to reduce the impact of errors associated with the boundaries.

This domain, shown in Figure 3.1, is based on a rotated grid system with 156x166 grid points in the horizontal, corresponding to a resolution of about 0.12° (approximately 13 km) over Ireland. In the vertical extent there are 40 unequally spaced levels.

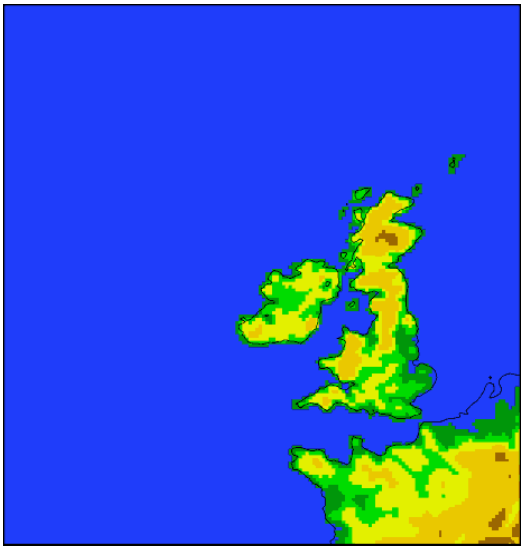

Figure 3.1: Model domain

The rationale for the validation exercise is to ensure that the model is capable of reproducing the essential features of the Irish climate, at the scale of the model, and to reveal any significant deficiencies. For this purpose the ECMWF ERA-40 global re-analysis data (Uppala *et al.* 2005) were used to drive the model, producing a dynamically downscaled simulation of the climate for the period 1961-2000, hereafter called the RCA-ERA-40 simulation. The actual simulation was launched from 1959 to allow time for the soil moisture to "spin up". Note that the observation-based ERA-40 driving data, while generally regarded as providing a very accurate description of the atmosphere, are not free from error (see comments on the relative humidity fields, for example, in section 3.4 below). Also, the data are only available at 6-hour intervals, a frequency that may be too

crude for the RCA to capture the essential features of very rapidly moving weather systems. Output products from the simulation, delivered with a 3-hour frequency, are listed in Table 3.1.

Geopotential at surface, 150, 500, 850, 925 and 1000 hPa
Temperature at surface and 2 metres, and at 150, 500, 850, 925 and 1000 hPa
3-hour maximum and minimum surface and 2-metre temperature
2-metre dew-point temperature
Temperature at three depths
Wind at 10m, 60m, 150, 500, 850, 925 and 1000 hPa
Maximum (3-hour) 10m wind
Surface friction velocity
Relative humidity at 2 metres, and at 150, 500, 850, 925 and 1000 hPa
2-metre specific humidity
Mean sea level pressure
Total, large-scale and convective precipitation
Soil moisture at three depths
Water runoff at two depths
Total cloud cover
Vertically integrated cloud liquid water and water vapour
Cloud top temperature (infrared)
Cloud water reflectivity (visible)
Water vapour brightness temperature and correction for clouds
Freezing height
Planetary boundary layer height
Averaged surface sensible, latent and momentum heat flux
Averaged surface short-wave and long-wave radiation
Averaged upward and downward short-wave and long-wave radiation at surface and top of atmosphere

Table 3.1: RCA output fields

3.2 Verification

To verify the outputs three data sources were exploited: UKCIP data, a dataset that includes monthly averages of 2-metre temperature and monthly total precipitation, on a 5 km grid covering Ireland; the Met Éireann climate archive, containing detailed information from the Irish synoptic and climate stations; and satellite data from the HOAPS database. The ERA-40 re-analysis fields are also available. For validation the simulation fields were either transformed to the UKCIP grid or spatially interpolated to the locations of the stations.

In this report only the essential validation results are presented; further information can be found on the C4I web site (http://www.c4i.ie).

Verification results for Ireland, based on the Irish observational data and the UKCIP and ERA-40 fields, are presented in section 3.3. Section 3.4 discusses the validation over sea using satellite data from the HOAPS database.

3.3 Validation over Ireland

3.3.1 Mean sea level pressure (MSLP)

Figure 3.2 shows the mean MSLP field over the model domain for the simulation period 1961-2000: RCA-ERA-40 (a), ERA-40 (b), and the difference between RCA-ERA-40 and ERA-40 (c). Relative to the reference ERA-40 data the large-scale circulation pattern is captured quite well by the model; there is a slight negative bias centred over England but the maximum difference is within 0.5 hPa of the ERA-40 values.

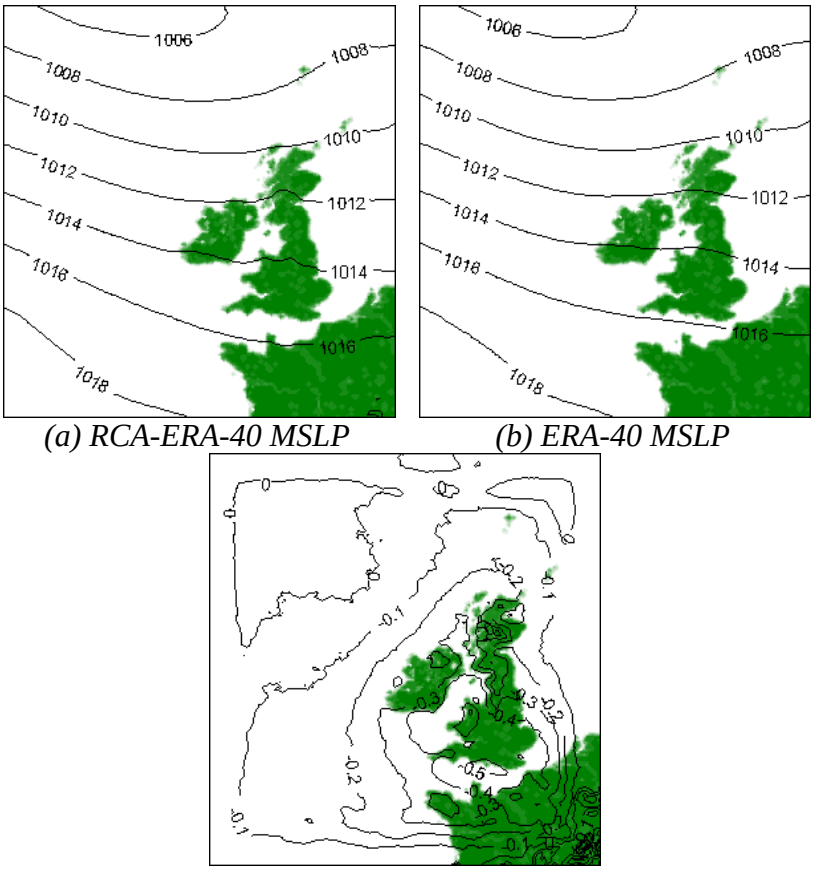

(a) RCA-ERA-40 MSLP *(b) ERA-40 MSLP*

(c) RCA-ERA-40 MSLP minus ERA-40 MSLP

Figure 3.2: Mean MSLP 1961-2000

3.3.2 Temperature, radiation and cloud cover

Figure 3.3 shows the validation results for the average January 2-metre temperature from 1961-2000: ERA-40 re-analysis data (a) and differences relative to UKCIP (b); RCA-ERA-40 (c) and differences relative to UKCIP (d). The model is in much better agreement with the observed temperatures (i.e. UKCIP) compared to the ERA-40 data. The main errors for the model occur around the coast and in some mountainous areas but overall are small (areas marked in white are within 0.25C of observations). The errors near the coast could be due to a lack of observational data and a consequent poor interpolation for the UKCIP data; those in mountainous areas could be partially attributed to the relatively crude (0.12°) representation of the orography by the model. Results for other months are very similar.

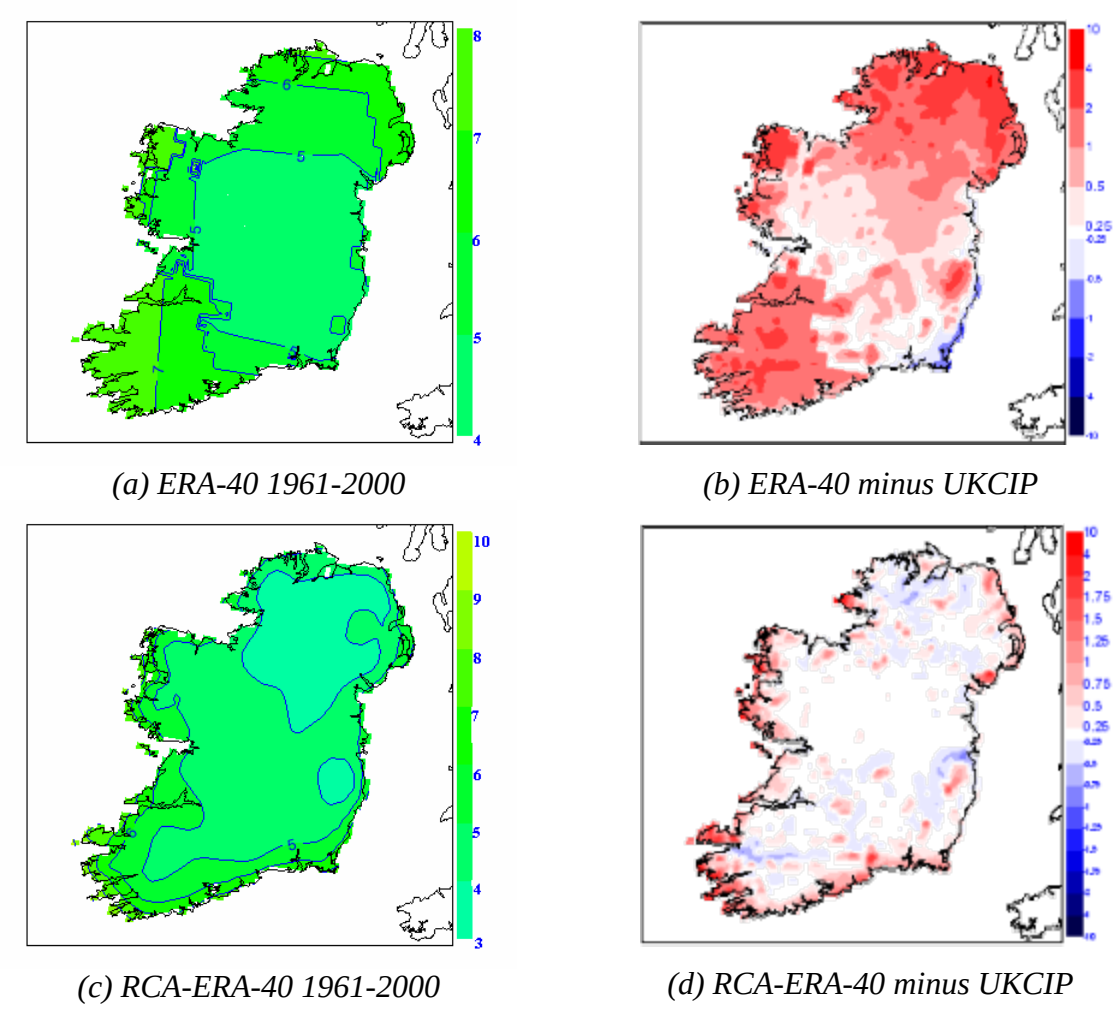

(a) ERA-40 1961-2000

(b) ERA-40 minus UKCIP

(c) RCA-ERA-40 1961-2000

(d) RCA-ERA-40 minus UKCIP

Figure 3.3: Average January 2-metre temperature

Figure 3.4 shows the yearly 2-metre temperature time-series for Valentia from 1961-2000. The inter-annual variability is captured well by the model, as are the longer-term trends. The 5-year running average values, plotted in bold, show an increase in temperature up to 1975, followed by a cooling to 1986, and a marked increase towards the end of the century.

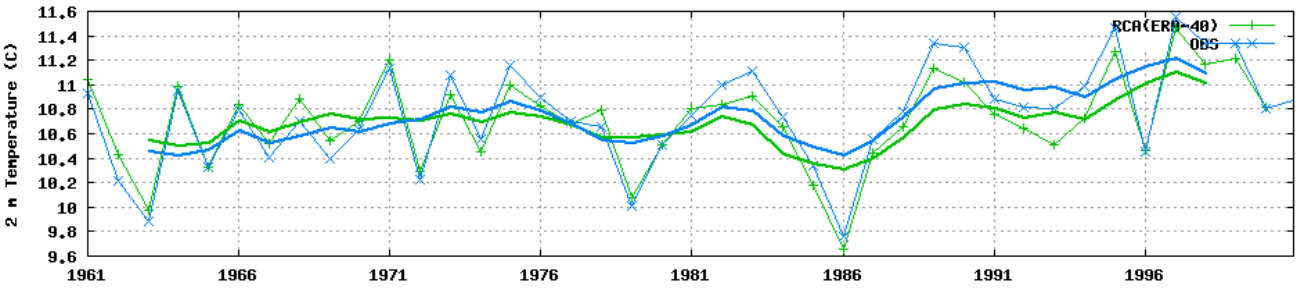

*Figure 3.4: Yearly 2-metre temperature time-series Valentia observatory 1961-2000. Observed (blue), RCA-ERA-40(green), 5-year running average in **bold**.*

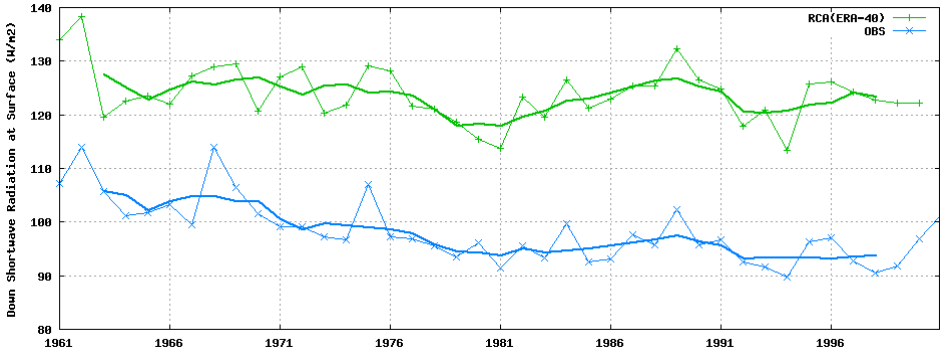

(a) Short-wave radiation

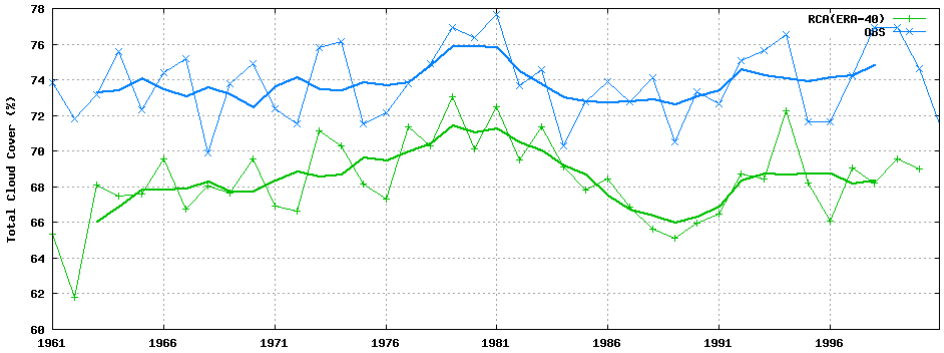

(b) Cloud cover

*Figure 3.5: Yearly time-series for Valentia observatory 1961-2000. Observed (blue), RCA-ERA-40(green), 5-year running average in **bold**.*

The yearly time-series of short-wave radiation at the surface and total cloud cover are also shown (Figure 3.5). In the case of the radiation the model values are systematically too high compared to the observations and while the patterns in the 5-year running average values are broadly similar, the model

fails to catch the slow decline in the observed values over the period. The long-term reduction in the observed radiation ("global dimming") is an intriguing feature that has been the subject of several studies (e.g. Stanhill 1998) and may be related to the buildup of atmospheric aerosols. As the model has a fixed set of parameters to calculate the radiation effects of aerosols, this may explain the lack of a trend in the simulated data. The systematic overestimation of the radiation is probably also related to the underestimation of cloud cover by the model.

To investigate the diurnal cycle of temperature, decadal monthly averages were calculated based on 3-hourly values from both the observation and simulation data. Figure 3.6 shows the results for Kilkenny for January and July in the 1960s and 1990s. The model slightly underestimates the range of the cycle in January, and overestimates the maximum temperature in July in the 1960s. However, both the model and observations show a shift towards warmer temperatures from the 1960s to the 1990s, and the amplitude of the diurnal cycles are generally well reproduced.

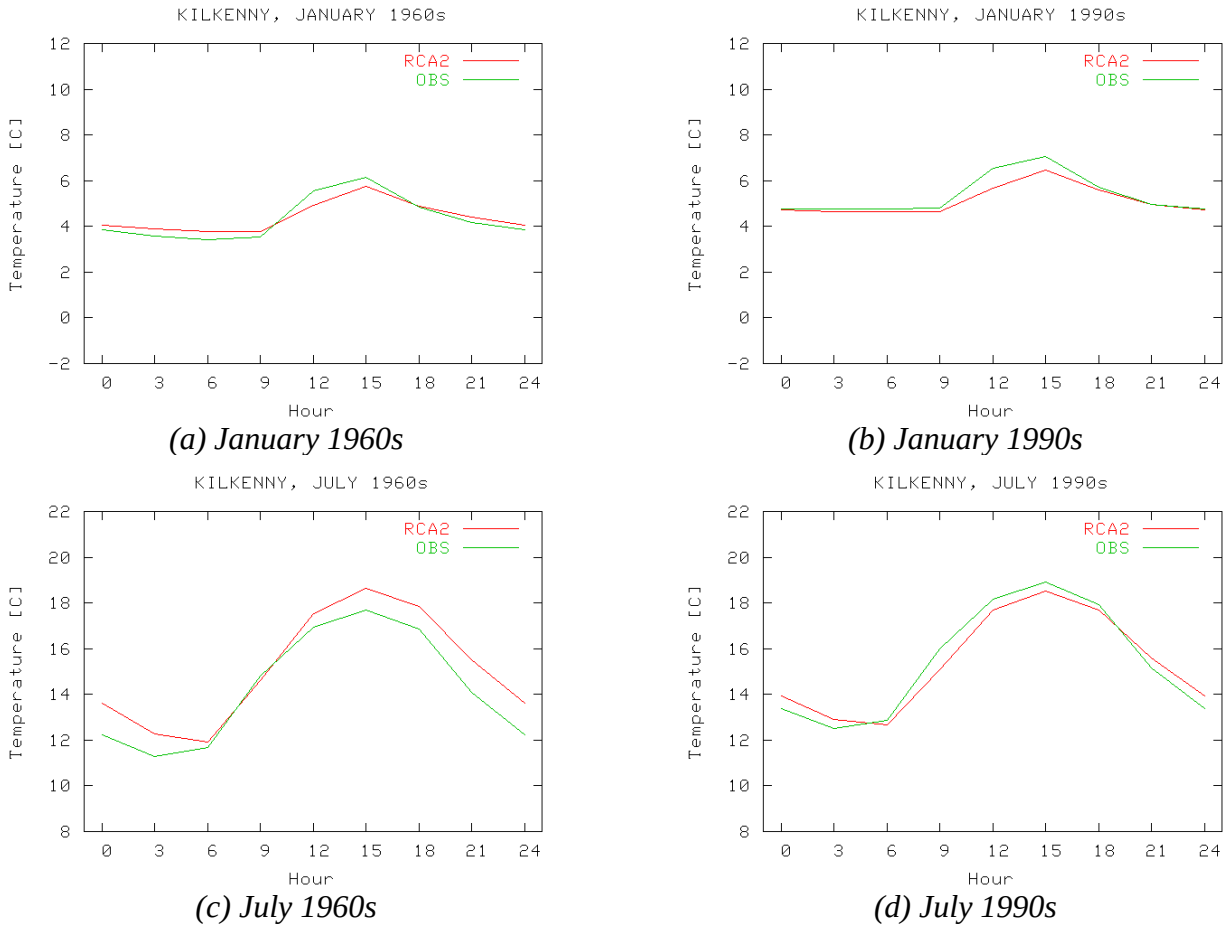

(a) January 1960s *(b) January 1990s*

(c) July 1960s *(d) July 1990s*

Figure 3.6: 2-metre temperature diurnal cycle for Kilkenny, Observed (green), RCA-ERA-40(red)

3.3.3 Precipitation

Sample results for the average monthly precipitation for the representative months January and April are shown in Figure 3.7. The plot for January shows that rainfall in the midlands is overestimated by about 20%. This is probably due to the model producing too many light precipitation events but it should also be noted that the observations generally underestimate rainfall amounts, particularly in windy conditions. In contrast, there is too little rain in mountainous areas, where the model underestimates rainfall by up to 15%. This could be partly due to an insufficient representation of the orography at the 0.12 degrees resolution of the model.

Agreement between the model and observations is better in April, a drier month, but the relative error is still similar, at about 20%. Overall, there is an overestimation of rainfall, again probably due to the model producing too many low precipitation events. Agreement in mountainous areas is better, however, suggesting that only the heavy rainfall over the mountains is difficult to simulate.

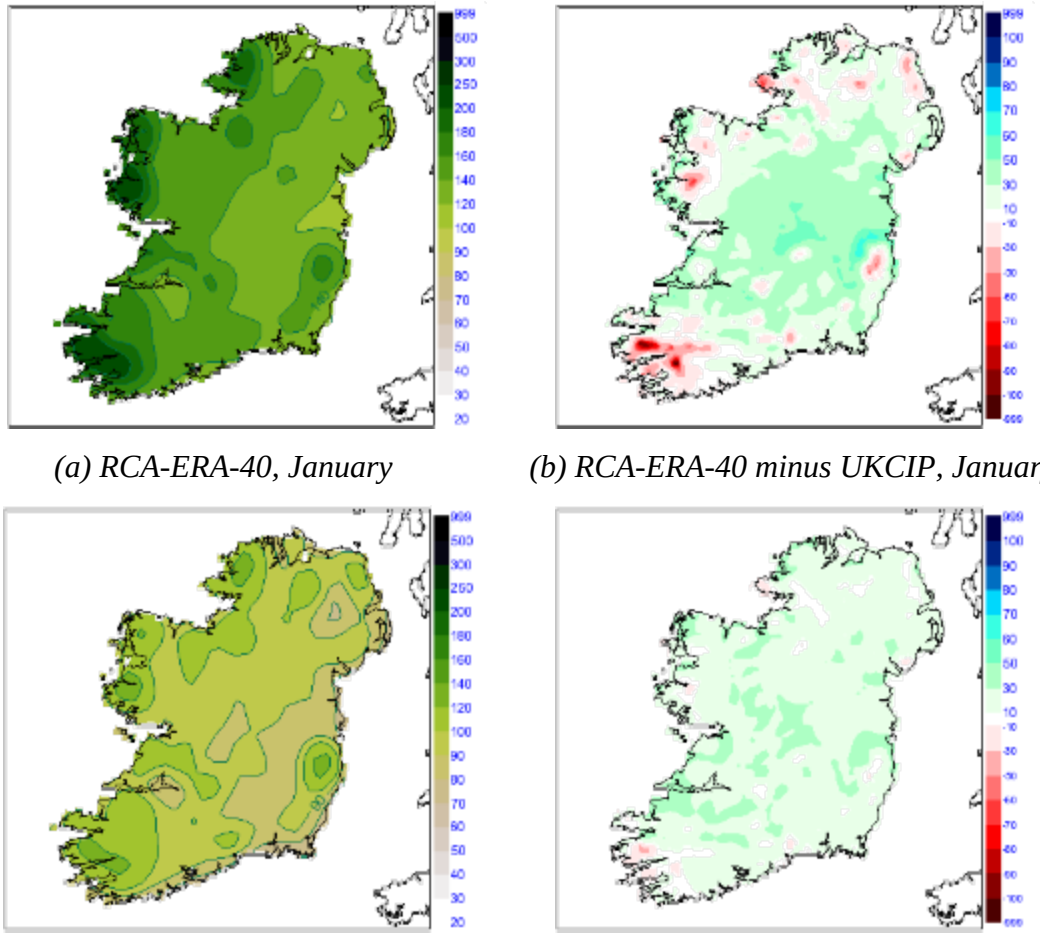

(a) RCA-ERA-40, January *(b) RCA-ERA-40 minus UKCIP, January*

(c) RCA-ERA-40, April *(d) RCA-ERA-40 minus UKCIP, April*

Figure 3.7: Average monthly 1961-2000 precipitation. (a) RCA-ERA-40, January (b) RCA-ERA-40 minus UKCIP, January (c) RCA-ERA-40, April (d) RCA-ERA-40 minus UKCIP, April

The yearly precipitation time-series plot for Belmullet (Figure 3.8) shows that the inter-annual variability and time trend are well reproduced. The model shows a consistent positive bias, as was seen in the monthly plots over Ireland discussed above.

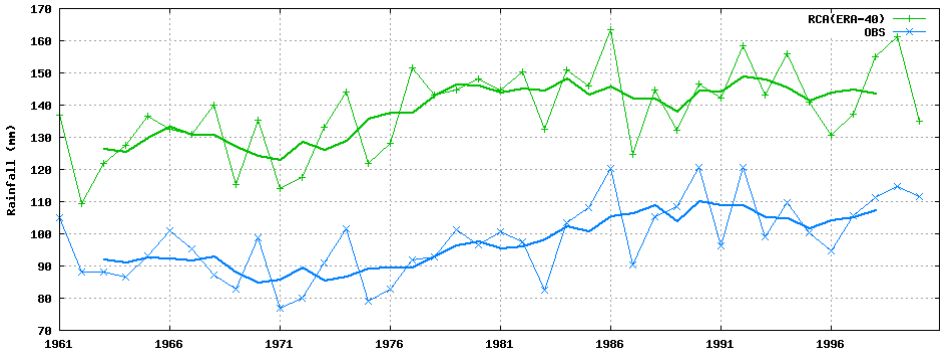

*Figure 3.8: Yearly precipitation time-series for Belmullet from 1961-2000. Observed (blue), RCA-ERA-40(green), 5-year running average in **bold**.*

The number of dry days per year (< 0.2 mm) for Belmullet is plotted in Figure 3.9a. The marked bias of the model to over-predict small amounts of rain is clearly seen in the data. However, both the model and observations show that the number of dry days has not changed much over the simulation period. The annual number of days with heavy rainfall (24-hour total exceeding 20.0 mm) is shown for Belmullet in Figure 3.9b. Here, the model is in better agreement with observations, with both showing an initial decrease in the 60s, followed by an increasing trend. A more detailed analysis of the simulated precipitation data is presented in section 4.

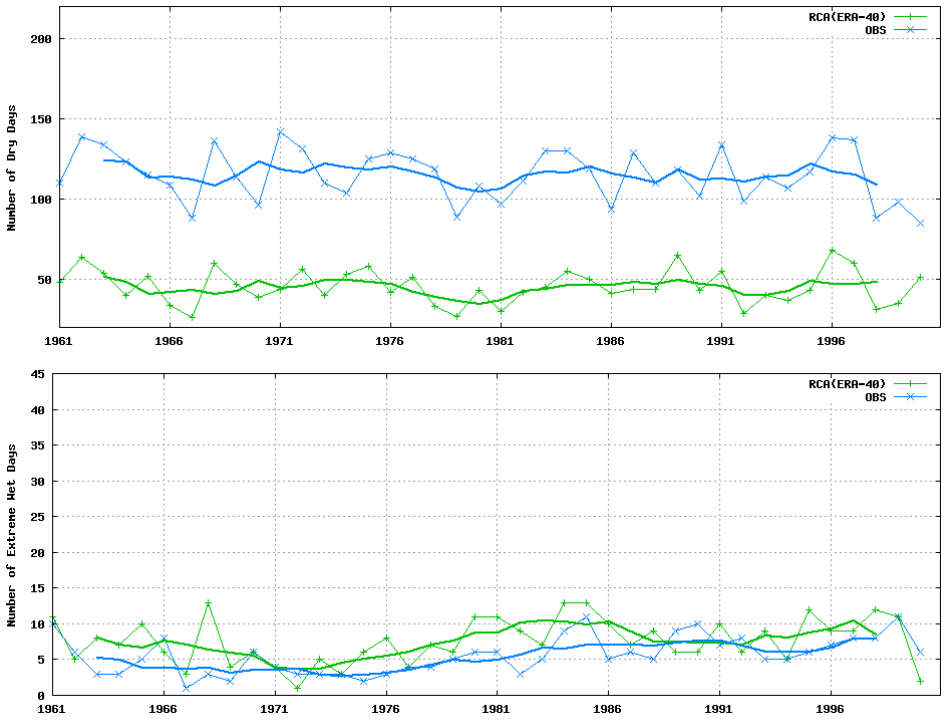

*Figure 3.9: Yearly time-series for Belmullet, 1961-2000, (a) number of dry days (< 0.2 mm), (b) number of heavy rainfall days (> 20.0 mm). Observed (blue), RCA-ERA-40(green), 5-year running average in **bold**.*

3.3.4 Wind

Figure 3.10 shows the yearly 10-metre wind speed for Belmullet. The peaks and troughs in wind values from year to year are captured well by the model, although the model winds are generally stronger than the observed values. For other stations the results are similar but the systematic differences vary from station to station.

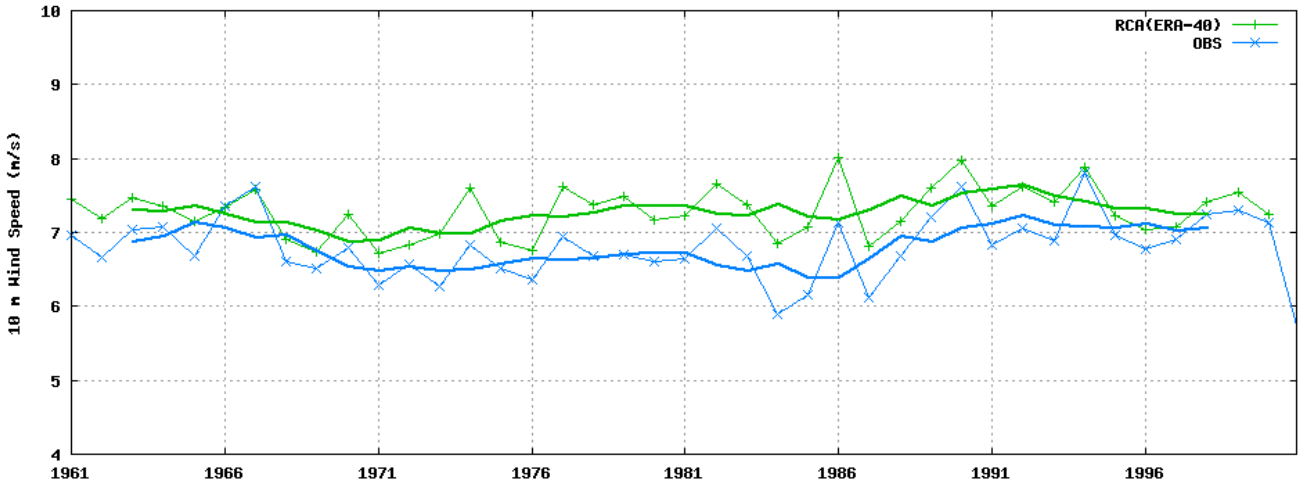

*Figure 3.10: Yearly 10-metre wind speed time-series for Belmullet from 1961-2000. Observed (blue), RCA-ERA-40(green), 5-year running average in **bold**.*

3.4 Validation over the ocean

Because of the influence of the sea on the Irish climate it is important to include the sea areas in the model validation. However, compared with land areas, surface observations (mainly reports from ships and buoys) are not plentiful and data quality is also a significant issue. Fortunately, the HOAPS dataset can be used to supplement the surface observations. Derived from satellite measurements it has an extensive set of meteorological parameters important for the water and energy budget.

The following products generated from the last decade of the 40-year RCA simulation (1991-2000) were validated using this database: the vertically integrated water vapour, 10-metre wind speed, net long-wave radiation and the sensible and latent heat fluxes. As an additional check the vertically integrated water vapour was compared against the ERA-40 data as this parameter is assimilated from observations in the re-analyses.

The spatial distribution of the vertically integrated water vapour is very similar in all three datasets (Figure 3.11). However, particularly in the summer months, the water vapour content is slightly higher in ERA-40 and RCA compared to HOAPS. The RCA bias is not unexpected as the model humidity is driven by the ERA-40 data. The slight overestimation in summer might explain the overestimation of precipitation in this season.

The spatial distribution of the 10-metre wind speed shows a good agreement between RCA and HOAPS (Figure 3.12). However, the speed is systematically underestimated by 3 to 4 ms^{-1} in winter and 2 ms^{-1} in summer. A scatter plot of the RCA simulated wind speed and the observed data from the K2 ocean buoy at 51° N, 13.3° W shows that the RCA winds have a small systematic positive bias but otherwise the fit is quite reasonable over the range of speeds encountered (Figure 3.13). This is slightly at odds with the HOAPS data which suggests that the model wind speeds are underestimated. The discrepancy may be explained by the fact that the ocean buoy measures the wind speed at a height of 3 metres instead of at the standard height of 10 metres i.e. observed values are a little too low. However, it is difficult to draw general conclusions from a single site. The accuracy of the satellite derived 10-metre wind speed is given as 1.4 ms^{-1} (Schulz *et al.*) and hence does not explain the difference.

The latent heat fluxes (Figure 3.14) are very well represented in our model simulation. The differences (slightly stronger negative heat fluxes in RCA compared to HOAPS) are within the uncertainties of the satellite data. Also the net long-wave radiation is well simulated. It is a little less negative than in HOAPS (Figure 3.15), which might be connected to the slightly overestimated water vapour content.

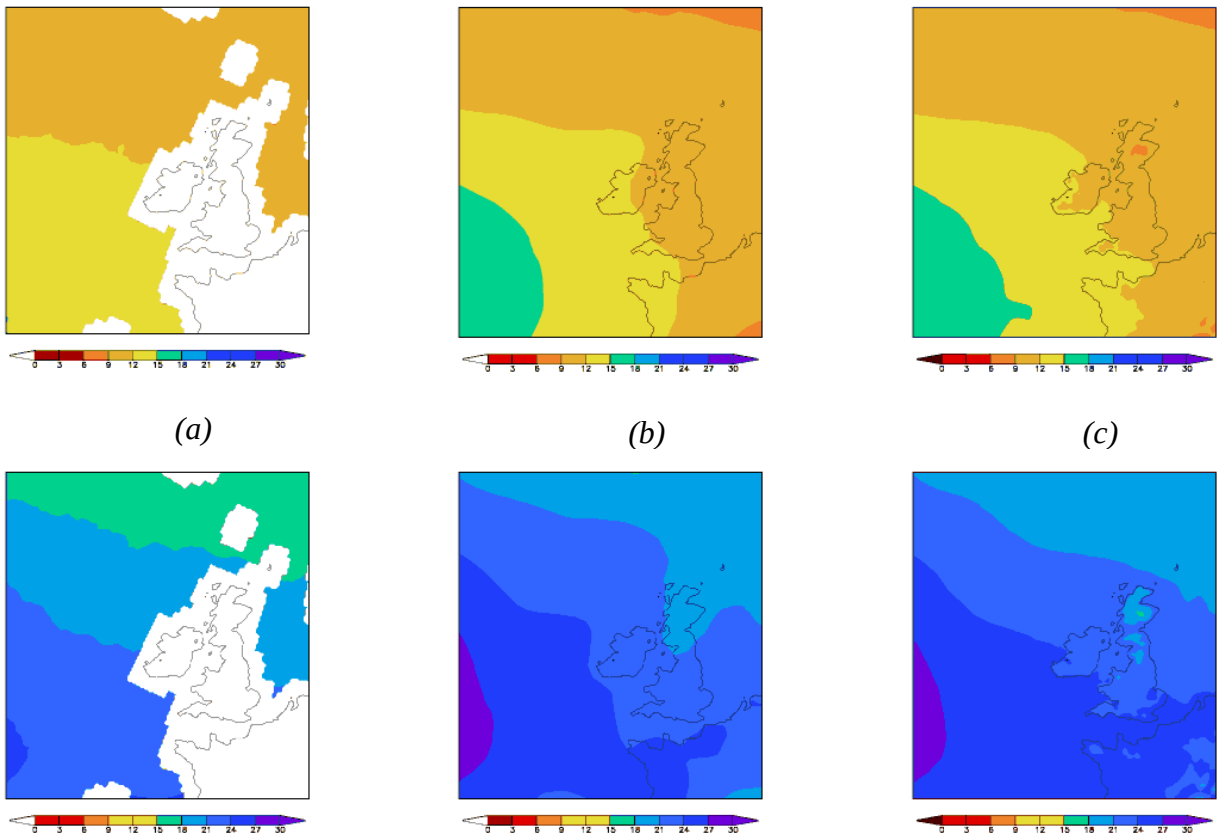

(a) *(b)* *(c)*

(d) *(e)* *(f)*

Figure 3.11: Vertically integrated water vapour [kg/m^2] as decadal monthly means for January 1991-2000 from (a) HOAPS, (b) ERA-40 and (c) RCA. (d) to (f) corresponding to (a) to (c) but for July 1991-2000.

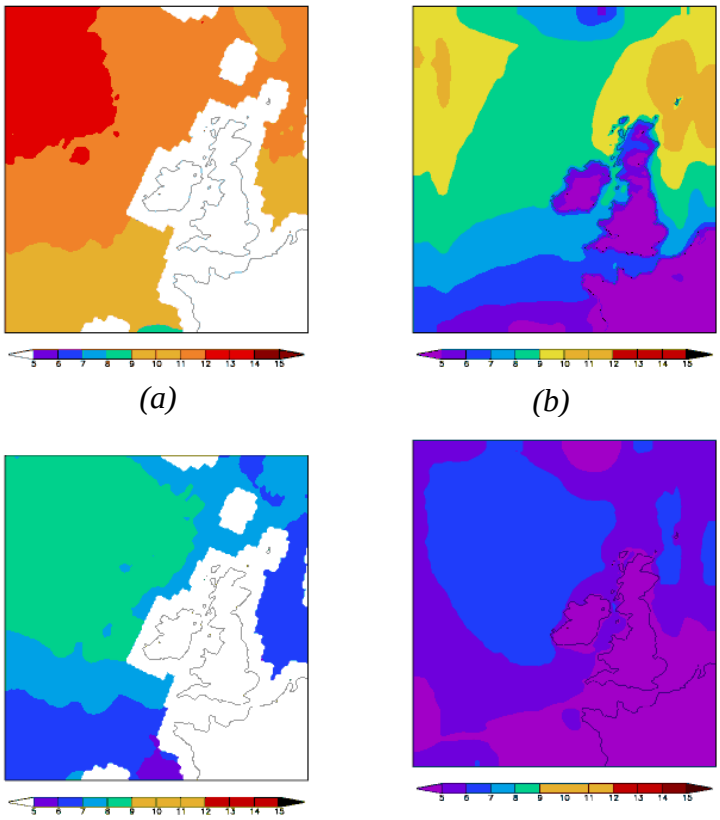

Figure 3.12: 10 m wind speed [ms^{-1}] as decadal monthly means for January 1991-2000 from (a) HOAPS and (b) RCA. (c) and (d) corresponding to (a) and (b) but for July 1991-2000.

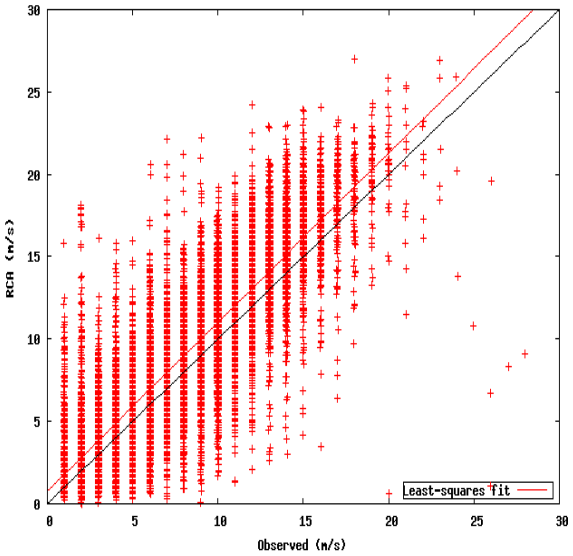

Figure 3.13: Scatter plot of the observed wind speed from ocean buoy 62081 (51° N, 13.3° W) for December 1991 to December 2000 compared to RCA. Buoy measurements are at a height of 3 m whereas the RCA output is at a height of 10 m (results interpolated to the location of the buoy). The red line indicates the linear least-squares fit.

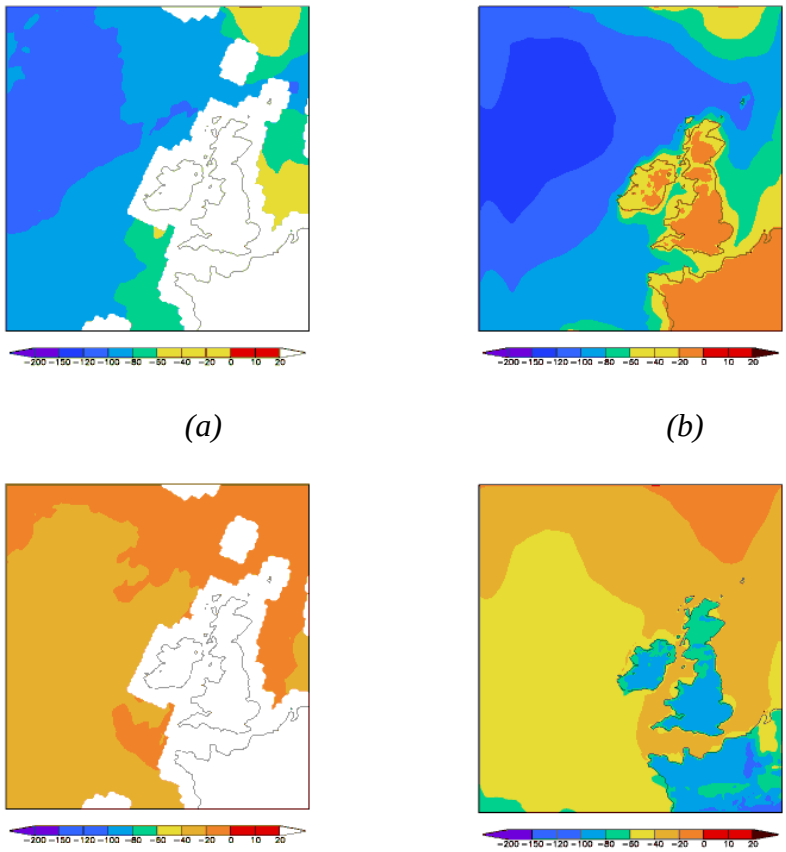

(a) *(b)*

(c) *(d)*

Figure 3.14: Latent heat flux [wm^{-2}] as decadal monthly means for January 1991-2000 from (a) HOAPS and (b) RCA. (c) and (d) corresponding to (a) and (b) but for July 1991-2000.

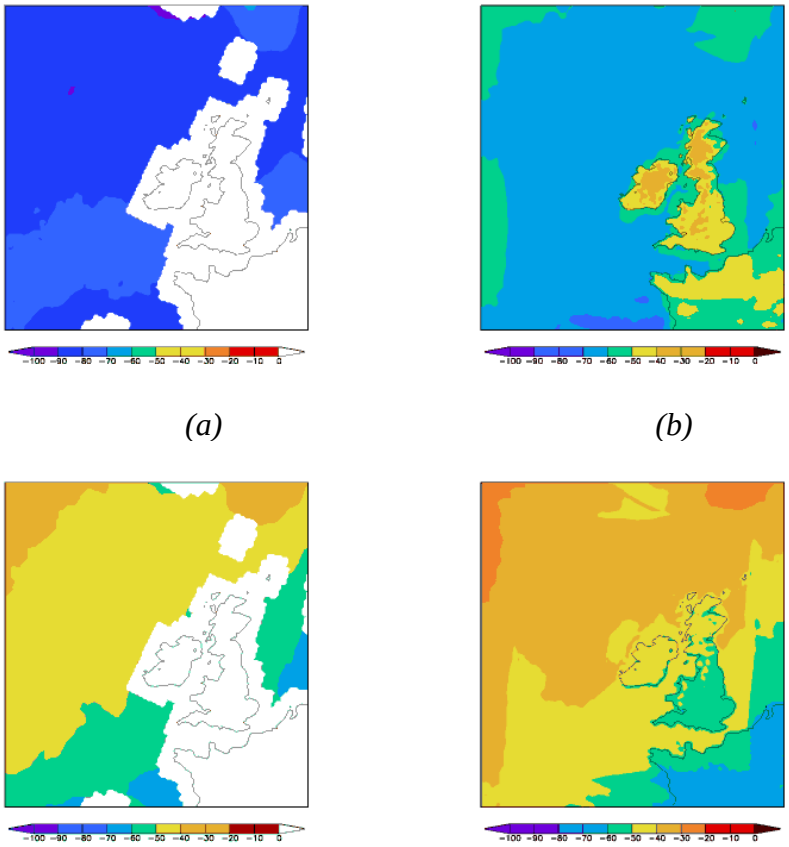

(a) *(b)*

(c) *(d)*

Figure 3.15: Net long-wave radiation [Wm^{-2}] as decadal monthly means for January 1991-2000 from (a) HOAPS and (b) RCA. (c) and (d) corresponding to (a) and (b) but for July 1991-2000.

3.5 Conclusions

The validation results confirm that the RCA is able to capture the essential features of the Irish climate. While there is evidence of systematic errors in the simulation of some weather elements, they are not regarded as serious enough to compromise the ability of the model to simulate the future climate. Some of the errors revealed in the validation run may be related to errors in the ERA-40 driving data.

References

Rummukainen M, Raisanen J, Bringfelt B, Ullerstig A, Omstedt A, Willen U, Hansson U, Jones C. 2001. A regional climate model for Northern Europe: Model description and results from the downscaling of two GCM control simulations. Climate Dynamics 17: 339-359. DOI: 10.1007/s003820000109

Schulz J, Meywerk J, Ewald S, Schluessel P. 1997. Evaluation of Satellite-Derived Latent Heat Fluxes. *Journal of Climate* **10**: 2782-2795.

Stanhill G. 1998. Long-term trends in, and spatial variation of, solar irradiances in Ireland. *Int. J. Climatol.*, **18**, 1015-1030

Uppala SM, Kållberg PW, Simmons AJ, Andrae U, da Costa Bechtold V, Fiorino M, Gibson JK, Haseler J, Hernandez A, Kelly GA, Li X, Onogi K, Saarinen S, Sokka N, Allan RP, Andersson E, Arpe K, Balmaseda MA, Beljaars ACM, van de Berg L, Bidlot J, Bormann N, Caires S, Dethof A, Dragosavac M, Fisher M, Fuentes M, Hagemann S, Hólm E, Hoskins BJ, Isaksen L, Janssen PAEM, McNally AP, Mahfouf J-F, Jenne R, Morcrette J-J, Rayner NA, Saunders RW, Simon P, Sterl A, Trenberth KE, Untch A, Vasiljevic D, Viterbo P, Woollen J 2005. The ERA-40 reanalysis. *Quart. J. Roy. Meteor. Soc.*: Submitted

4 Validation of simulated precipitation patterns over Ireland for the period 1961–2000*

The Rotated Empirical Orthogonal Function (REOF) method was used to analyse the annual and interannual variability of the precipitation patterns over Ireland as simulated by the Rossby Centre Regional Climate Model (RCA) for the period 1961-2000. The annual and monthly precipitation results show that the model captures the major spatial pattern of each month but the simulation shows a larger percentage in the leading principal component (PC) and tends to have a less pronounced seasonal cycle compared to the observations. The simulation for the wet winter season is in slightly better agreement with the observations compared with the drier summer season. Over Ireland the distribution of the observed precipitation shows two major REOF patterns. One pattern shows more precipitation in the south-west of the country compared with north-western areas. This pattern is simulated quite well. The second pattern shows a precipitation maximum in the west and north-west of Ireland. The frequency of this pattern shows a strongly increasing trend, which is slightly underestimated in the model simulation. Both patterns show seasonal and interannual variability. The wavelet energy density analysis shows that the interannual variability is more important than the seasonal one. In general the model overestimates the monthly average precipitation but captures the major spatial and seasonal patterns.

4.1 Introduction

Any model that aspires to provide useful guidance on future climate change must be capable of realistically simulating the current and past climate. However, with the strong spatial and temporal variability of precipitation, it is a challenging task for a model to reproduce the observed climatology, especially the intensity of extreme events. In recent years many studies have been carried out to evaluate changes in precipitation patterns for various periods and regions. In this study we focus on Ireland, a country that in spite of its relatively high latitude has a temperate maritime climate thanks to the warm North Atlantic current, the impact of which is most noticeable along the west coast. The prevailing westerly winds and the local orography to a large extent determine the precipitation patterns for the country (Keane and Collins, 2004), with the highest values generally occurring in regions with high orography.

Although the precipitation distribution is determined by fairly simple mechanisms and, measured over a long period, is rather evenly distributed throughout the year, there is considerable temporal and spatial variability if the focus is shifted to short time periods. In a principal component analysis (PCA) of monthly precipitation between 1941 and 1970, for example, Logue (1984) found that with data expressed as percentages of the annual average, the leading principal component (PC1) is a measure of a tendency for rainfall to be higher in summer compared to winter and has a maximum in the midlands and north-east of the country. The second component (PC2) shows a tendency for the first half of the year to be relatively wet and the second half relatively dry; it has a maximum in the south-east.

* NOTE: This is a preview of an article submitted for publication.

The pressure distribution over the North Atlantic Ocean, which can be characterized by the North Atlantic Oscillation Index (NAO), influences the strength of the surface westerly flow (Rogers, 1985). The link between the NAO and precipitation over Europe has been investigated in many previous studies (Rex, 1951; Namias, 1964; Moses, 1987; Wilby, 1997; Davies, 1997). Also, the evaluation of the atmospheric moisture budget reveals coherent large-scale changes since 1980 (Hurrell, 1995). Kiely (1998, 1999) studied the changing precipitation climate in Ireland and identified 1975 as a significant year (coinciding with the evolution of the NAO): after 1975 the mean precipitation increased as well as the number of extreme precipitation events. The most pronounced increase in the number of extreme precipitation events occurred in August, September and October. In the monthly mean precipitation there are abrupt increases in March and October after 1975. Investigations of precipitation variations in Ireland in the decades after 1970 were also carried out by McElwain and Sweeney (2003). They studied the recent trends in temperature and precipitation using Irish observation data. The analysis of the precipitation changes supports the findings of the United Kingdom Climate Impacts Programme (UKCIP) with evidence of a trend towards a winter increase in the north-west of the country and summer decreases in the south-east. In general, the changes are consistent with the summary in the IPCC report (Houghton, 2001) that precipitation amounts have increased by 0.5 -1% every decade in the mid/high latitudes of the Northern Hemisphere in the 20th century.

Using a climate model to analyse the Irish climate presents its own problems. Although major progress has been achieved in simulating the climate with global and regional climate models, some inadequacies, especially regarding the intensity of extreme events, still remain. Analysis of the Atmospheric Model Intercomparison Project (AMIP) decadal simulations over the United States and the adjoining oceans show, for example, that in general the models have less interannual variation compared with the observations, with more variance being explained by the leading (annual cycle) PC, whereas the observations show a less peaked spectrum (Boyle, 1998). Because of the relatively coarse resolution of GCM models some local processes cannot be simulated and only the leading PC is well captured. Gutowski (2003) analysed ten years of a regional climate simulation over the central U.S. region and found that the model showed less spread compared with the observations in its pattern of spatial correlation versus distance from an anchor station, suggesting that resolved model circulation patterns producing 6-hourly precipitation data are limited in the range of precipitation patterns they can produce compared to the real world. The correlation also indicated that replicating observed precipitation intensity distribution for 6-hour accumulation periods requires a grid spacing smaller than about 15 km, suggesting that models with a grid spacing substantially larger than this will be unable to simulate the observed diurnal cycle of precipitation.

Because of the strong spatial and temporal variability of precipitation, it is a challenging task even for a regional climate model to reproduce precipitation that matches the observations, especially the intensity of extreme precipitation. The purpose of this paper is to study the quality of the precipitation simulations produced by a high resolution regional climate model and, in particular, the annual and interannual variability of the modeled precipitation over Ireland.

4.2 Experiment design and analysis procedure

4.2.1 Model setup and datasets

The RCM used in this study is the Rossby Centre Regional Atmospheric Model (RCA) developed from the High Resolution Limited Area Model (HIRLAM). A brief introduction of RCA is given by Jones (2001). The model domain that was used is shown in Figure 3.1, section 3.1. The model was run with a horizontal resolution of approximately 13 km with 40 vertical levels and a time integration step of 540 seconds. The integration period extended from 1 January 1959 to 31 December 2000. The ERA-40 re-analysis data (available at 00, 06, 12 and 18 UTC each day) were used as driving data. In this study, simulated monthly precipitation values were evaluated against gridded observation data for Ireland from the United Kingdom Climate Impacts Program (UKCIP) for the time period 1961 to 2000. These observation data are available on a grid with a horizontal resolution of 5 km. Monthly and annual precipitation anomalies were calculated for both the simulation and the observations for the whole time series. For the REOF analysis, the anomalies were normalized by the corresponding standard deviation.

4.2.2 Analysis procedure

4.2.2.1 REOF analysis

Empirical orthogonal functions (EOF) and principle component analysis (PCA) are widely used to study the spatial pattern of various meteorological parameters. Because of the large spatial variability of rainfall over Ireland it is difficult to obtain the local modes using EOF or PCA. Therefore, the varimax-rotated empirical orthogonal function (REOF) method was used. This means that the initial EOF modes were linearly transformed using the varimax method, which maximizes the variance of the squared correlation coefficient between the time series of each REOF mode and each original EOF mode. The method increases the spatial variability of the obtained modes. Therefore, the significant anomalies appear where regional phenomena are dominant, which makes the mode easier to interpret (Horel, 1981; Richman, 1986; Jolliffe, 1987; Richaman, 1987; Kawamura, 1994; Chen, 2003).

The REOF method was used to study the spatial patterns of the precipitation anomalies both from the observations and model simulation. For the calculation of the covariance matrix only land grid points were used. Apart from the normal method, where the spatial pattern shows the climatic characteristics of the precipitation anomaly distribution, the so-called nonstandard method was used: the spatial field is used as the time function, while the time series is considered to be the spatial field, and therefore the eigenvectors show the time evolution of the precipitation over the whole country. For the nonstandard method the original data were used.

4.2.2.2 Wavelet analysis

Wavelet analysis is a common tool for analyzing localized variations of a time series. The results show the dominant modes of variability and its variations in time (Torrence, 1998). In this paper a Morlet

wavelet was used as the wavelet mother function to study the period of the REOF time coefficient series:

$$\psi_0(x) = \pi^{-\frac{1}{4}} e^{i\omega_0 x} e^{-x^2/2} \qquad (1)$$

where ω_0 is the non-dimensional frequency. The continuous wavelet transform of a continuous time series is defined as the convolution of f(x) with a scaled and translated version of $\psi_0(x)$

$$W_\psi(a,b) = \frac{1}{\sqrt{a}} \int_{-\infty}^{\infty} f(x)\, \psi\left(\frac{x-b}{a}\right) dx \qquad (2)$$

where *a* is the dilate scale, *b* is the localized time index. In order to evaluate the energy distribution of the wavelet, the energy density is calculated in the following form:

$$E(a,b) = \frac{1}{C_\psi} \frac{|W_{ab}(f)|^2}{a^2} \qquad (3)$$

where

$$C_\psi = \frac{1}{2\pi} \int_{-\infty}^{x} \frac{|\psi(\omega)|^2}{|\omega|} d\omega = 2\pi \qquad (4)$$

4.3 Results

4.3.1 The spatial pattern of annual and monthly anomalies

First, we examine the annual anomalies from the observed data to compare them to the simulation data. The two leading PCs separately account for 35.2% and 29.4% of the total variance. In the case of the first leading PC (Figure 4.1a), the anomalies are positive except for some small patches along the east and south-east coasts. The largest positive values are located in the north-west and west regions. This is different from the mean annual precipitation distribution shown in Figure 4.1c. In the second PC distribution (not shown), the largest positive anomaly value is located in the north-west of the country, with negative values elsewhere, especially in the south-east. This pattern is likely to be more pronounced in later data according to McElwain's (2003) analysis of Malin Head (north coast) precipitation data which shows an increasing trend from the late 1970s, possibly connected with the evolution of the NAO index. The third spatial pattern shows a negative anomaly over the whole of Ireland with the largest negative value located over the north-east of the country. The fourth and fifth spatial patterns explain very little of the variance; more than 80% is explained by the first three eigenvectors.

Figure 4.1b shows the first leading component from the simulation data and should be compared with Figure 4.1a; the first two component patterns now explain 37.4% and 36.5% of the variance. The distributions for the first patterns are very similar but the highest value is a little weaker in the simulation. Comparing the second component, the pattern is different and the simulation shows a positive anomaly over the whole country. The comparison shows that the model can simulate the

leading regional spatial pattern of the precipitation anomaly quite well; agreement is good for the leading PC but becomes increasingly poor for higher PCs.

In the climatological mean values for Ireland, precipitation is subject to seasonal variation although spatial distribution details (location of maxima and minima) are relatively stable (Keane and Collins, 2004). However, local differences in the spatial distribution between individual months must not be overlooked. The first three principal components of simulated precipitation of each month are compared to the observed ones for the 40 year period. For January and October (Figures 4.2 and 4.5) the first two leading components of the simulation show similar spatial patterns compared to those from the observation analysis. The largest positive anomaly values are located in the north-west and south-east of the country in the first and second leading PCs, respectively. The first PC is particularly similar to the annual spatial precipitation pattern (Figure 4.1a); its distribution reveals strong gradients with high values in the north-west of the country and lower values in the south-east. In contrast, the summer spatial patterns differ more from the annual spatial patterns, and agreement is poor between the observation and simulation analyses. An exception is the month of August, where the first two leading PCs are captured very well (not shown). In other summer months (April to July), only one PC is captured. In April (Figure 4.3), the first and third PCs of the observation data correspond to the first and second PCs of the simulation analysis. The agreement for the first pattern shows some deviation. For July (Figure 4.4) the situation is similar. The third PC of the simulation corresponds to the second PC of the observation analysis. In this case the agreement for the first pattern is even worse compared to April. For other months (February, March, May, June, September, November and December), the first leading PC is captured well, while higher PCs are not captured.

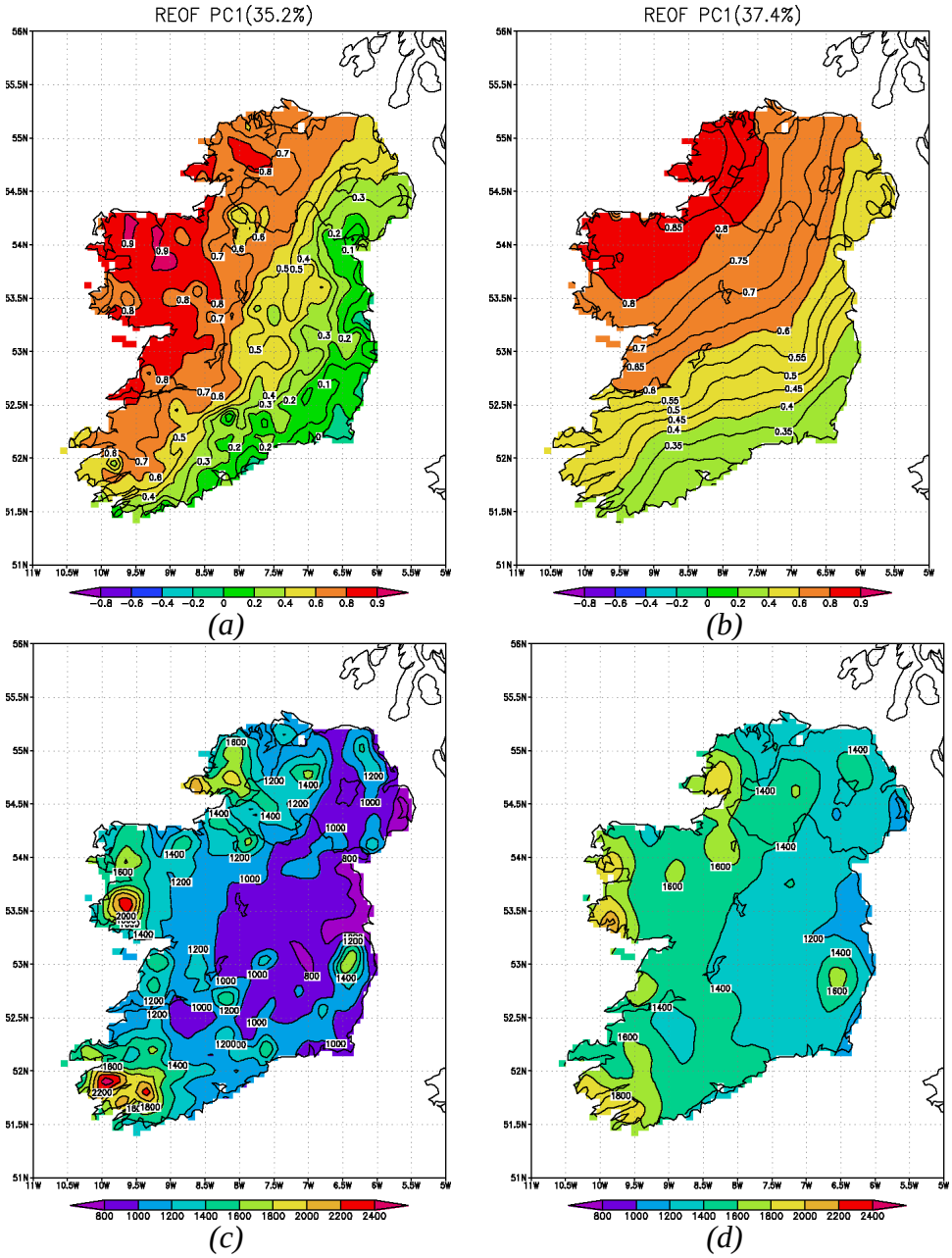

Figure 4.1: Leading PC for the observed (a) and simulated (b) annual precipitation data and the annual average precipitation (c) observation (d) simulation for 1961-2000

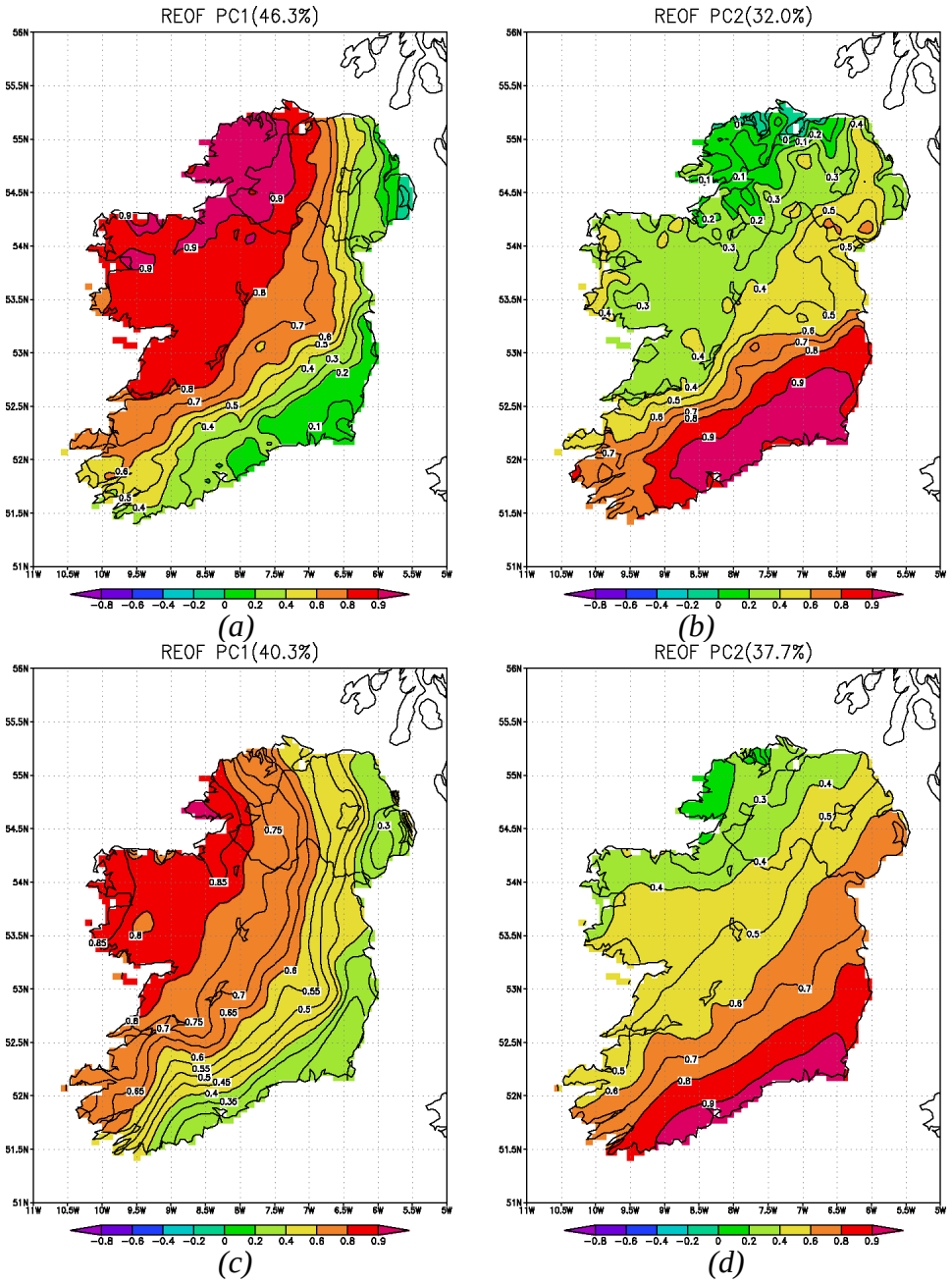

Figure 4.2: The leading PCs from the observation (a,b) and simulation (c,d) analyses in January

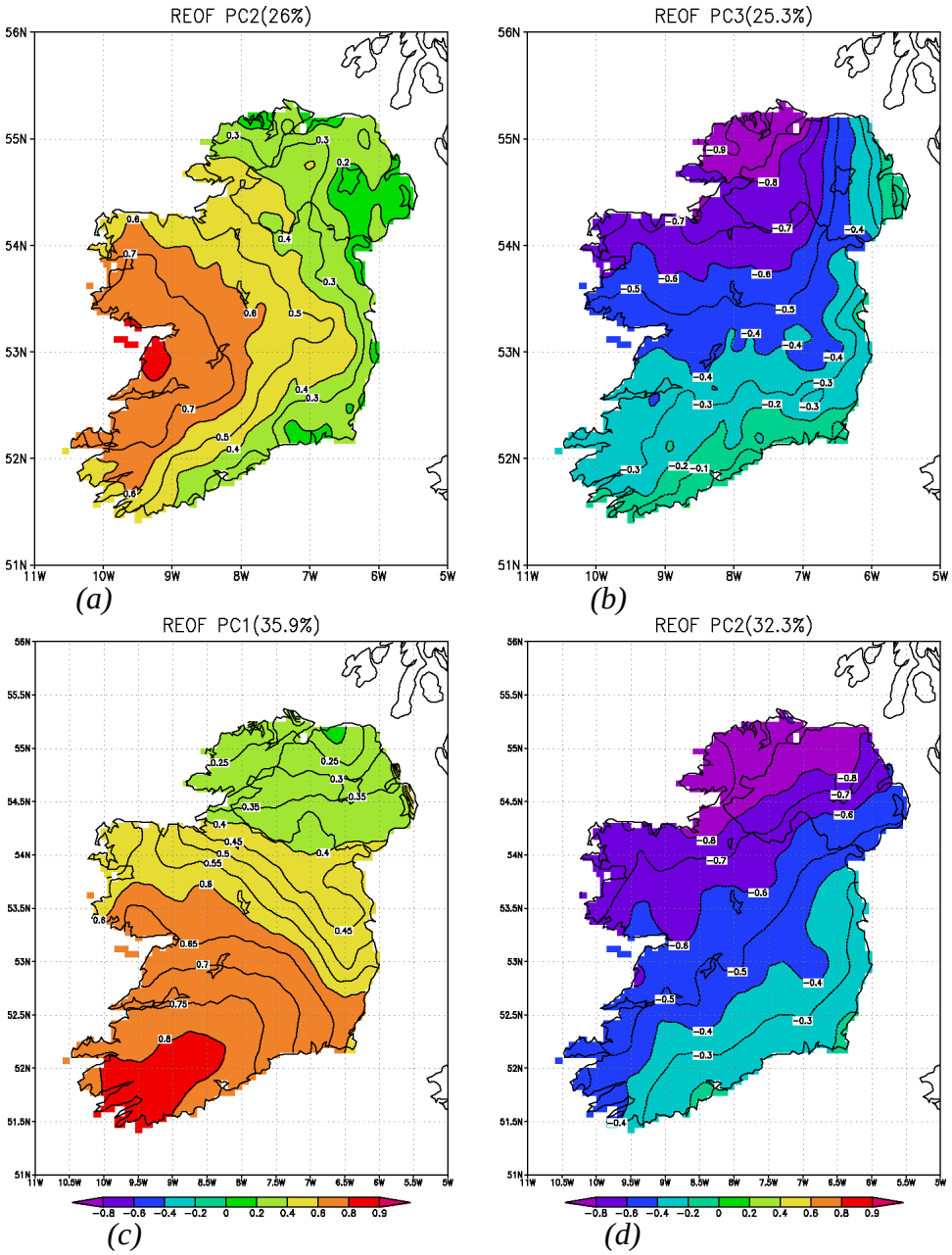

Figure 4.3: The leading PCs from the observation (a,b) and simulation (c,d) analyses in April

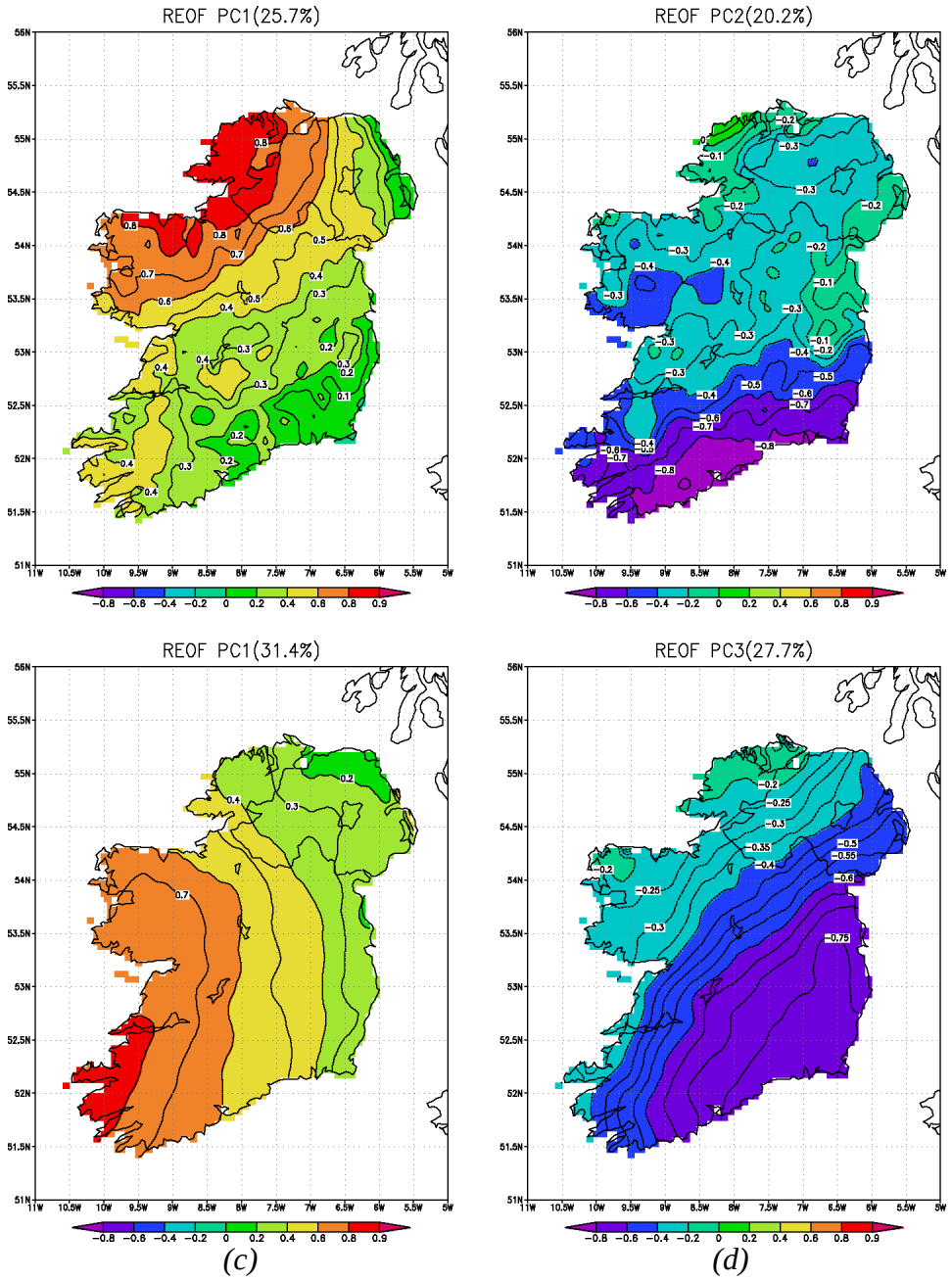

Figure 4.4: The leading PCs from the observation (a,b) and simulation (c,d) analyses in July

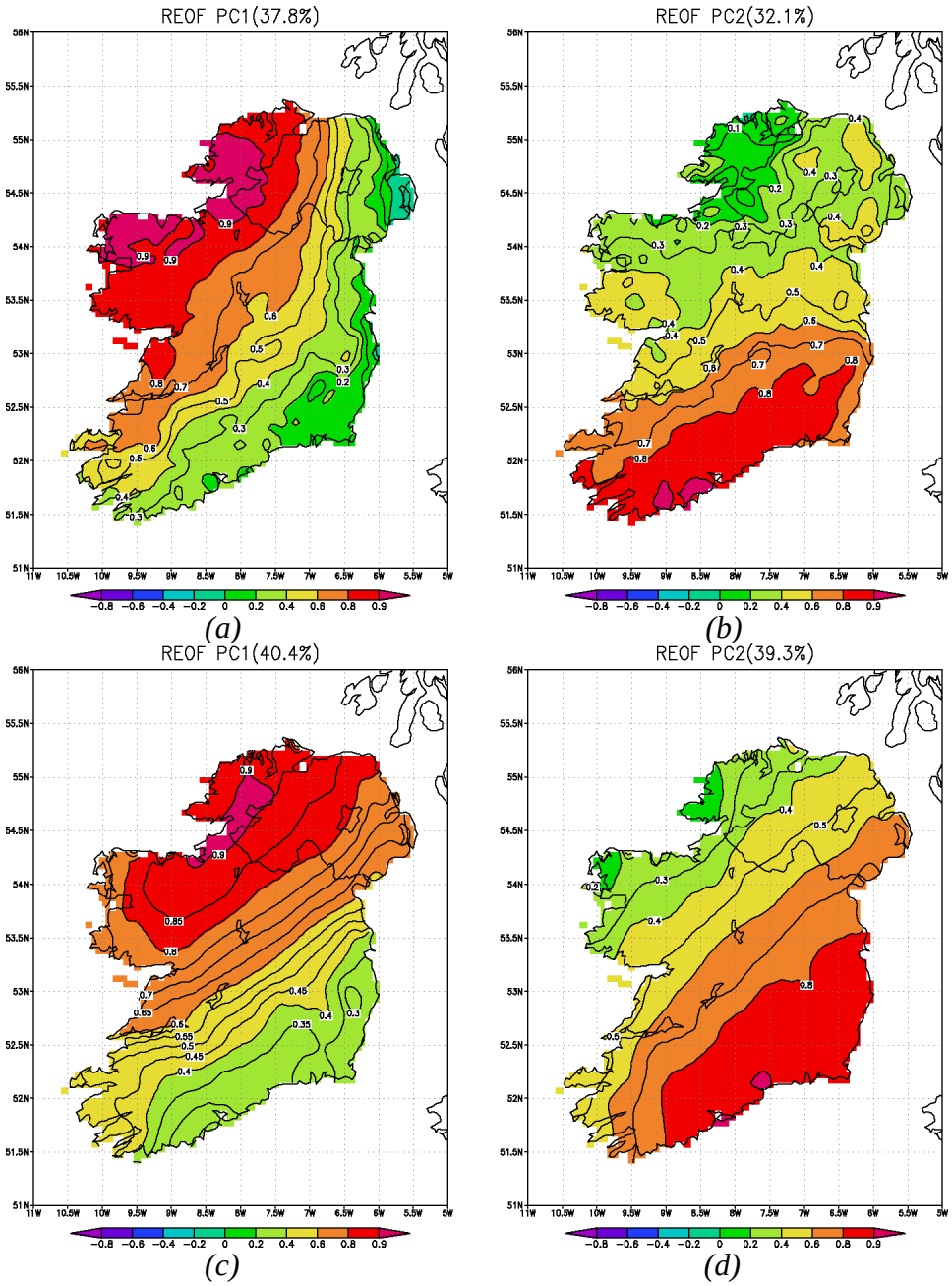

Figure 4.5: The leading PCs from the observation (a,b) and simulation (c,d) analyses in October

For most months the simulation captures the spatial characteristics of the precipitation pattern at least for the leading PC. Generally the simulation agrees better with the observation analysis in the wet winter season compared to the dry summer season. In the observation data there is a fast transit from the wet to the dry season in spring, which is too slow in the simulation. Also, in autumn the transition from the dry to the wet season is slower in the simulation than in the observations. The simulated spatial pattern of November is very different from the observed one and is very similar to the simulated October pattern.

Figure 4.6 is a bar chart of the percent variance explained by the leading PC for different months and the annual average. In the dry season the variance explained by the first principal component is much smaller than in the wet season. The difference between winter and summer is larger in the observation analysis compared to the simulation analysis. Thus in summer there is more spatial variability in the observation analysis compared to the simulation analysis. A reason for this could be the occurrence of more convective precipitation in the summer months compared to the winter months.

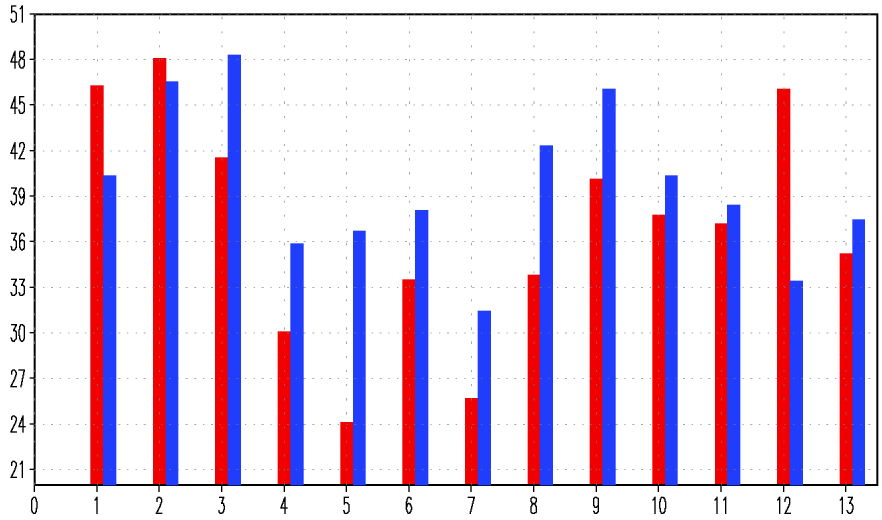

Figure 4.6: Bar chart of the percent variance explained by the leading components for the observation (red) and simulation (blue); months are numbered 1-12, with the annual data labeled as number 13.

In general the model has a less pronounced seasonal cycle in the spatial variability than the observations; it leads to a worse agreement in the summer months, where the spatial variability is larger in the observation analysis compared to the simulation analysis. This might also result in a worse agreement between the observation and simulation analyses of the leading PCs in the summer months compared to the winter months.

4.3.2 Spatial pattern evolution

The analysis of the monthly and annual precipitation shows that the model can capture the leading PC in most cases. To study the time evolution of the monthly data the nonstandard REOF is used. In order to see the trend more clearly the eigenvector series are smoothed using a one year moving average process. For the first and second PCs of the observation and simulation data the evolution of the precipitation over Ireland shows two major patterns.

In the first PC the high precipitation center is located in the south and south-west of the country (Figures 4.7a and 4.7c), with good agreement between the simulation and observation data although the simulation data tend to have more precipitation over the country on average. The simulation values are a little weaker than the ones from the observations in the south-western rainfall maximum, while in the midlands, the simulated rainfall is a little stronger.

Before 1975, the precipitation amount of the first PC is relatively small, except for a few peak values (Figure 4.8a). After 1975, the precipitation amount from this PC is generally higher than before 1975 and shows a pronounced decadal variability. The first PC explains 43.3% and 42.4% of the variance for the observation and simulation data, respectively. Because the area of the midlands, where the precipitation is slightly overestimated, is larger than the area of the slightly underestimated precipitation maximum in the south-west (Figures 4.7a and 4.7b), the simulated data eigenvector is stronger compared with the observation analysis for the whole time period.

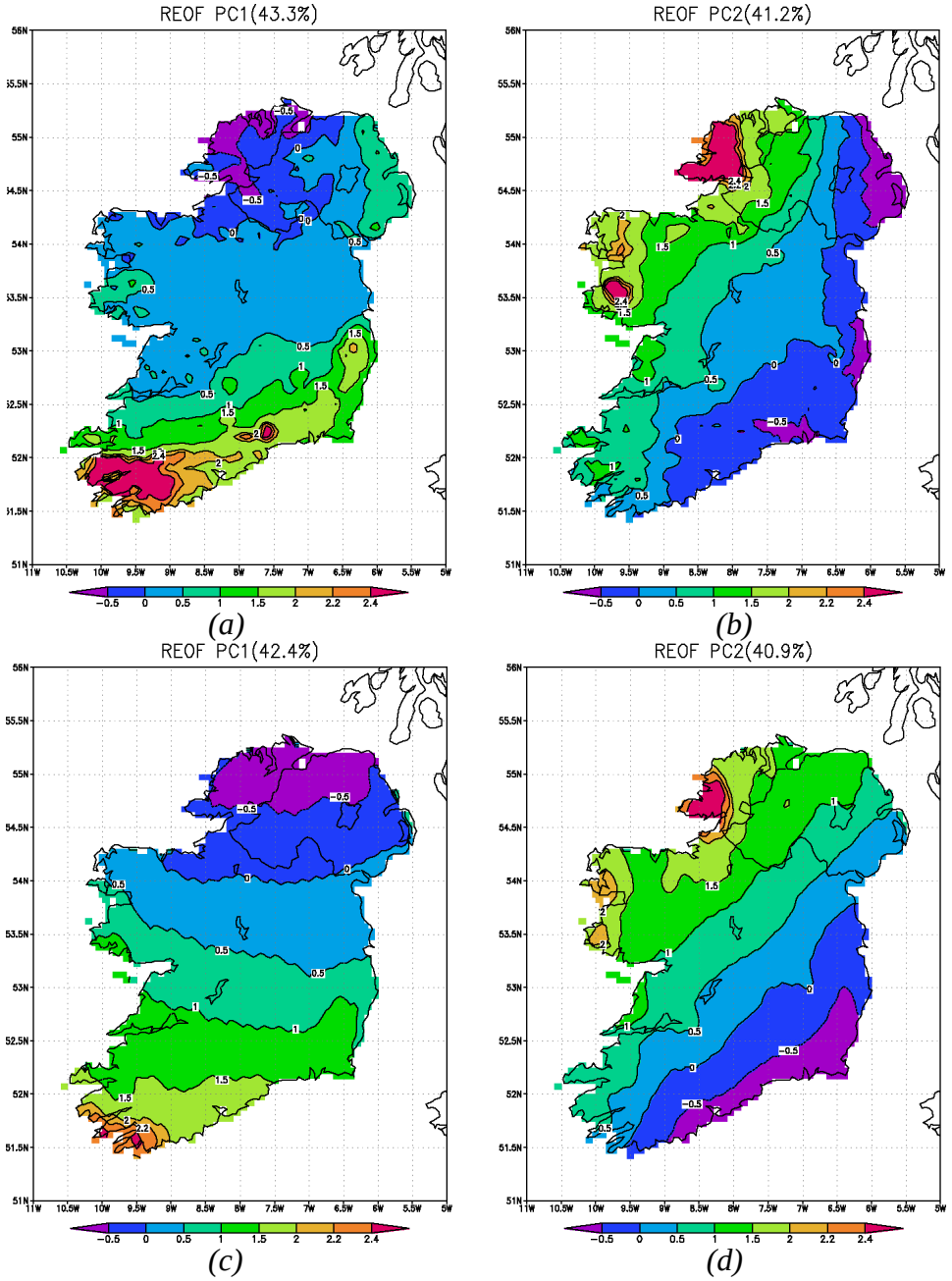

Figure 4.7: The first and second PC of observation (a,b) and simulation (c,d) for 1961-2000

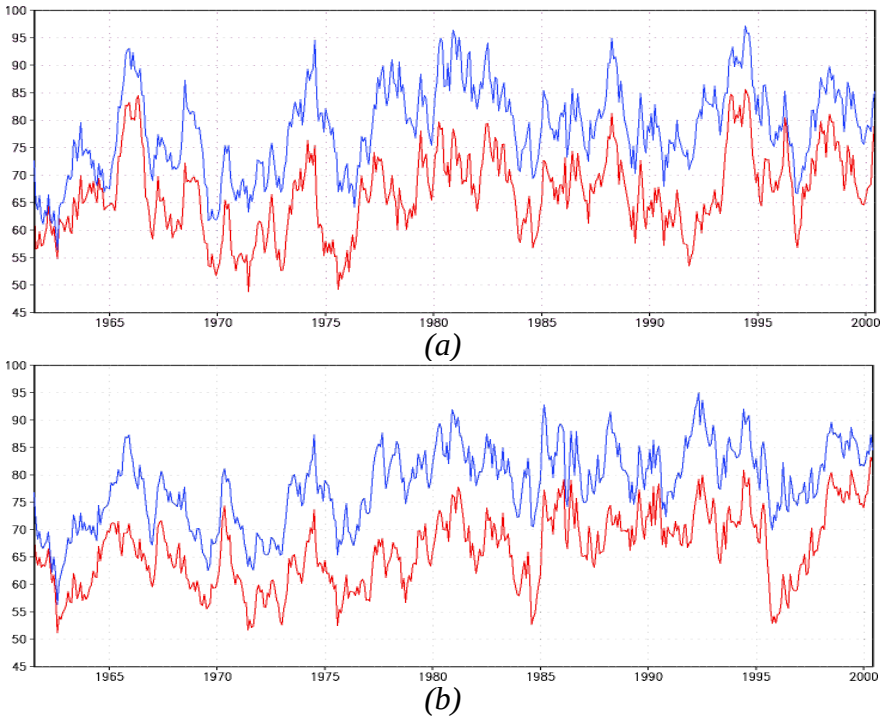

Figure 4.8: The first (a) and second (b) eigenvector of observed (red) and simulated (blue) precipitation (one year moving average) in mm/month

The second pattern explains 41.2% and 40.9% of the variance for the observation and simulation data respectively, with the precipitation maxima located in the west and north-west of the country (Figures 4.7b and 4.7d). In general the simulation data show the same deficiencies as in the first pattern: the simulated precipitation maxima are less pronounced than in the observation analysis. However, the time evolution of the second pattern is different from the first pattern (Figure 4.8b). Before 1975 it is still similar, while after 1975 the time series shows a stable increasing trend in the observation and simulation analysis.

Because the first two PCs that explain more than 80% of the variance show comparably low values for the time period before 1975, the precipitation is comparably low in this time period over the whole country. The increase in the average intensity as well as in the variability of the first PC with its precipitation maximum in the south-west after 1975 is consistent with Kiely's (1999) research. According to the second PC the precipitation shows a gradual increase in the west and north-west after 1975.

A more detailed frequency analysis of the first two eigenvectors would shed further light on the time evolution of the two major precipitation patterns. Unfortunately, the unsmoothed data (not shown) are very noisy and therefore a maximum entropy method (MEM) was used to identify the dominant frequencies. Here the singular spectrum analysis method (SSA) was used to analyze the original series. The 4 leading oscillatory components were used to reconstruct the time series, providing a smoothed series that can be used to identify trends in the precipitation (Ghil, 2000, Dettinger, 1995). Figure 4.9 shows the results of the MEM analysis of the reconstructed time series of the observations and the simulation. There are two major frequencies. One has a period of about 4 months, reflecting the

seasonal variation, while the other has a period of about one year. Both frequencies are detectable in the observation and simulation data. Although the spatial patterns are different between the first and second PC, the frequency analysis is similar. These two periods characterize quite well the evolution of precipitation over time.

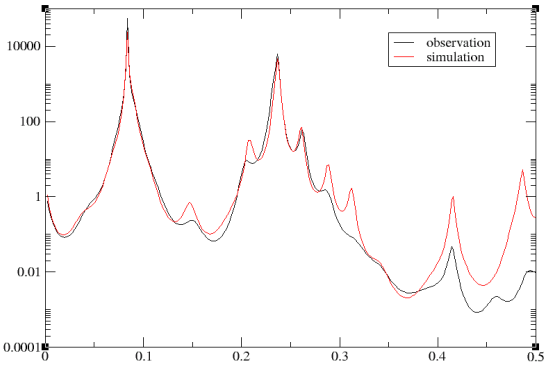

Figure 4.9: Results of the MEM analysis of the reconstructed first eigenvector series Abscissa: frequency (month^{-1})

Since the major spatial distribution shows two periods, the question is which period is dominant? To answer this question a wavelet analysis was used to study the same time series. Comparing the energy density evolution of the first PC, the annual period is strongest both for the observation (Figure 4.10a) and simulation data (Figure 4.10b), with the seasonal period energy relatively weak.

(a)

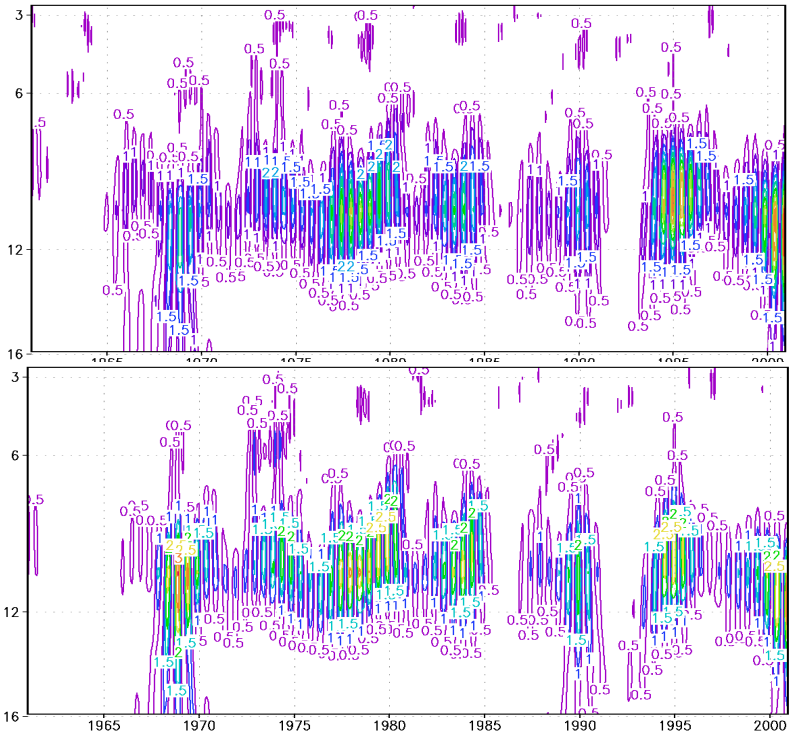

(b)

Figure 4.10: The energy density evolution of the first eigenvector from (a) observation and (b) simulation (ordinate: period in month)

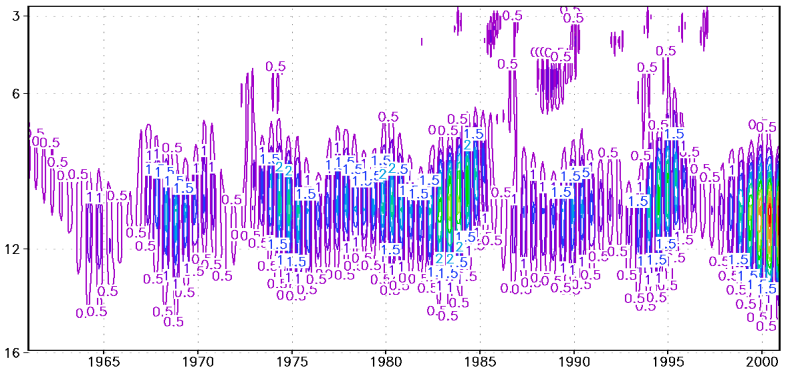

(a)

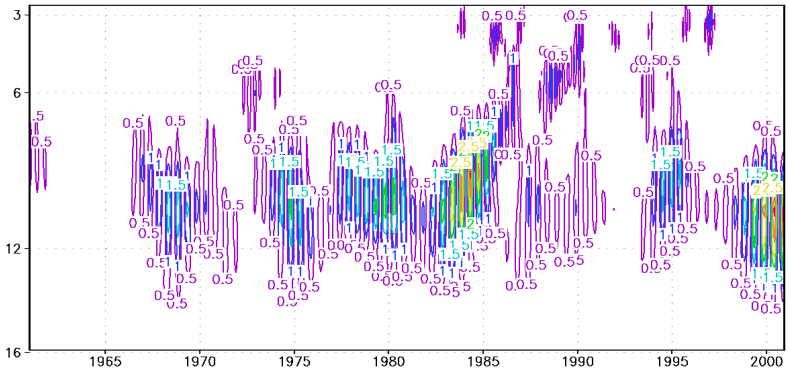

(b)

Figure 4.11: The energy density evolution of the second eigenvector from (a) observation and (b) simulation (ordinate: period in month)

Note that there is good agreement between the time evolutions for both sets of data. The dominant annual period is also evident in the energy density analysis of the second eigenvector (Figures 4.11a and 4.11b), but the time evolution is different. From about 1975, in contrast to the first eigenvector, there is a continuously strong energy density (Figure 4.11a) in the observation analysis, which is however not as continuous in the simulation analysis.

4.4 Discussion and conclusions

The REOF method was used to analyse the annual and interannual variability of the precipitation patterns over Ireland as simulated by a high resolution regional climate model.

Although the precipitation does not show a pronounced seasonal cycle, the local variation of the spatial distribution is very obvious. The annual and monthly precipitation analysis results show that the model can capture the leading spatial pattern in most months. However, the simulation shows a stronger signal in the leading PC and tends to have a less pronounced seasonal cycle compared to the observations. The transit from the wet winter to the dry summer season and from the dry to the wet season is too slow in the model simulation. In summertime the precipitation amounts are overestimated in our simulation (Figure 4.12). The orographically induced precipitation maxima are underestimated in the simulation, while the precipitation in the Irish Midlands is overestimated.

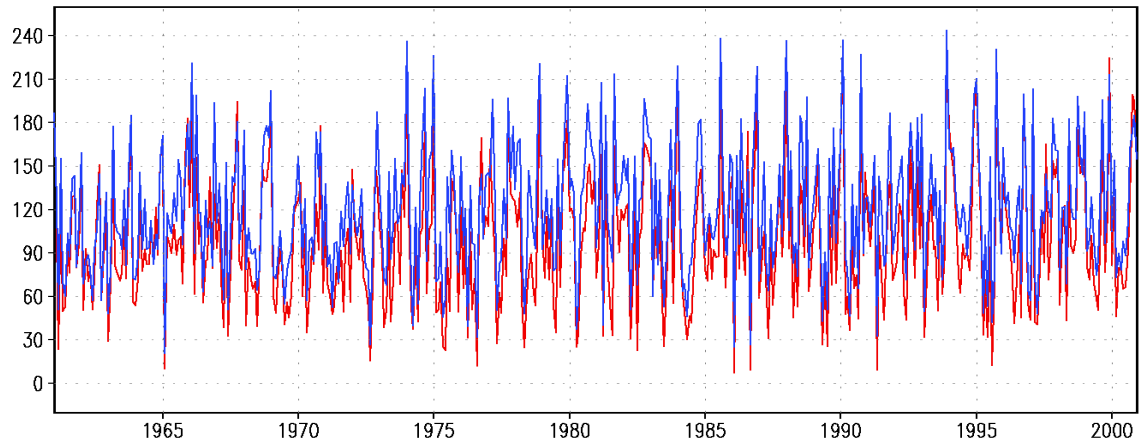

Figure 4.12: Observed (red) and simulated (blue) average rainfall over Ireland in mm/month

The time evolution of the leading spatial patterns of the original rainfall analysis shows two major patterns of the precipitation distribution for Ireland. In one pattern, the precipitation maximum is located in the south-west of Ireland. The evolution of this pattern shows a strong decadal variability, which is very well simulated by the model. The time evolution of the second pattern, linked to precipitation maxima in the west and north-west of Ireland, shows a strong continuously increasing trend, even if the simulation slightly underestimates this trend. Both of the patterns have a seasonal and an annual period. The wavelet energy density analysis shows that the annual period is dominant.

References

Boyle JS. 1998. Evaluation of the annual cycle of precipitation over the United States in GCMs: AMIP simulations. *Journal of Climate* **11**: 1041-1055

Chen GTJ, Jiang ZH, Wu MC. 2003. Spring heavy rain events in Taiwan during warm episodes and the associated large-scale conditions. *Monthly Weather Review* **131**: 1173-1188

Davies JR, Kelly MP, Osborn T. 1997. Explaining the climate of British Isles. In *climates of British Isles: Present, Past and Future.* Hulme M,Barrow E(eds). Springer: Berlin: 386-406

Dettinger MD, Ghil M., Strong CM, Weibel W., and Yiou P., 1995: Software expedites singular-spectrum analysis of noisy time series. *Eos, Trans. American Geophysical Union* 76(2): 12, 14, 21

Ghil M., Allen MR., Dettinger MD, Ide K., Kondrashov D., Mann ME, Robertson AW, Saunders A, Tian Y, Varadi F., Yiou P. 2002. Advanced special methods for climatic time series, *Review of Geophysics* **40(1)**: 1-41

Gutowski J. R., Decker S. G., Donavon R. A., Pan Z. T., Arritt R. W., Takle E. S. 2003. Temporal-spatial scales of observed and simulated precipitation in central U.S. climate. *Journal of Climate* **16**: 3841-3847

Hurrell JW. 1995. Decadal trends in the North Atlantic Oscillation: Regional temperature and precipitation. *Science* 269: 676-679

Horel JD. 1981. A rotated principal component analysis of the interannual variability of the Northern Hemisphere 500-mb height field. *Monthly Weather Review* **109**: 2080-2092

Houghton JT, Ding Y, Griggs G, Noguet M, Van der Linden P, Dai X, Maskell K, Johnson CA (eds). 2001. IPCC 2001: Climate change 2001: The scientific basis. Cambridge: Cambridge University press.

Jolliffe IT. 1987. Rotation of principal component: some comments. Journal of Climatology **7**: 507-510

Jones C. 2001: A brief description of RCA2, SWECLIM Newsletter **11**: 9-14

Kawamura R.1994. A rotated EOF analysis of global sear surface temperature variability with interannual and interdecadal scales. Journal of Physical Oceanography 24:707-715

Keane T, Collins JF. 2004, *climate,weather and Irish agriculture:* 27-62

Kiely G, Albertson JD., Parlange MB. 1998. Recent trends in diurnal variation of precipitation at Valentia on the west coast of Ireland. *Journal of Hydrology* 207: 270-279

Kiely G. 1999. Climate change in Ireland from precipitation and streamflow observation. *Advances in Water Resources* 23: 141-151

Logue JJ. 1984. Regional variation in the annual cycle of rainfall in Ireland as revealed by principal component analysis. *Journal of climatology* 4: 597-607

McElwain L, Sweeney J. 2003. Climate change in Ireland-recent trends in temperature and precipitation. *Irish Geography* 36: 97-111

Moses T, Kiladis GN, Diaz HF, Barry RG. 1987. Characteristics and frequency of reversals in mean sea level pressure in the North Atlantic sector and their relationship to long-term temperature trends. *Journal of climatology* 7:13-30

Namias J. 1964. Seasonal persistence and recurrence of European blocking druing 1958-160. *Tellus* 16: 394-407

Rex DF. 1951. The effect of Atlantic blocking action upon European climate. *Tellus* 3: 100-112

Richman MB. 1986. Rotation of principal component. *Journal of Climatology* 6: 293-335

Richman MB. 1987. Rotation of principal component: a reply. *Journal of Climatology* 7: 511-520

Rogers JC. 1985. Atmospheric circulation changes associated with the warming over the northern North Atlantic in the 1920s. *Journal of climate and applied meteorology* 24: 1303-1310

Termoni P. 2003. Monitoring and improving the temporal interpolation of lateral-boundary coupling data for a limited-area model. *Monthly Weather Review* 131: 2450-2463

Torrence C., Compo GP. 1998. A practical guide to wavelet analysis. *Bulletin of the American Meteorological Society* 79(1): 61-78

Wilby RC, O'Hare G, Barnsley N. 1997. The North Atlantic Oscillation and British Isles climate variability,1865-1996. *Weather* 52: 266-27

5 Simulation of future climate: 2021-2060

Projections for the future Irish climate were generated by downscaling the ECHAM4 GCM data using the RCA model. Simulations were run for a reference period 1961-2000 and a future period 2021-2060; differences between the periods provide a measure of expected climate change.

Results show a general warming in the future climate with mean monthly temperatures increasing typically between 1.25 and 1.5 degrees. The largest increases are seen in the south-east and east, with the greatest warming occurring in July. For precipitation the most significant changes occur in the months of June and December. June values show a decrease of about 10%, noticeably in the southern half of the country. March, July and August are largely unchanged but all other months show overall increases. December values show increases ranging between 10% in the south-east and 25% in the north-west. There is also some evidence of an increase in the frequency of extreme precipitation events (20 mm or more per day) in the north-west. For cloud cover and short-wave radiation the signals are more mixed with no obvious trends in the future. However, the results need to be treated cautiously as the ECHAM4 model has a static aerosol representation and the RCA downscaling does not capture the decreasing trend in short-wave radiation, possibly linked to increasing aerosol concentrations, seen in the past climate at stations such as Valentia.

5.1 Introduction

There are several GCM datasets that can be used to drive the RCA to produce projections for the future Irish climate. None can be regarded as definitive as even with perfect models there is considerable uncertainty regarding the concentrations of future greenhouse gases (GHG) that are implicated in climate change; these are subject to social and political influences that can only be modeled on a "scenario" basis. In reality all of the GCM models have flaws that compound the uncertainty. Nevertheless, for the same GHG scenario there is reasonable agreement between different GCM simulations up to about mid century (see Houghton *et al.* 2001). This provides the justification for this study. The results should be treated with caution as they are based on the data from a single GCM. Ideally, we should downscale the data from several GCMs, using an "ensemble" approach to quantify the uncertainty. The current study should be seen as a first step along this path.

Simulation data from the Max Planck Institute ECHAM4/OPYC3 coupled atmosphere-ocean general circulation model (Roeckner *et al.* 1996) were chosen to drive the RCA. This transient simulation, extending from 1860 to 2100, used observed GHG concentrations up to 1990 and the "SRES-B2" scenario for the future (i.e. moderately increasing GHG concentrations; see http://www.grida.no/climate/ipcc/emission/095.htm for details). It is important to note that the GCM simulation was not linked to any meteorological observations in simulating the past climate; snapshots of the weather on particular days in the past will have little in common with the observed weather but averaged over seasons they should be in agreement. In practice the agreement is not perfect, particularly at a regional level (see section 5.2), and for downscaling with the RCA model it is essential to generate a reference simulation, linked with the current and past climate, that can be used to assess the future simulation. The reference run (RCA-P) was chosen to cover the 40-year period 1961-2000[1] while the future run (RCA-F) covered the period 2021-2060. Differences between the two runs give a

[1] 1961-1990 is the official WMO climate reference period. We use a longer period to aid comparison with the future period.

measure of the expected change in the Irish climate.

Only the main results are presented here; further information can be found on the C4I web site http://www.c4i.ie.

5.2 Results

5.2.1 Mean sea level pressure (MSLP)

Figure 5.1 shows the MSLP field averaged over the 40-year integration period from 1961 to 2000. Differences between RCA-P and ERA-40 (Figure 5.1c) show that the ECHAM4-driven model produces a slightly stronger gradient across Ireland, resulting in a stronger westerly airflow compared with the observation-based ERA-40 data.

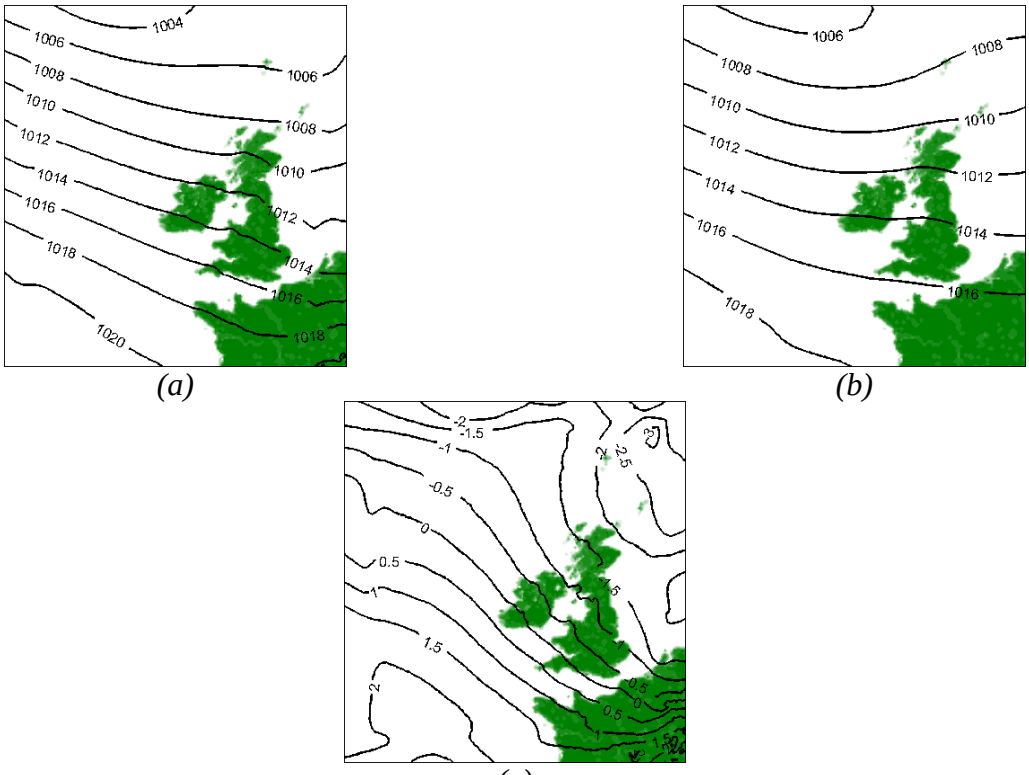

Figure 5.1: Average MSLP 1961-2000 in hPa, (a) RCA-P, (b) ERA-40, (c) RCA-P minus ERA-40.

Plots of the mean differences between RCA-P and RCA-F are shown in Figure 5.2. The differences are small but in the future period the mean pressure is slightly lower over the whole model domain – this is also reflected in the difference plot where all values are negative. The pressure gradient is slightly increased, particularly in the north of the model domain. Further discussion of the MSLP can be found in Section 8.

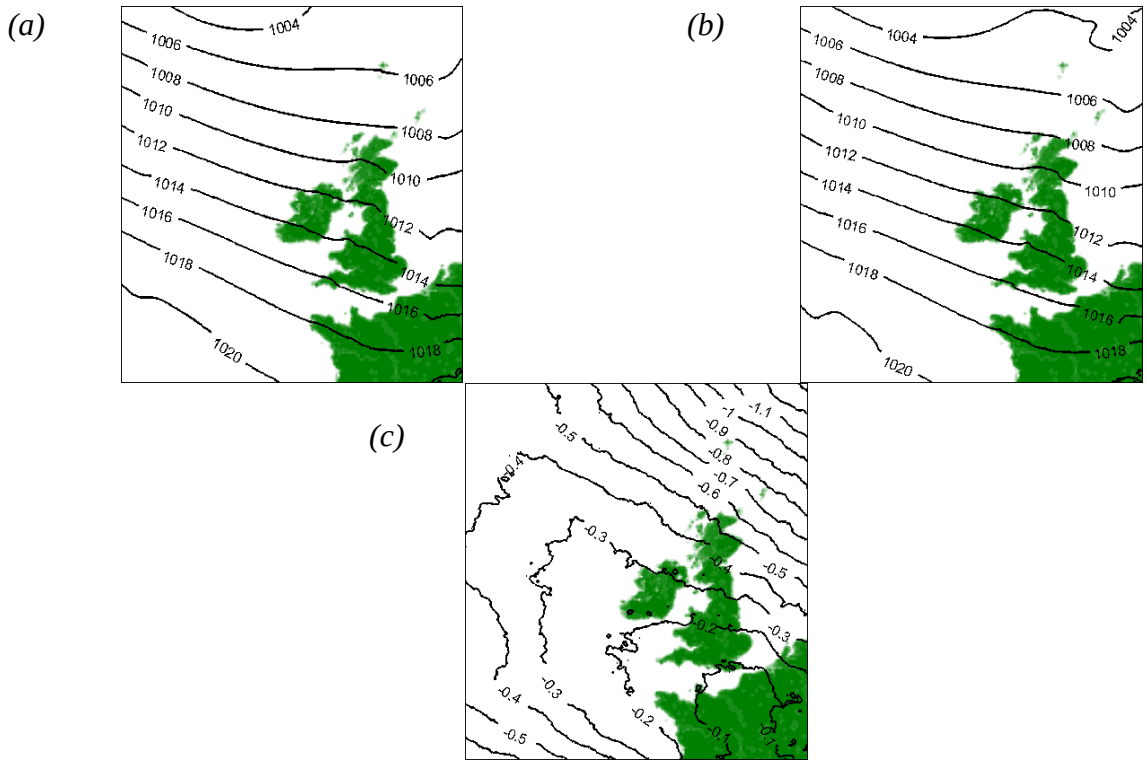

Figure 5.2: Average MSLP in hPa for ECHAM-driven RCA: (a) RCA-P, (b) RCA-F and (c) (RCA-F) – (RCA-P)

5.2.2 2-metre Temperature

Figure 5.3 shows the January and July average monthly 2-metre temperature over Ireland for 1961-2000 and differences relative to the observation-based UKCIP dataset. In general the RCA-P data are too warm: January temperatures are about 1.5º C above observations and while the July data are in better agreement, there is still a warm bias in many areas. In addition, the annual variability is not as large as observed.

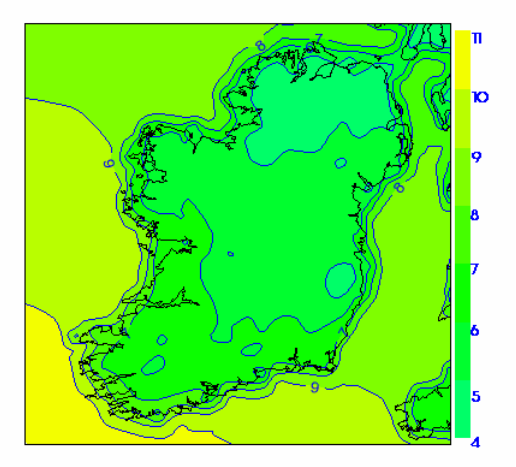

(a) January RCA-P

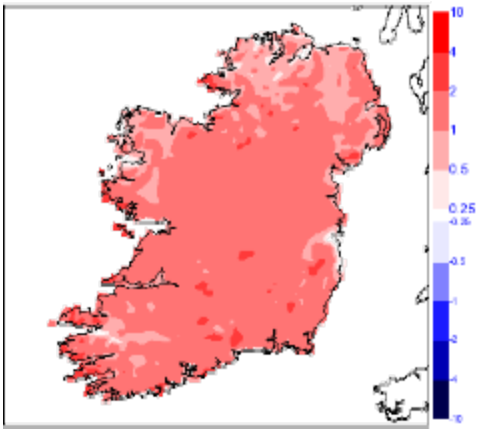

(b) January RCA-P minus January UKCIP

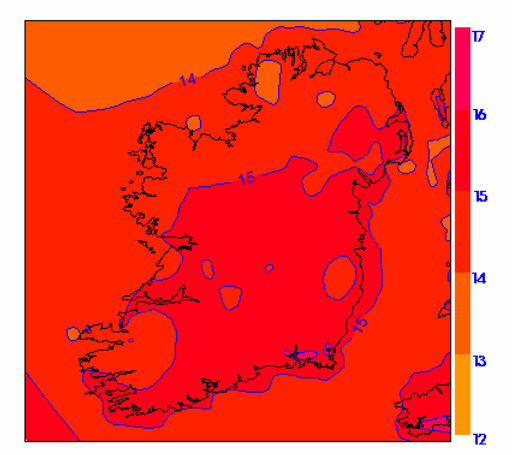

(c) July RCA-P

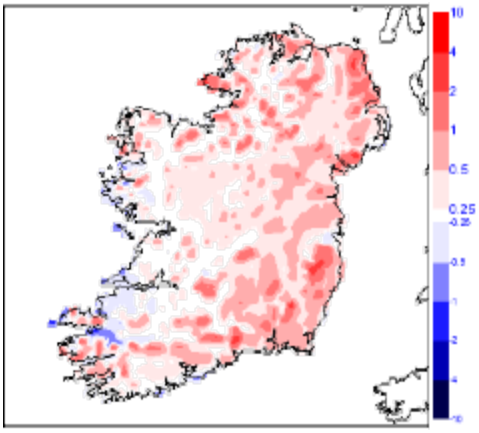

(d) July RCA-P minus July UKCIP

Figure 5.3: January and July monthly average 2-metre temperature for 1961-2000

The results reflect poorly on the ability of the ECHAM4 data to capture the essential features of the Irish climate. However, the importance of the simulations is not in reproducing the present climate, but rather in providing a reference dataset for evaluating trends in the future climate.

Figure 5.4 compares the past (1961-2000) and future (2021-2060) ECHAM4-driven simulations. It can be seen that the average January temperatures over Ireland have increased between these two periods by about 1.25º (Figure 5.4b), with the largest increase in the south-east and east. The average July temperatures have increased even more, by about 1.50ºC (Figure 5.4d), again with the largest increase in the south and south-east.

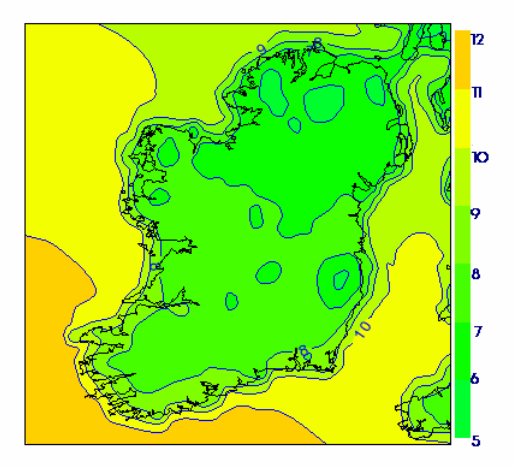

(a) January RCA-F

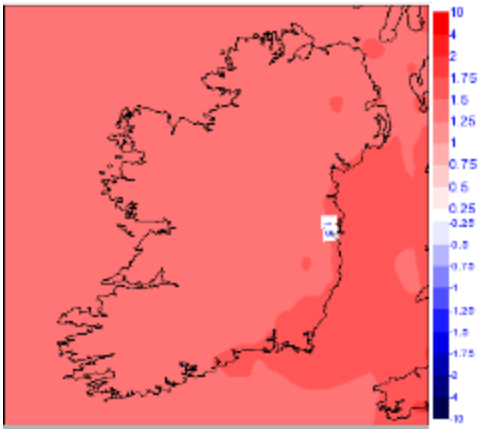

(b) January RCA-F minus January RCA-P

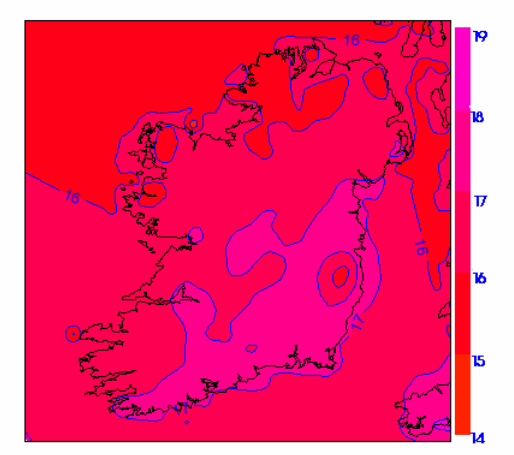

(c) July RCA-F

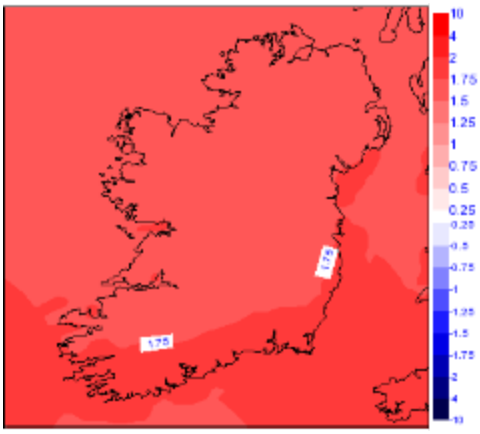

d) July RCA-F minus July RCA-P

Figure 5.4: January and July monthly average 2-metre temperature for 2021-2060, and differences with RCA-P (1961-2000)

The yearly 2-metre temperature time-series for Valentia is shown in Figure 5.5. The RCA-P results (purple) show good inter-annual variability, but fail to reproduce the observed temperatures (blue) during the cooler 1980s. The change in temperatures between RCA-P and RCA-F (shown in red) is clearly visible, with an increase of about 1°C at the start of the future period rising to about 2°C by the 2050s. The inter-annual variability still exists, although almost all temperatures are warmer than those for the present climate.

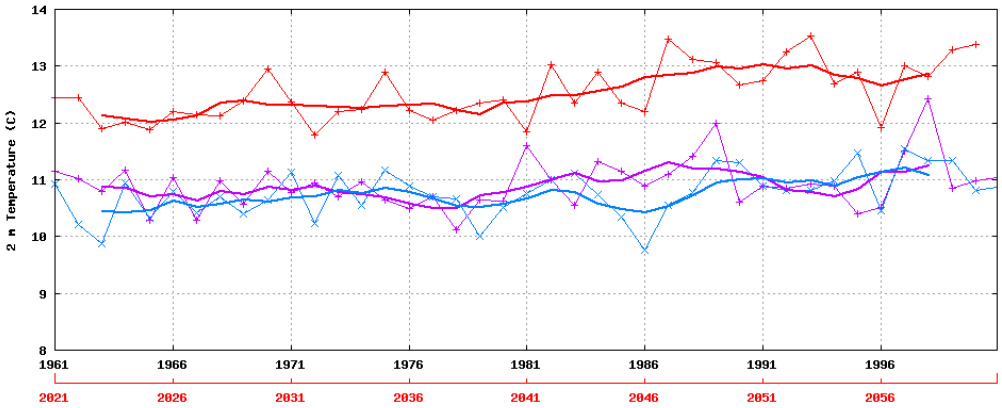

*Figure 5.5: Yearly 2-metre temperature time-series Valentia observatory. 1961-2000 Observed (blue), 1961-2000 RCA-P (purple), 2021-2060 RCA-F (red), 5-year running averages in **bold**.*

5.2.3 Radiation and Cloud Cover

Figure 5.6 shows the yearly time-series of the short-wave radiation at Valentia. Observations are plotted in blue, RCA-P in purple, RCA-F in red, and with 5-year running averages plotted in bold. The observations show a trend of decreasing short-wave radiation incident at the surface over the period 1961-2000. RCA-P produces more short-wave radiation than observed, and does not show any overall trend during the simulation period. Similarly, the RCA-F plot shows no significant trend in the data. Failure to capture the trend could be attributed to the fact that the ECHAM4 model has static aerosol concentrations; the "global dimming" effect, which is probably linked to increasing concentrations of aerosols and a consequent reduction in radiation reaching the surface of the earth, is not taken into account (see also section 3.3.2).

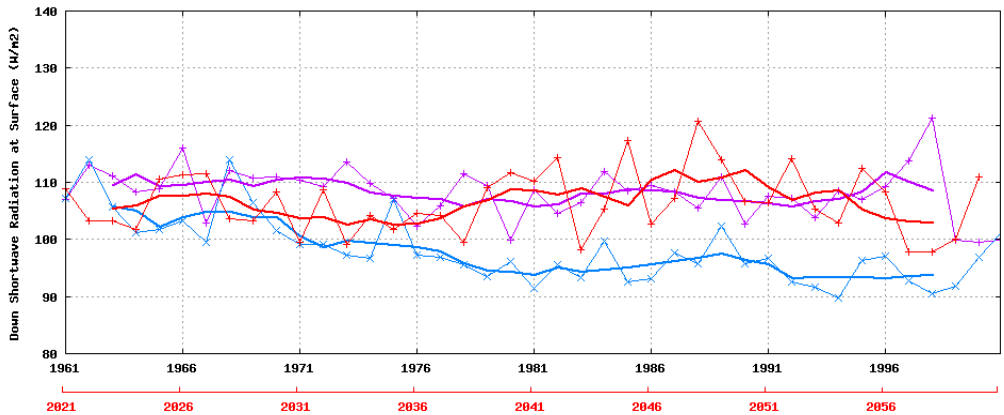

*Figure 5.6: Yearly time-series of short-wave radiation at Valentia observatory. 1961-2000 Observed (blue), 1961-2000 RCA-P (purple), 2021-2060 RCA-F (red), 5-year running averages in **bold**.*

Although there are no strong long-term trends in the simulated short-wave radiation at Valentia, there are some inter-annual differences that could be due to changes in cloud cover. Plots of the yearly mean cloud (Figure 5.7) and relative changes between the RCA-F (red) and RCA-P (purple) data show some correlation with the short-wave radiation plots (Figure 5.6).

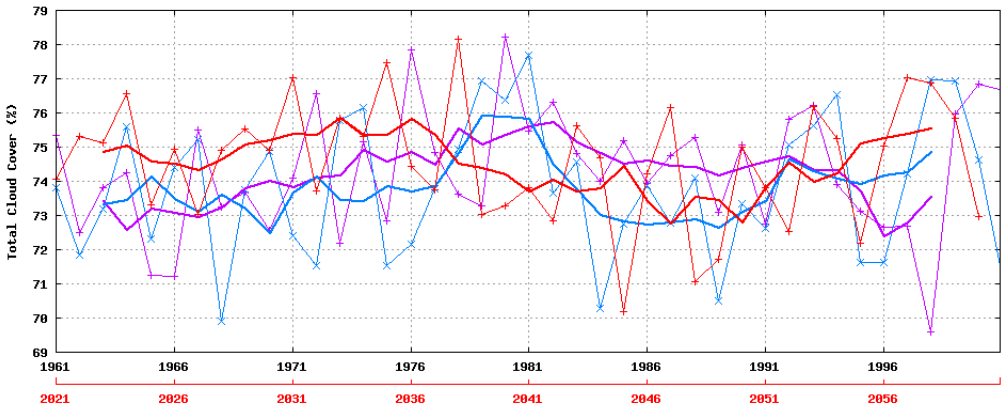

Figure 5.7: Yearly time-series of cloud cover at Valentia observatory. 1961-2000 Observed (blue), 1961-2000 RCA-P (purple), 2021-2060 RCA-F (red), 5-year running averages in ***bold****.*

5.2.4 Precipitation

June and December show the largest changes in average monthly precipitation between RCA-P and RCA-F, as shown in Figure 5.8. Over most of the southern half of the country, as well as in mountainous areas in the west and north, the June monthly rainfall amounts in the future simulation are over 10% lower than those in the 1961-2000 reference period. It is the only month which is significantly drier compared to the reference period. March, July and August are largely unchanged but all other months show overall increases in precipitation. December shows the largest increase with changes ranging from around 10% in the south-east, to 25% in the north-west (Figure 5.8d).

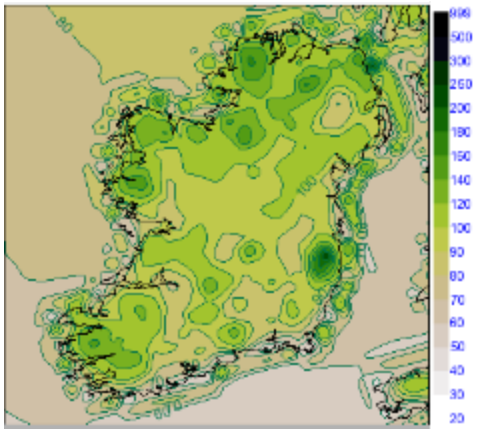

(a) June RCA-F

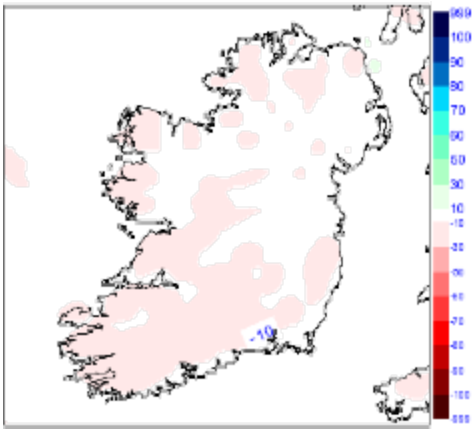

(b) June RCA-F minus June RCA-P

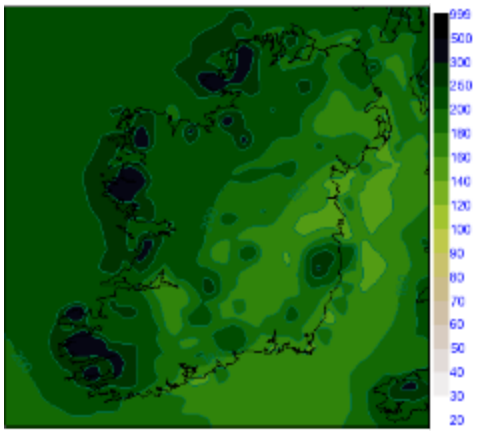

(c) December RCA-F

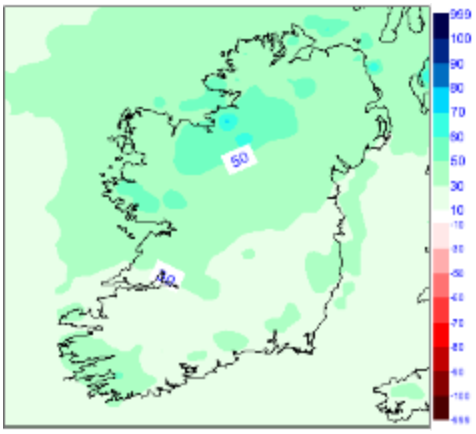

(d) December RCA-F minus December RCA-P

Figure 5.8: June and December monthly rainfall accumulation for 2021-2060, and differences with RCA-P (1961-2000)

The yearly rainfall time-series for Belmullet is shown in Figure 5.9. The RCA-P simulation (purple) produces higher rainfall values than those observed (blue), showing that the ECHAM4 climate for the period 1961-2000 is too wet. The precipitation results for the RCA-F period (red) show an increase in rainfall amounts for most years compared to the RCA-P reference simulation. With 5-year running average values RCA-F shows higher rainfall amounts for almost all years compared with RCA-P. The variability in the trend of the future precipitation is not as large as that for RCA-P, showing that higher annual rainfall amounts occur more consistently in the future than in the present climate.

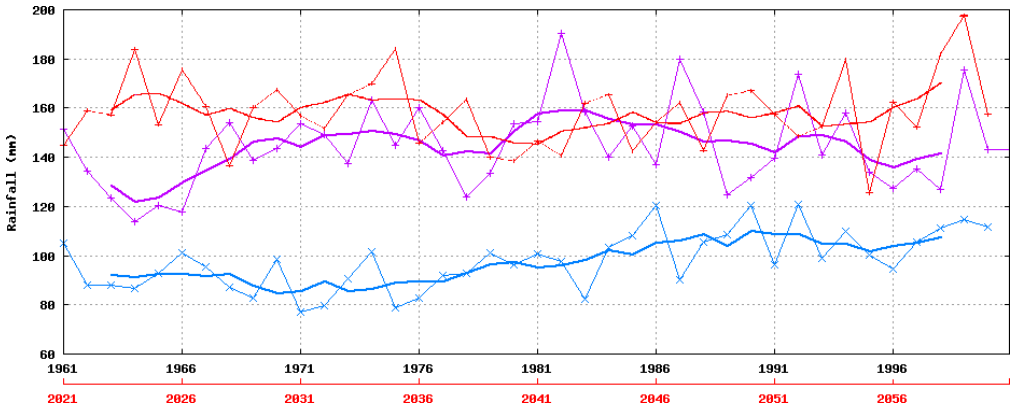

*Figure 5.9: Yearly rainfall time-series for Belmullet. 1961-2000 Observed (blue), 1961-2000 RCA-P (purple), 2021-2060 RCA-F (red), 5-year running averages in **bold**.*

The number of dry days per year (< 0.2 mm) for Belmullet is shown in Figure 5.10a. As in the case of the validation run (Section 3) the model produces small amounts of rain too frequently, resulting in fewer dry days. Compared with the reference period the number of dry days in the future simulation is similar.

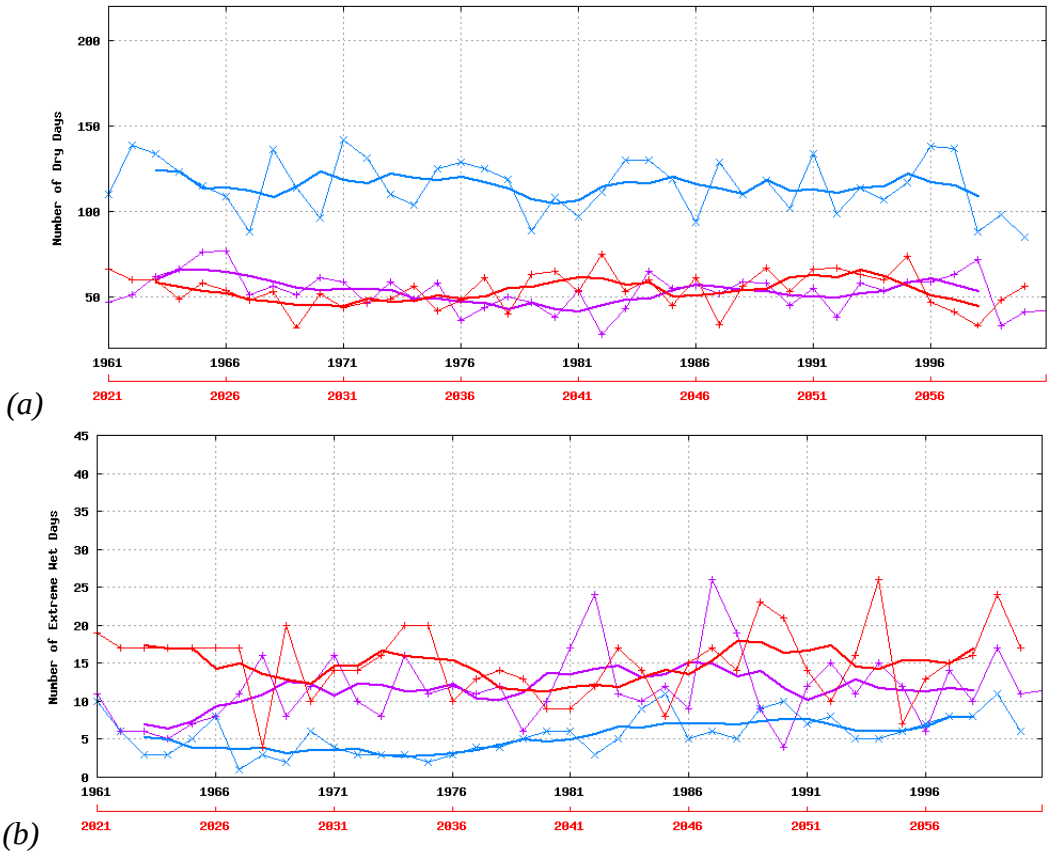

*Figure 5.10: Yearly time-series for Belmullet: (a) number of dry days (< 0.2 mm), (b) number of heavy rainfall days (> 20.0 mm). Observed (blue), RCA-P (purple), RCA-F (red), 5-year running average in **bold**.*

The frequency of heavy precipitation (> 20 mm) days per year is shown for Belmullet in Figure 5.10b. For the reference period the model over-predicts the frequency of such events. This is quite likely related to the more pronounced westerly flow in the ECHAM4 data which may give rise to a moister atmosphere with increased precipitation. The average number of heavy rainfall days seems to have increased in the RCA-F results although both periods remain within the range of 4 to 26 days per year.

5.2.5 10-metre wind

Analysis of the 10-metre winds revealed a deficiency in the model post-processing of the winds. Winds are currently being recalculated using winds from the lowest model levels. Results for the ECHAM4 simulations will be made available on the C4I web site http://www.c4i.ie.

5.3 Conclusions

Projections for the future Irish climate have been generated using the RCA model to downscale ECHAM4 GCM data. Simulations were run for a reference period 1961-2000 and a future period 2021-2060; differences between the periods provide a measure of expected climate change.

Results show a general warming in the future climate with mean monthly temperatures increasing typically between 1.25 and 1.5 degrees. The largest increases are seen in the south-east and east, with the greatest warming occurring in July. For precipitation the most significant changes occur in the months of June and December. June values show a decrease of about 10%, noticeably in the southern half of the country. March, July and August are largely unchanged but all other months show overall increases. December values show increases ranging between 10% in the south-east and 25% in the north-west. There is also some evidence of an increase in the frequency of extreme precipitation events (20 mm or more per day) in the north-west. For cloud cover and short-wave radiation the signals are more mixed with no obvious trends in the future. However, the results need to be treated cautiously as the ECHAM4 model has a static aerosol representation and the RCA downscaling does not capture the decreasing trend in short-wave radiation, possibly linked to increasing aerosol concentrations, seen in the past climate at stations such as Valentia.

References

Houghton JT, Ding Y, Griggs DJ, Noguer M, van der Linden PJ, Dai X, Maskell K, Johnson CA Eds. 2001: Climate Change 2001: The Scientific Basis. Cambridge University Press, 881 pp.

Roeckner E, Arpe K, Bengsson L, Christoph M, Claussen M, Duemenil L, Esch M, Giorgetta M, Schlese U, Schulzweida U. 1996. The Atmospheric General Circulation Model ECHAM-4: Model Description and Simulation of Present-Day-Climate. Max-Planck Institute for Meteorology, Report No. **218**, Hamburg, Germany, 90 pp.

6 The impact of climate change on river flooding under different climate scenarios

Application of the HBV model to the Suir catchment area shows that the hydrological model is capable of capturing the local variability of river discharge with reasonable accuracy when driven by observations (calibration) or high resolution ERA-40 driven RCA simulation output (validation). In both cases the same model parameters were used in the HBV model.

Using ECHAM4 driven RCA simulation data for the future period (2021-2060) the hydrological model shows a significant increase in the more intense discharge episodes, a pattern that is also shown in the return values of extreme discharge.

6.1 Introduction

The IPCC has stated that mean surface temperatures may rise 0.3-0.6°C per decade in the 21th century (Houghton, 2001). As increased temperatures will lead to greater amounts of water vapour in the atmosphere and an accelerated global water cycle, it is reasonable to expect that river catchment areas will be exposed to a greater risk of flooding. While many impact studies have already been carried out to assess such risks in other countries (Bergstrom, 2001, Pilling, 2002, Arnel, 2003), this study examines the risks for Ireland using the Suir catchment area as a test case.

The Land Surface Parameterization (LSP) scheme is an important part of the RCA climate model; it acts as a bridge connecting the atmosphere and water cycle. Significant efforts have been made to improve the representation of the land surface-atmosphere interaction during the last two decades, particularly for the hydrological component. However, because of the different spatial resolutions of the climate and hydrological models, it is still difficult to couple the models directly. For the hydrological model, the most important processes in the context of climate change and river flooding are known to be precipitation and evapotranspiration. In this study, the precipitation values from different RCA simulations are used to drive the hydrological model in the Suir catchment area, while for evapotranspiration, the monthly mean climate values from Johnstown Castle are used as proxies in the catchment area.

6.1.1 HBV model

The HBV hydrological model of the Swedish Meteorological and Hydrological Institute (SMHI) is used in this study (Bergstrom 1995; Lindstrom 1996). The model is a semi-distributed, conceptual hydrological model using sub-basins as the primary hydrological units, taking into account area-elevation distribution and basic land-use categories (forest, open areas and lakes). The sub-basins option is used in geographically or climatologically heterogeneous basins or large lakes. The model handles snow accumulation and melt, soil moisture and runoff generation and includes a simple routing procedure. It has been widely used in Europe and other parts of the world in applications such as hydrological forecasting, water balance mapping and climate change studies.

6.1.2 Datasets

To investigate the influence of climate change on regional water resources and flooding, three global datasets were used to drive the RCA model. For the past climate (1961-2000), ERA-40 and ECHAM4 data were used, while for the future climate simulation (2021-2060) the model was driven by ECHAM4 data consistent with the SRES-B2 scenario. As the ERA-40 data are based on observations and are generally regarded as providing an accurate description of the atmosphere, they provide an excellent means for testing the performance of the climate model in a hydrological application. To consider the effect of the different boundary data on the future climate simulation run, the ECHAM4 past climate simulation was used as a control.

6.2 Results

6.2.1 Calibration

In the HBV model the parameters with the largest uncertainty are related to the soil moisture parameterization scheme. The main parameters are FC (maximum soil moisture storage in millimeters), LP (fraction of FC above which potential evapotranspiration occurs and below which evapotranspiration will be reduced) and the coefficient BETA (determining the relative contribution to runoff from a millimeter of precipitation at a given soil moisture deficit). These parameters are dependent on the properties of the catchment, such as the land-use type, the wilting point and soil porosity. Because of the uncertainty, the Monte Carlo Random Sampling (MCRS) method is popularly used for the parameter estimation. However, as the HBV program source code is not available, the above method is difficult to apply. In order to overcome this obstacle, quasi-stratified sampling in the form of Latin Hypercube Sampling (McKay, 1979) was used. In this method, the limited sampling numbers can produce similar results to the Monte Carlo approach (Yu, 2001).

For the calibration of Suir catchment run, observed precipitation data for the period January 1960 to December 1964 and monthly mean climate evapotranspiration data were used to drive the HBV model. The actual catchment area and rainfall stations are shown in Figure 6.1. Note that the calibration period includes relatively dry and wet years. Although insufficient observation data coverage limited the duration of the calibration to 5 years, it should be sufficient according to the model documentation of SMHI, which recommends the use of 5-10 years of data. The performance of the model was judged using a modified R^2 statistical correlation measure, defined as follows.

$$R^2 = \frac{\left(\sum (QR - QR_{mean})^2 - \sum (QC - QR)^2\right)}{\sum (QR - QR_{mean})^2}$$

QC = computed discharge

QR = observed discharge

QR_{mean} = the mean of QR over the calibration period

For the calibration of Suir catchment data, the R^2 value (unity for perfect performance) was 0.787.

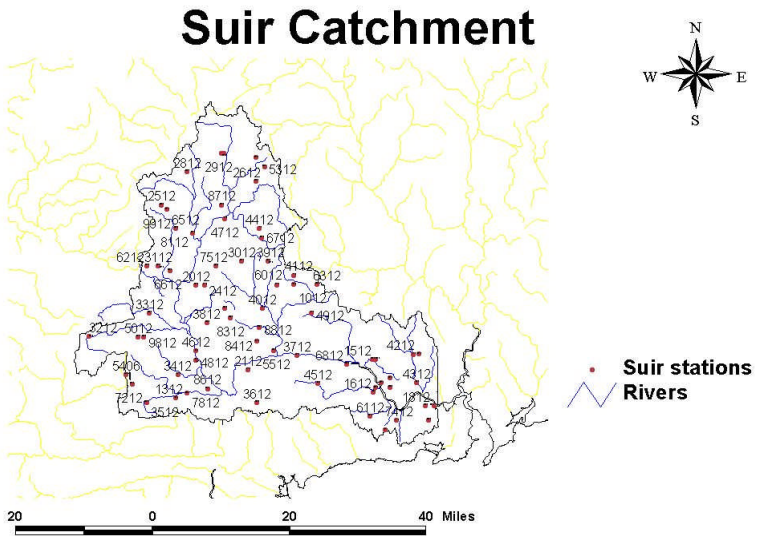

Figure 6.1 Suir catchment area and rainfall stations.

Figure 6.2 presents the calibration results. Except for the peak values, which are slightly underestimated, the variation in the simulated discharge coincides with the observed discharge fairly well.

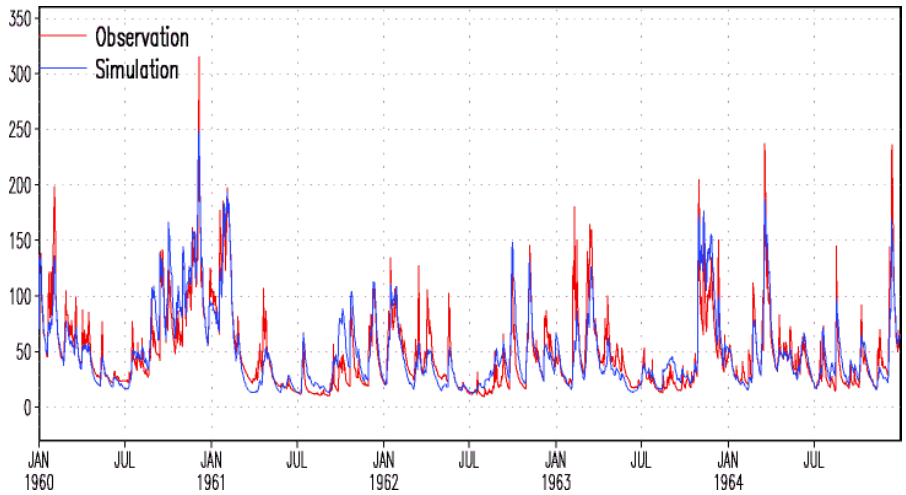

Figure 6.2: Observed and simulated (observed precipitation) discharge [m^3/s]

6.2.2 Validation

In the validation run the parameter values are kept the same as in the calibration, but simulations are repeated with independent input series from different present day simulation results. Results are shown in Figure 6.3. The evolution of the simulated discharge shows good agreement with observed data, similar to the calibration run and with peak values underestimated. On the whole, the simulation is a little worse compared to the calibration run with an R^2 value of only 0.545, while the correlation coefficient reaches 0.79. This confirms that the model simulates the evolution of the discharge well, whereas the underestimated peak values caused the R^2 value to be relatively low. Figure 6.4 shows the return values of the annual extremes of the observation and ERA-40 driven simulation. The distribution of return values for the different return periods show a good agreement, although they are systematically underestimated by 15-20%.

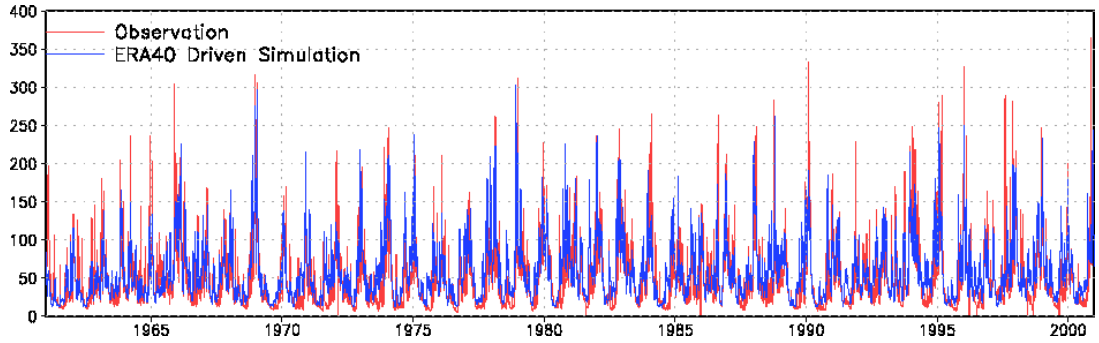

Figure 6.3: Observed and simulated (ERA40 driven simulation) discharge [m^3/s]

(a)

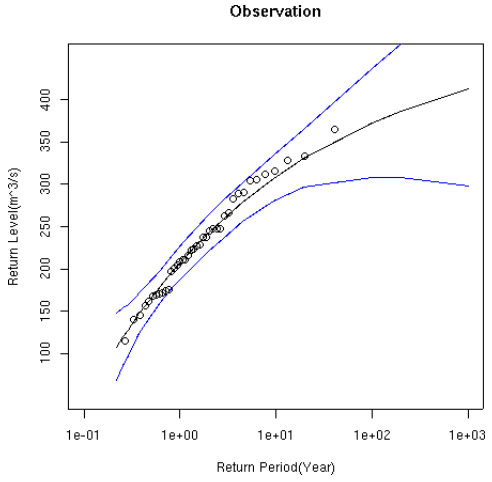

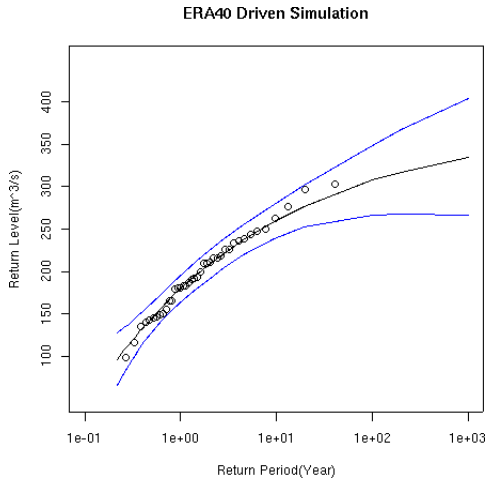

(b)

Figure 6.4: Return values of observed (a) and simulated (ERA-40 driven simulation) (b) maximum annual discharge

6.2.3 Future

Figure 6.5 shows the impact of climate change on the river discharge. For the past climate, the ECHAM4 driven control simulation slightly over-predicts the discharge compared to the observations

(Figure 6.5a), and the timing of peak events is slightly shifted. Although we cannot expect an exact agreement concerning the timing of peak events between observation and simulation because the ECHAM4 data are not based on atmospheric observations, the number of peak values is similar, which gives us confidence in the future projections. In the future run (Figure 6.5b), the frequency and intensity of heavy discharges (e.g. > 350 m^3s^{-1}) have clearly increased compared to the control run (Figure 6.5a). The return value analysis (Figure 6.6) also shows similar results with the 10-year return value increasing from about 290 m^3s^{-1} to 360 m^3s^{-1}. Figure 6.7 shows the effect of climate change on the annual cycle of the discharge: it remains unchanged in the dry season, but increases by up to 20% in December and January.

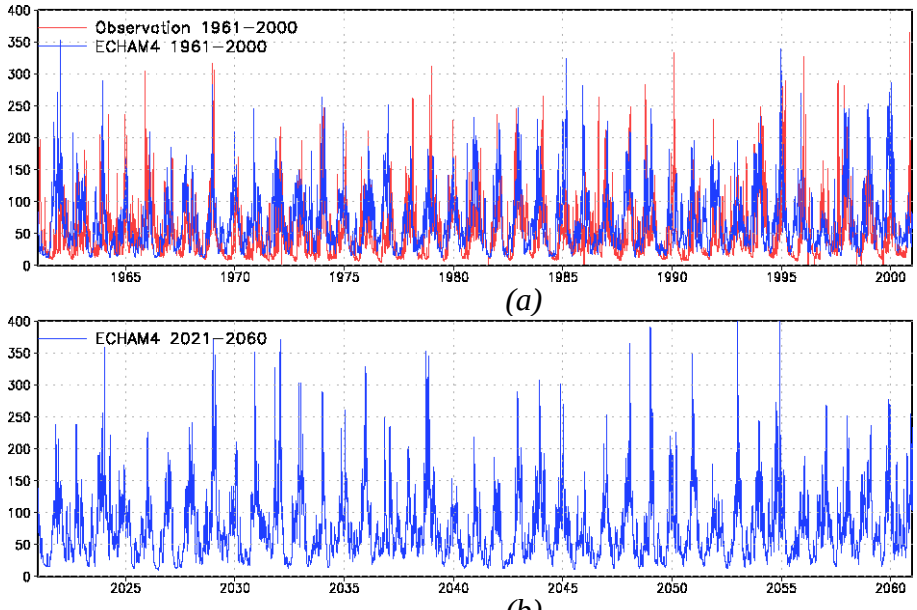

(a)

(b)

Figure 6.5: Simulated discharge using the ECHAM4 driven RCA simulation for the past and future climate and observed discharge [m^3s^{-1}]

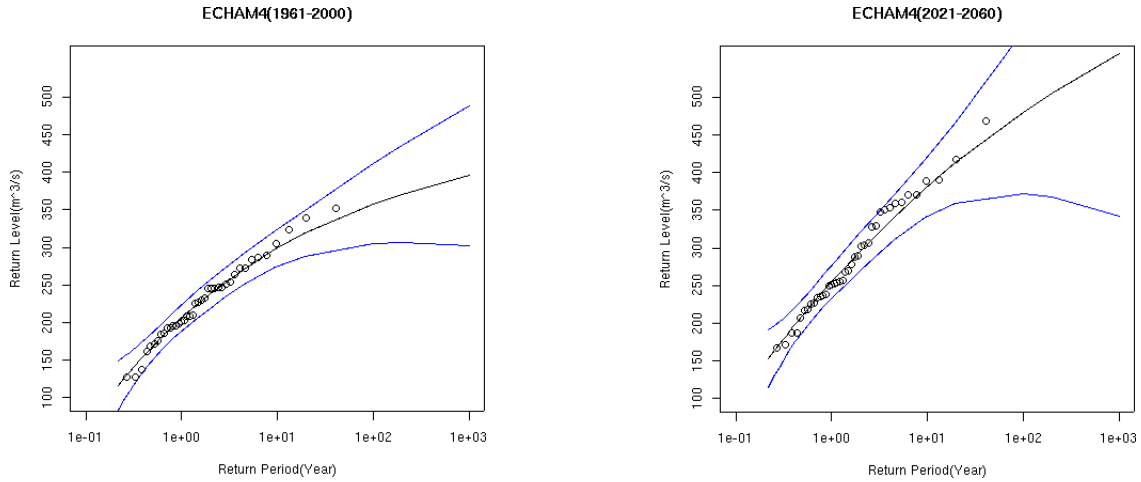

(a) (b)

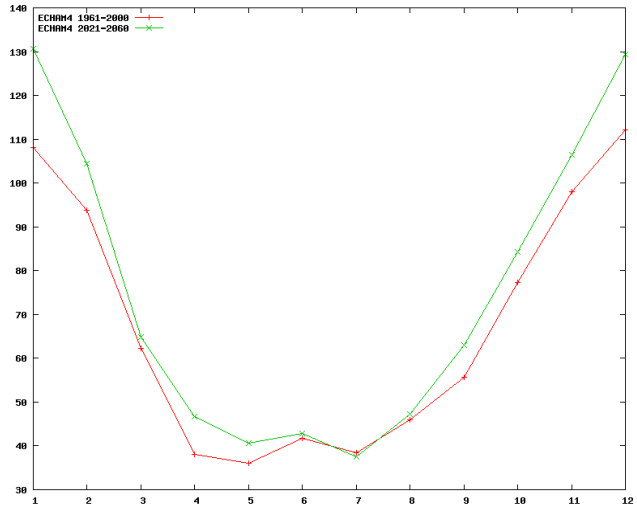

Figure 6.7: Annual cycle of simulated discharge driven by ECHAM4 data for the past and future climate [m^3s^{-1}]

6.3 Conclusions

Application of the HBV model to the Suir catchment area shows that the hydrological model is capable of capturing the local variability of river discharge with reasonable accuracy when driven by observations (calibration) or high resolution ERA-40 driven RCA simulation output (validation). In both cases the same model parameters were used in the HBV model.

Using ECHAM4 driven RCA simulation data for the future period (2021-2060) the hydrological model shows a significant increase in the more intense discharge episodes, a pattern that is also shown in the return values of extreme discharge.

References

Arnell, N.W. 2003: Relative effects of multi-decadal climatic variability and changes in the mean and variability of climate due to global warming: future streamflow in Britain. *Journal of Hydrology*, **270**: 195-213.

Bergstrom, S., 1995: The HBV model, Chapter 13 of *Computer models of watershed hydrology*, Water Resources Publications. 443-476

Bergstrom, S., Carlsson B., Gardelin M., Lindstrom G., Pettersson A. and Rummukainen M., 2001: Climate change impacts on the runoff in Sweden-assessments by global climate models, dynamical downscaling and hydrological modelling. *Climate Research*, **16**: 101-112

Houghton JT, Ding Y, Griggs DJ, Noguer M, van der Linden PJ, Dai X, Maskell K, Johnson CA Eds. 2001: Climate Change 2001: The Scientific Basis. Cambridge University Press, 881 pp.

Lindstrom, G., Johansson B., Persson M., Gardelin M. and Bergstrom S., 1997: Development and test of the distributed HBV-96 model. *Journal of Hydrology*, **201**: 272-288

McKay, M.D., Conover W.J. and Beckman R.J. 1979: A comparison of three methods for selection values of input variables in the analysis of output from a computer code. *Technometrics*, **2**: 239-245.

Pilling, C.G. and Jones J.A.A. 2002: The impact of future climate change on seasonal discharge, hydrological processes and extreme flows in the Upper Wye experimental catchment, mid-Wales. *Hydrological Processes*, **16**: 1201-1213.

Yu, P.S., Yang T.Ch. and Chen S.J., 2001: Comparison of uncertainty analysis methods for a distributed rainfall runoff model. *Journal of Hydrology*, **244**: 43-59.

7 Cyclones statistics and tracks in the climate simulations: past and future

To assess the ability of the regional climate model to realistically reproduce the frequency and intensity of cyclones, data from the RCA simulation (1961-2000) driven by ERA-40 re-analysis data were compared against the ERA-40 data, using an algorithm developed to identify and track cyclones. Analysis of the frequency and intensity of cyclones shows that the RCA is in good agreement with ERA-40. The number of weak cyclones with core pressures between 990 and 1000 hPa is overestimated by 20 to 30% but the number of intense cyclones with core pressures of less than 950 hPa is very well captured.

For the future period climate data from the ECHAM4 driven RCA simulation were used (based on the SRES-B2 emission scenario of greenhouse gas concentrations). Results for the reference (1961-2000) and future (2021-2060) simulations were compared. When all cyclones with core pressures less than 1000 hPa are considered the total numbers and the seasonal and spatial distributions are similar. However, the frequency of very intense cyclones with core pressures less than 950 hPa, show substantial changes: a 15% increase in the future simulation with even stronger increases in winter and spring while autumn numbers show a decrease. In terms of impacts, it is interesting to note that in the future simulation the tracks of the very intense cyclones, mostly located north of Ireland, extend further south relative to the reference simulation.

7.1 Introduction: tracking cyclones

The following algorithm was used to track the movement of cyclones.

On a horizontal grid of N_x x N_y points a low pressure centre is identified at grid point *(i, j)* if these criteria are met:

- the pressure value, *p(i, j)*, is less than a given threshold, e.g. 1000 hPa;
- the point is a local minimum of pressure.

A point *(i, j)* is defined to be a local minimum of surface pressure if its pressure value *p(i, j)* is less than the pressure values of all points contained in the surrounding four grid boxes (i.e., the surrounding 80 grid points, see Figure 7.1). This corresponds to *p(i, j)* being the minimum pressure within a distance of approximately 53 km in all directions. Since for each point we examine the four surrounding grid boxes, we do not take into account the boundary points and the three nearest points to the boundaries.

For example, a point will be identified as the centre of a cyclone if for the pressure value *p(i, j)*, we have:

$$p(i, j) < 1000 \text{ hPa}$$

and

$$p(i, j) < p(i + k, j + l), \quad k = -4,\ldots..,+4 \quad (k \neq 0)$$

where

$$4 < i < N_x - 3 \quad \text{and} \quad 4 < j < N_y - 3.$$

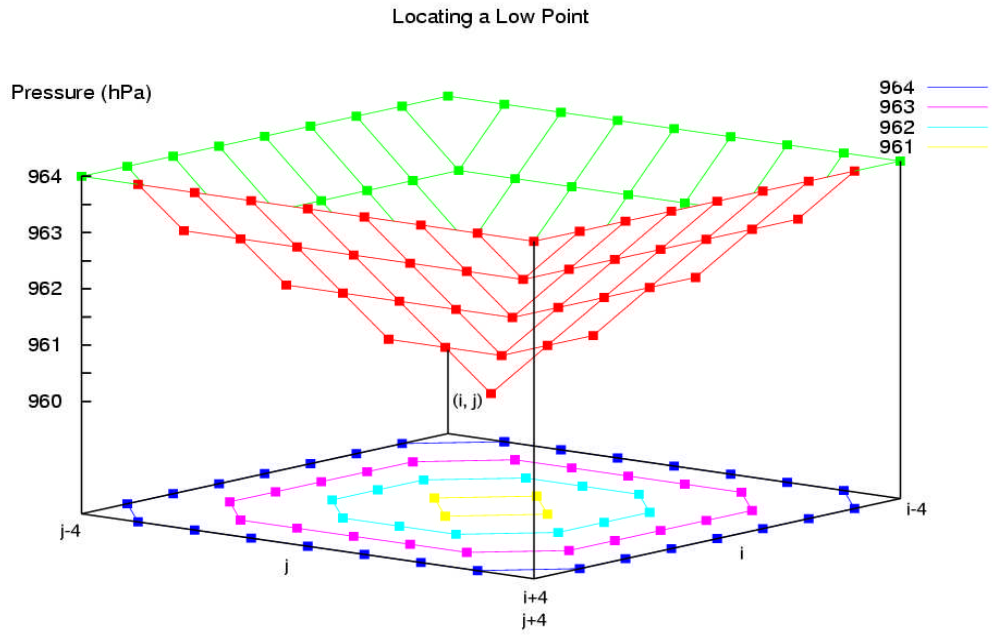

Figure 7.1: Locating a low point

7.1.1 Cyclone statistics

The algorithm was applied to the RCA model results and the ERA-40 re-analysis data. As the ERA-40 data are only available at 6-hour intervals the same interval was used for the RCA data. Figure 7.2a shows the frequency of lows occurring at varying pressure values for both data sets. The data bins along the x-axis have an increment of 1 hPa.

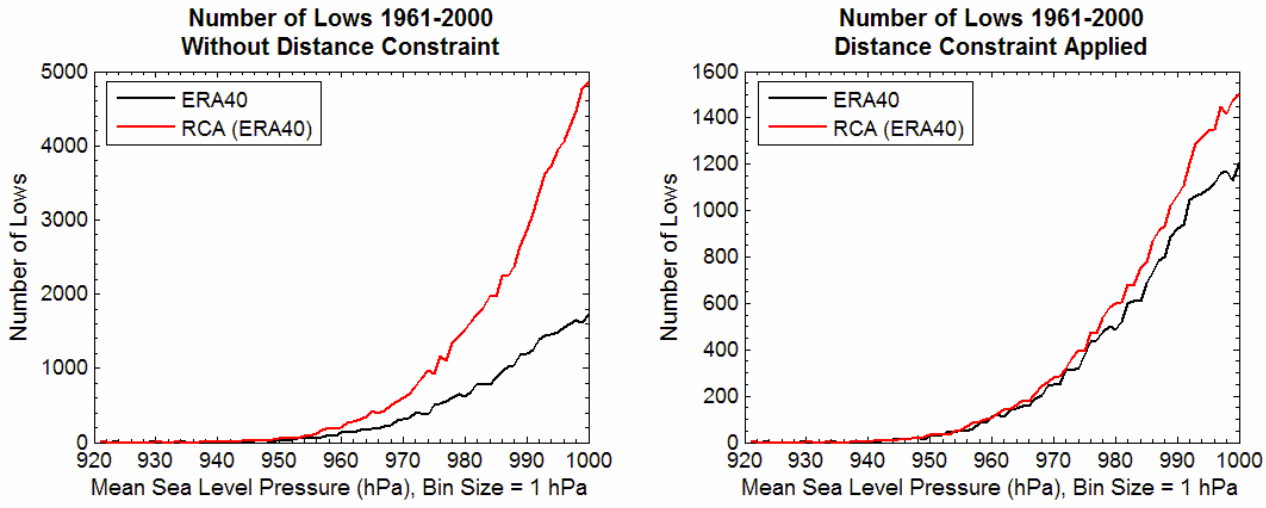

(a) *(b)*

Figure 7.2: Frequency of lows occurring at varying pressure (a) without using a distance constraint and (b) using a distant constraint

Although both curves in Figure 7.2a follow a similar trend, the RCA model returns substantially more lows, particularly at higher pressure values. The discrepancy arises from the fact that the RCA model tends to split a large-scale low pressure system with only one local minimum in the ERA-40 data into several local minima that are counted as separate lows in our algorithm (Figure 7.3). This is a common occurrence in the RCA simulations and since the local minima obviously belong to the same system we introduce an extra constraint in the algorithm: two local minima are considered to belong to the same system if they are less than 1000 km apart. The distance of 1000 km was chosen since this is a typical extension of a low-pressure system. With this constraint the low-pressure system is assigned the minimum pressure value and its position is taken to be the position of this minimum. The revised statistics (Figure 7.2b) show much better agreement with ERA-40.

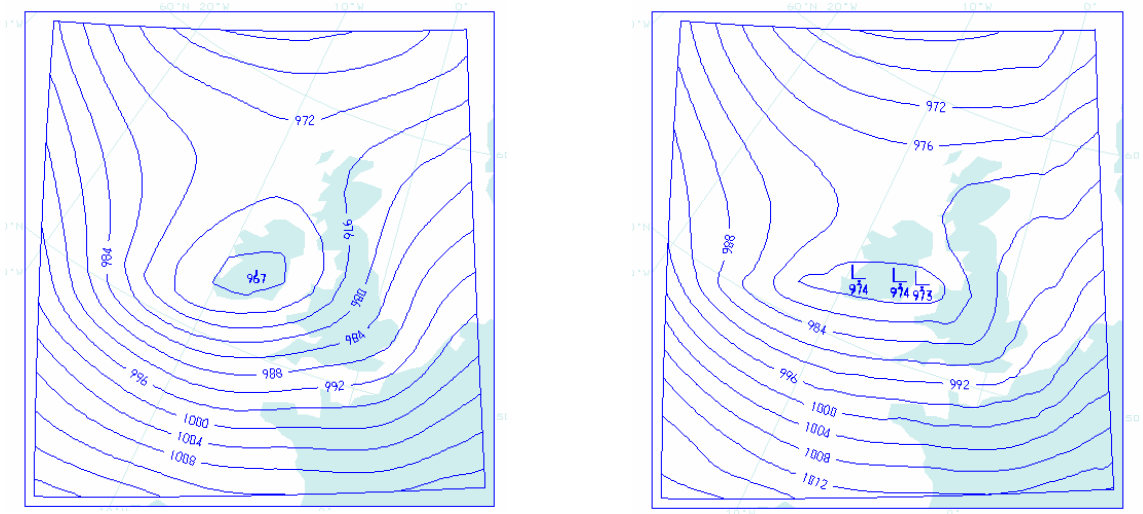

Figure 7.3: An example of (a) one local minimum in ERA-40 and (b) three local minima in RCA

Figure 7.4a shows the annual number of lows with a core pressure of less than 1000 hPa. The patterns are very similar for the RCA and ERA-40 data with the RCA numbers being slightly higher. This is also reflected in the ratio plot shown in Figure 7.4b.

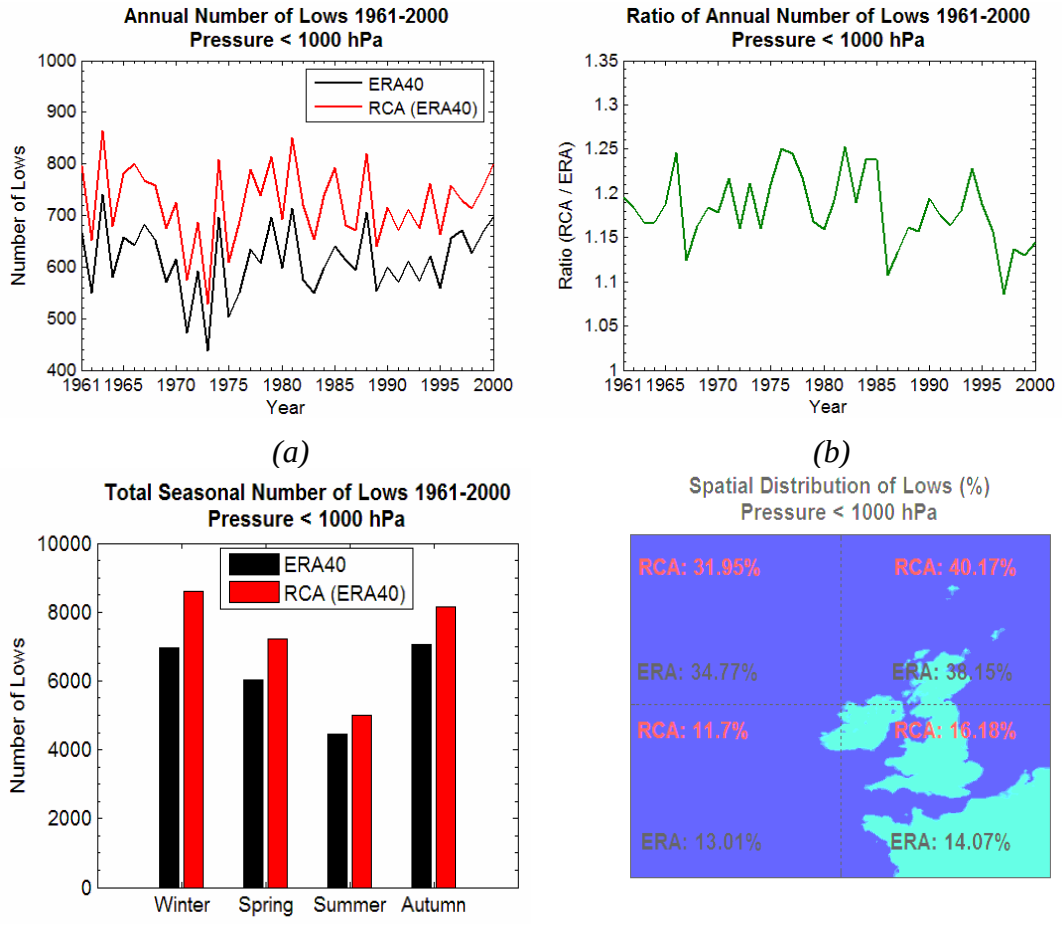

Figure 7.4: (a) ERA-40 and RCA annual number of lows, (b) ratio of annual number of lows RCA/EA40, (c) total seasonal number of lows and (d) spatial distribution of lows with a core pressure of less than 1000 hPa in RCA and ERA-40 for the time period 1961-2000.

The seasonal number of lows over forty years is depicted in Figure 7.4c. Both the RCA model and the ERA-40 data follow the same trend with the greatest and lowest number of lows occurring in winter and summer respectively. Figure 7.4d shows the spatial distribution of the cyclones split into quadrants. The percentages are broadly similar but RCA has slightly more lows in the eastern half of the area compared with ERA-40. As expected, most of the lows fall into the northern half of the area.

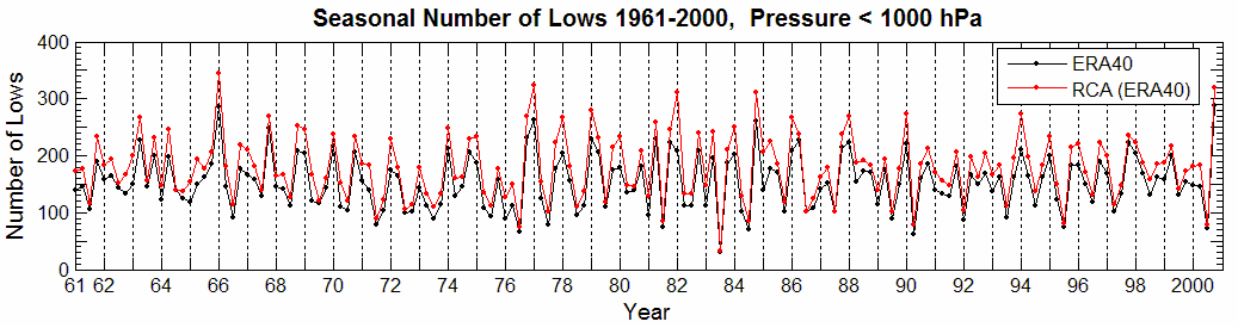

Figure 7.5: Seasonal number of lows with a core pressure of less than 1000 hPa from ERA-40 and RCA for 1961-2000.

The time-series plot of the number of lows, stratified by season, over the whole area (Figure 7.5) shows that the RCA model is able to capture the seasonal variations quite well.

7.1.2 Intense cyclones

In this section statistics are presented for cyclones with core pressures less than 950 hPa. Note that with the lower pressure threshold the RCA model results agree more closely with the ERA-40 re-analysis data. This is evident from the plot depicting the annual number of lows (Figure 7.6a).

The seasonal and spatial distribution of the cyclones are shown in Figure 7.6b and 7.6c respectively. As expected, most of the intense cyclones occur in winter and are located in the northern half of the area.

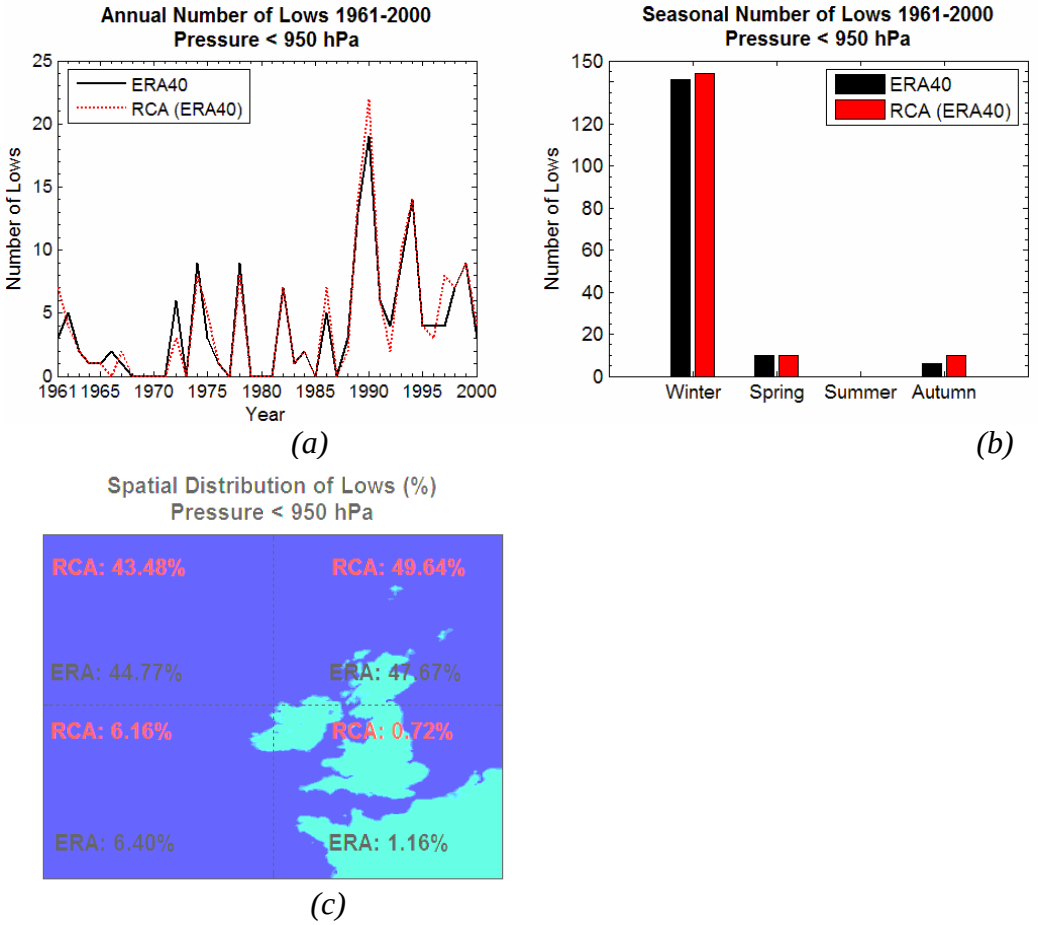

Figure 7.6: (a) Annual and (b) total seasonal numbers of lows and (c) spatial distribution of lows with a core pressure of less than 950 hPa in ERA-40 and RCA

A time-series plot of the seasonal number of lows (Figure 7.7) shows good agreement between RCA and ERA-40. Note the increase in frequency in the 1990s.

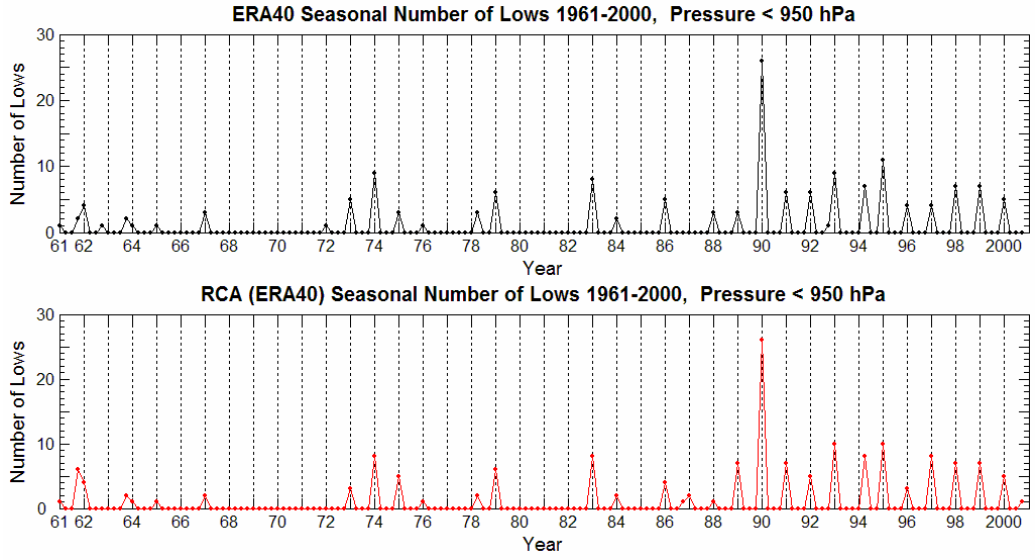

Figure 7.7: Seasonal number of lows with a core pressure of less than 950 hPa from ERA-40 (top) and RCA (bottom) for 1961-2000.

It is encouraging that the results compare quite well for these intense cyclones not only in the annual numbers, but also in the spatial and seasonal distributions, since extreme events are interesting in terms of impacts.

7.2 Cyclone tracking

In this section the spatial movement of cyclones with a core pressure less than 950 hPa is examined. To track the movement of the systems the cyclone centres are located at output times t and $t + \Delta$, where Δ is the data output frequency, set to 6 hours to suit the ERA-40 data. A cyclone at time t is considered to be the same cyclone identified at time $t + \Delta$ if the estimated speed of movement, based on the great circle distance between the positions, is less than 120 km/hr. In addition, only cyclones that exist for at least 24 hours are considered.

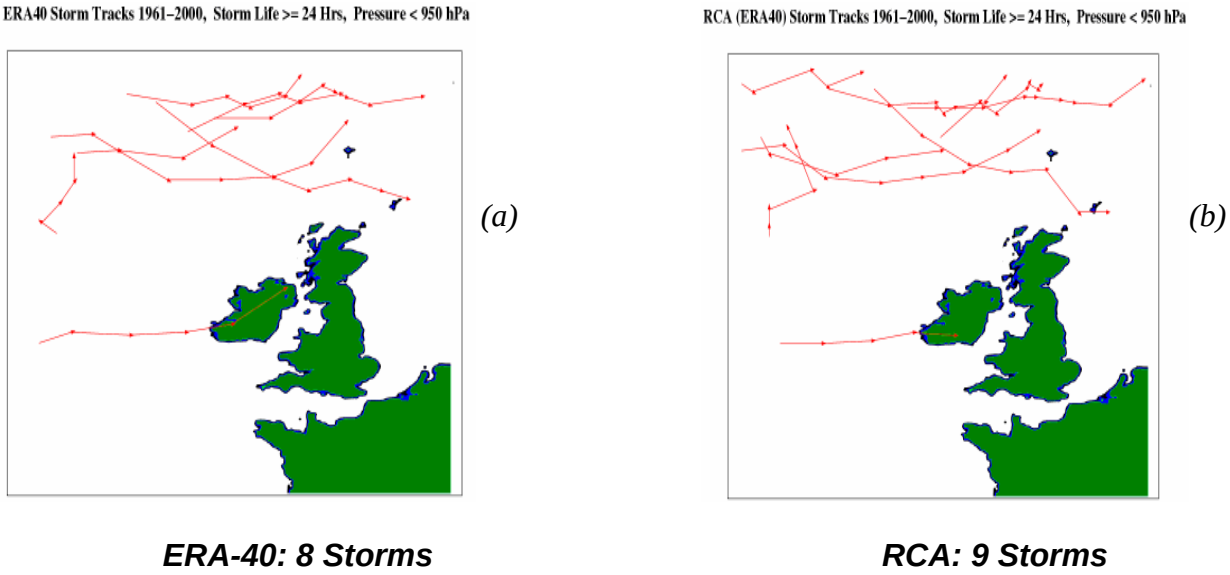

Figure 7.8: Tracks of storms with a core pressure of less than 950 hPa with a life of at least 24 h from (a) ERA-40 and (b) RCA for the time period 1961-2000

Applied to the RCA and the ERA-40 fields (Figure 7.8) we can see that the RCA model is in good agreement with ERA-40.

Results for one particular storm that caused widespread damage when it crossed Ireland and the UK on 25 January 1990 are shown in Figure 7.9. The RCA track of this so-called Burns' Day storm, while a little too far south, agrees well with ERA-40. However, the intensification of the system lags ERA-40 although it does eventually catch up with an extreme pressure of 950 hPa.

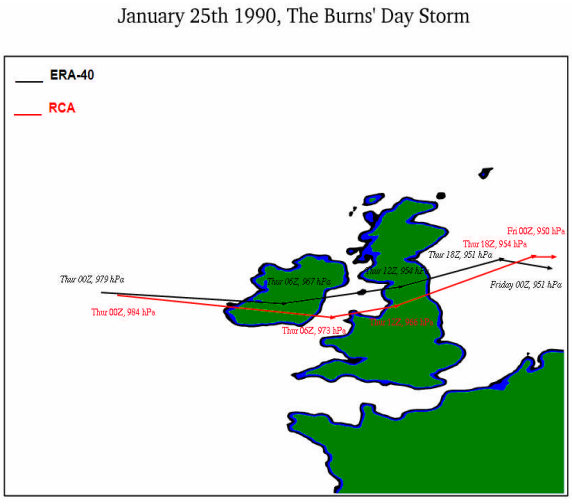

Figure 7.9: Tracks of the Burns' Day storm from ERA-40 (black arrows) and RCA (red arrows) for Thursday, 25 January 1990, 00 UTC to Friday, 26 January 1990, 00 UTC

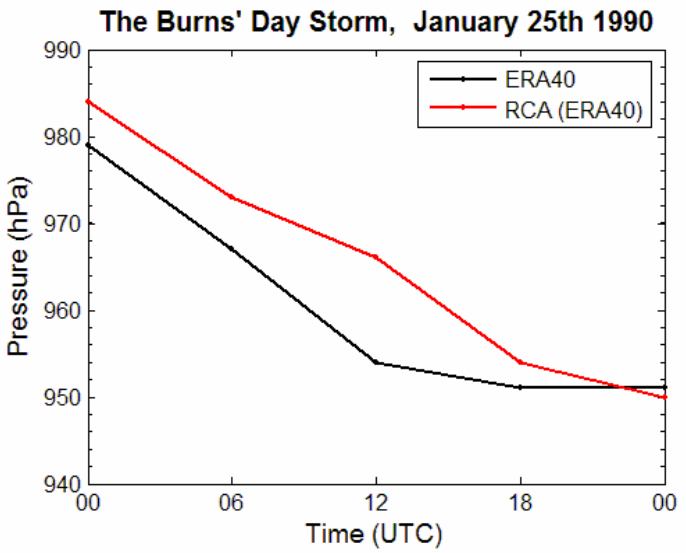

Figure 7.10: Core pressure values for the Burns' Day storm from ERA-40 and RCA for Thursday, 25 January 1990, 00 UTC to Friday, 26 January 1990, 00 UTC

7.3 Simulation of the future climate

This section examines the impact of climate change on the frequency and intensity of cyclones, using the two ECHAM4 driven RCA simulations for 1961-2000 (reference simulation) and 2021-2060 (future simulation) described in Section 5. Data at 3-hour intervals are used.

Figure 7.11 shows the frequency of lows occurring at varying pressure values for both sets of data. The differences between the simulations are generally small but for the higher core pressure values the number of cyclones in the future simulation is slightly less compared with the reference simulation.

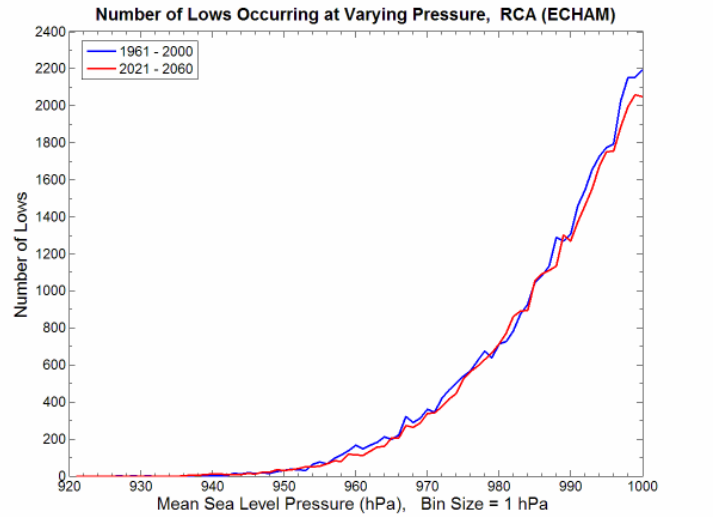

Figure 7.11: Number of lows occurring at varying pressure for 1961-2000 (blue line) and for 2021-2060 (red line)

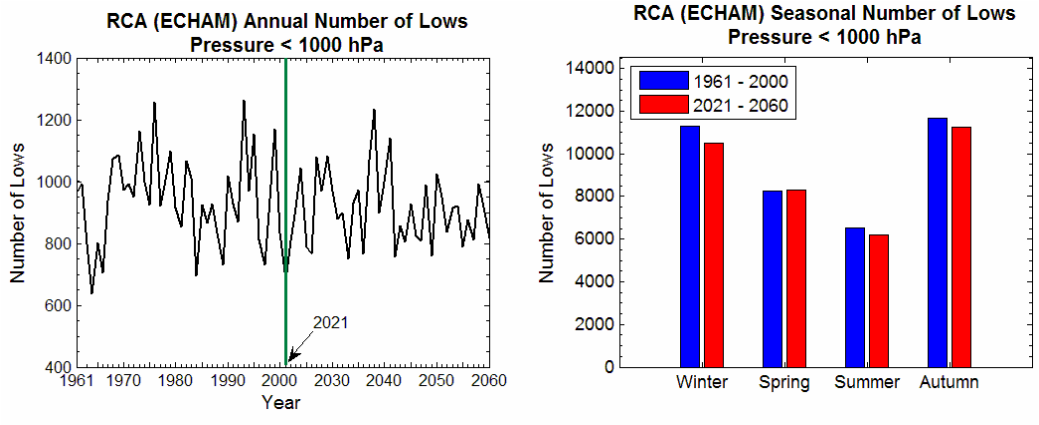

(a) *(b)*

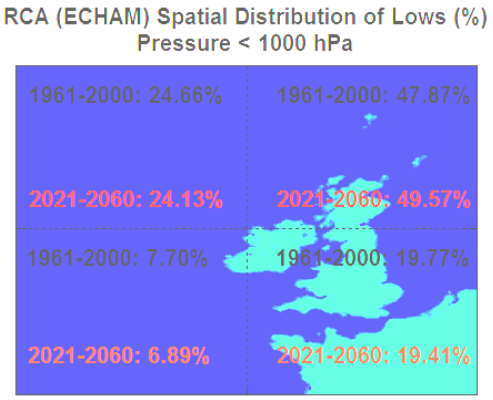

(c)

Figure 7.12: (a) Annual, (b) total seasonal numbers and (c) spatial distribution of lows with a core pressure of less than 1000 hPa for 1961-2000 and 2021-2060 as simulated by RCA driven by ECHAM4

Figure 7.12 shows (a) the annual, (b) the total seasonal number and (c) the spatial distribution of lows with a core pressure of less than 1000 hPa. Again, the differences between the simulations are small and similar results are found when the core pressure threshold is reduced to 960 hPa.

However, with a core pressure threshold of 950 hPa a different pattern emerges (Figure 7.13). Even if there is a substantial decadal variability (Figure 7.13a), there are at least three peaks in the annual number of lows in the future simulation, which exceed all the peaks in the reference simulation. Furthermore the intense storms are more frequent in winter and spring (Figure 7.13b), whereas there is a substantial decrease in autumn. Although the spatial distributions are similar (Figure 7.13c), the future simulation shows more of these intense cyclones in the south-east quadrant, which is the quadrant with the highest land proportion and therefore more important in terms of impacts. In the future simulation the storm tracks also extend further south relative to the reference simulation (Figure 7.14).

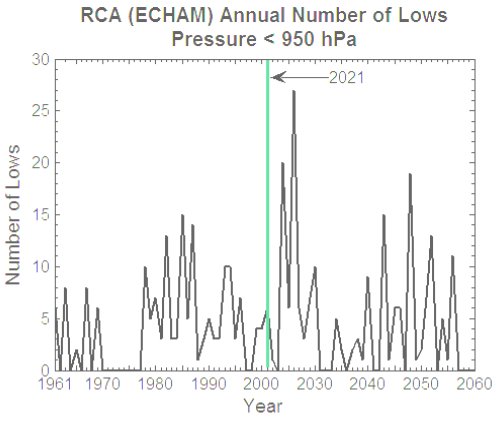

(a)

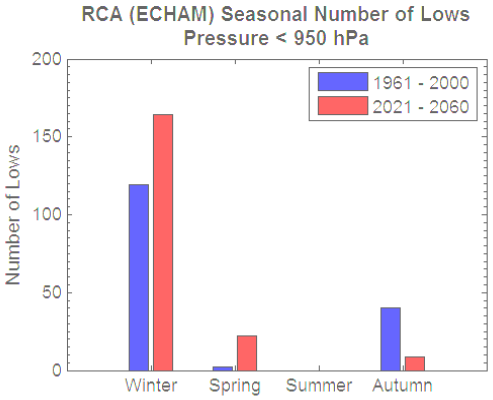

(b)

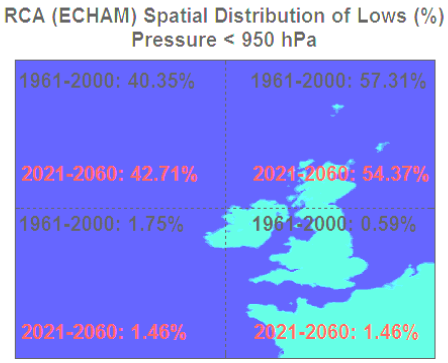

(c)

Figure 7.13: (a) Annual, (b) total seasonal numbers and (c) spatial distribution of lows with a core pressure of less than 950 hPa for 1961-2000 and 2021-2060 as simulated by RCA driven by ECHAM4

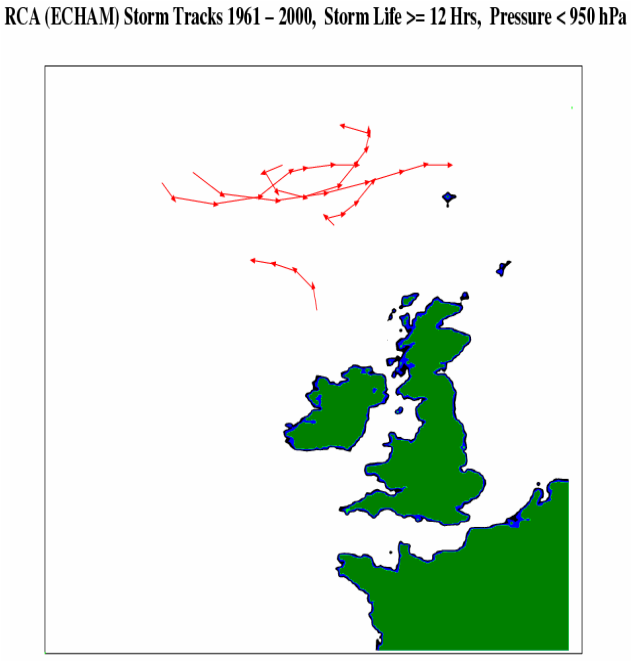

(a)

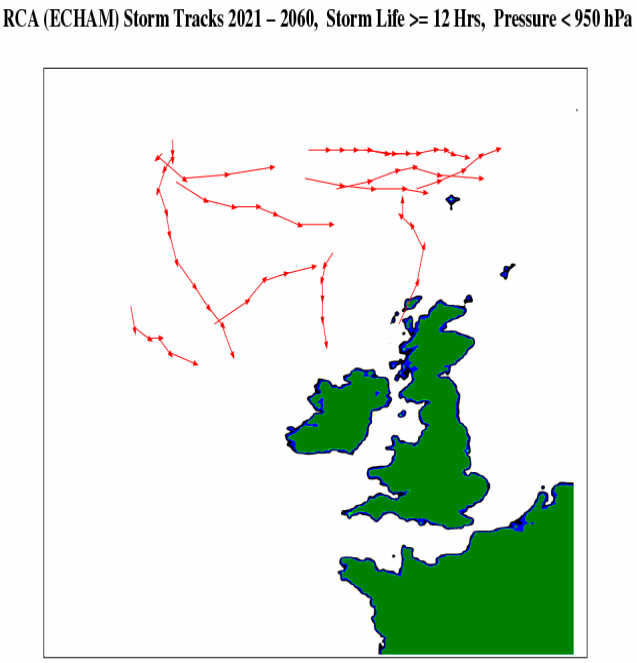

(b)

Figure 7.14: Tracks of storms with a core pressure of less than 950 hPa for at least 12 h from RCA driven by ECHAM4 for (a) the time period 1961-2000 and (b) the time period 2021-2060

7.4 Conclusions

To assess the ability of the regional climate model to realistically reproduce the frequency and intensity of cyclones, the RCA simulation (1961-2000) driven by ERA-40 re-analysis data was compared with the ERA-40 data. Data from the latter are based on a wide variety of atmospheric observations and therefore provide an accurate reference for evaluating the RCA simulation. Analysis of the frequency and intensity of cyclones shows that the RCA is in good agreement with ERA-40. The number of weak cyclones with core pressures between 990 and 1000 hPa is overestimated by 20 to 30% but the number of intense cyclones with core pressures of less than 950 hPa is very well captured.

For the future period climate data from the ECHAM4 driven RCA simulation were used (based on the SRES-B2 emission scenario of greenhouse gas concentrations). Results for the reference (1961-2000) and future (2021-2060) simulations were compared. When all cyclones with core pressures less than 1000 hPa are considered the total numbers and the seasonal and spatial distributions are similar. However, the frequency of very intense cyclones with core pressures less than 950 hPa, show substantial changes: a 15% increase in the future simulation with even stronger increases in winter and spring while autumn numbers show a decrease. Previous studies on cyclone activity in the North Atlantic region show different results for the total number of lows: Zhang and Wang (1997) and Lambert (1995) found a decrease; König *et al*. (1993) found no significant changes; Hall *et al*. (1994) and Sinclair and Watterson (1999) found an increase. However, the increased intensity of cyclones in the future climate of the North Atlantic area close to Ireland and the UK during the winter months is a common feature in these studies (e. g. Lambert (1995), Geng and Sugi (2003)). In terms of impacts, it is interesting to note that in the future simulation the very intense cyclones (core pressures below 950 hPa) extend further south relative to the reference simulation (Figure 7.14).

References

Geng Q, Sugi M. 2003. Possible change of extratropical cyclone activity due to enhanced greenhouse gases and sulfate aerosols – study with a high-resolution AGCM. *Journal of Climate,* **16**: 2262-2274.

Hall NMJ, Hoskins BJ, Valdes PJ, Senior CA. 1994. Storm tracks in a high-resolution GCM with doubled carbon dioxide. *Quarterly Journal of the Royal Meteorological Society,* **120**: 1209-1230.

König W, Sausen R, Sielmann F. 1993. Objective Identification of Cyclones in GCM Simulations. *Journal of Climate,* **6**: 2217-2231.

Lambert SJ. 1995. The effect of enhanced greenhouse warming on winter cyclone frequencies and strengths. *Journal of Climate,* **8**: 1447-1452.

Sinclair MR, Watterson IG. 1999. Objective Assessment of Extratropical Weather Systems in Simulated Climates. *Journal of Climate,* **12**: 3467-3485.

Zhang Y, Wang W-C. 1997. Model-Simulated Northern Winter Cyclone and Anticyclone Activity under a Greenhouse Warming Scenario. *Journal of Climate*, **10**: 1616-1634.

8 Influence of an increased sea surface temperature on North Atlantic cyclones *

Since Ireland and the UK are surrounded by water the sea surface temperature (SST) has a major impact on the climate of these islands. The question is if an increased SST in the North Atlantic could lead to more severe storms. In this study the influence of an increased SST on the frequency and intensity of cyclones is investigated using two 16-year simulations with the Rossby Centre regional climate model, RCA, on a model domain including Western Europe and large parts of the North Atlantic. The RCA model is driven by ERA-40 re-analysis data at the lateral and lower boundaries, using the original SST (standard experiment) and an SST increased by 1 K (sensitivity experiment). This increase in SST is typical of the predictions from general circulation model (GCM) simulations within this century for the North Atlantic region according to the SRES-B2 emission scenario. Using this approach, rather than driving RCA by the output of a GCM for present day and for the future climate, ensures that we can separate the influence of the SST on the development of cyclones from other influences.

The total number of cyclones is found to be only slightly higher, whereas the intensity of cyclones is strongly increased in the sensitivity experiment compared to the standard experiment. In the 16-year period three hurricanes with pressure gradients of up to 50 hPa per 100 km, wind speeds of up to 42 m/s and substantial amounts of rain (up to 50 mm/h) appear in northern latitudes between 30 and 35 degrees in the sensitivity experiment which do not appear in the standard experiment. The study suggests that the remnants of such hurricanes could influence European coastal areas in a world with a warmer SST.

8.1 Introduction

High SSTs are well known to have an influence on the intensity of hurricanes in tropical regions (e. g. Chan *et al*., 2001). In a case study by Davis and Bosart (2002), looking at hurricane Diana in 1984, an increase in the SST by 1-2 K resulted in a storm with a core pressure that was about 27 hPa deeper after 60 h of integration with a numerical model. This deepening was caused by enhanced water vapour fluxes from the ocean into the atmosphere. De Maria and Kaplan (1994) used the SST as a predictor for the maximum potential intensity of tropical cyclones. Even though Hobgood (2003) stated that the surface air temperature, which is closely linked to the SST, is not the only parameter determining the intensities of hurricanes, and that the vertical temperature structure of the atmosphere and the surface pressure are also important, it is obvious that the SST and the associated latent heat fluxes play a key role in the development of hurricanes.

For extratropical cyclones there are only a few studies, restricted to the western North Pacific region, that deal with the influence of the SST on their development. Gyakum and Danielson (2000) found that the combination of warm SST anomalies with cold airmasses over the western North Pacific, leading to enhanced sensible and latent heat fluxes from the ocean into the atmosphere, favours explosive cyclogenesis. Also, Chen *et al*. (1992), looking at explosive cyclones off the East Asian coast, reported rapid cyclogenesis in the Kuroshio Current region connected with warm SST anomalies. However, enhanced sensible and latent heat fluxes are not the only sources for cyclogenesis. Amongst others

* NOTE: this is a preview of an article submitted for publication.

Pavan *et al*. (1999) state that baroclinicity and thus temperature gradients are also important for the development of cyclones.

Previous studies using GCMs to study future changes in the frequency and intensity of cyclones due to increased greenhouse gas concentrations, which also include changes in the SST towards warmer conditions, differ in their results depending on the used methodology and on the used GCM. König *et al*. (1993), determining local minima in the 1000 hPa geopotential height field and local maxima in the 850 hPa vorticity field, suggest no significant changes in the number of cyclones over the North Atlantic. Hall *et al*. (1994) report that the eddy kinetic energy near the storm tracks increases by roughly 10% in a doubled CO_2 concentration simulation with even more pronounced increases downstream, especially for the North Atlantic storm track; whereas Zhang and Wang (1997) suggest a decrease in the cyclone activity under increased greenhouse gas concentrations when looking at 1000 hPa geopotential heights and vorticity, root-mean-square (rms) of 500 hPa geopotential heights as well as Eady growth rate maximum. Lambert (1995) also looked at the number of intense cyclones under doubled CO_2 concentration conditions using 1000 hPa geopotential heights and found that even if the total number of cyclones decreases, the number of intense cyclones increases in the Northern hemisphere during winter. This is consistent with findings from Sinclair and Watterson (1999) for the mean sea level pressure minima but not for the vorticity maxima. They state that the sea level pressure is generally reduced in a doubled CO_2 concentration atmosphere, which leads to lower core pressures but not to increased intensities of the cyclones. Thus they suggest looking at the vorticity rather than pressure minima. Nevertheless, even if looking at the vorticity maxima, Sinclair and Watterson (1999) find increased winter cyclone activity near the downstream end of the principal storm tracks, which would indeed affect our region of interest around Ireland and the UK. Because of the differences in the results, using GCMs to investigate the future development in the frequency and intensity of cyclones, which stem from different methods and different GCM projections, it is important to reduce the sources of uncertainty. This can be done by looking at cyclone statistics with different methods for the present day climate.

McCabe *et al.* (2001) looked at trends in winter frequencies and intensities of extratropical cyclones in the Northern Hemisphere using sea level pressure fields from the National Centers for Environmental Prediction – National Center for Atmospheric Research (NCEP-NCAR) re-analysis project for 1959-1997. They detected an increasing winter cyclone frequency in high latitudes (north of 60° N) and a decreasing winter cyclone frequency in low latitudes (between 30° N and 60° N) over the 39 years. The cyclone intensity in both latitudinal bands has increased during the 39 years according to their study. Geng and Sugi (2001) investigated winter cyclone characteristics using mean sea level pressure distributions from NCEP-NCAR re-analysis data over the North Atlantic. They reported trends towards higher cyclone density over the northern North Atlantic and towards lower cyclone density over the eastern coast of the North Atlantic as well as over Western Europe. At the same time they found more intense cyclones in large regions over the past 40 years along with a considerable decadal variability. These results are consistent with the results of McCabe *et al*. (2001). Paciorek *et al*. (2002) report increasing numbers of intense storms as well as positive trends for Eady growth rate, temperature variance and high percentiles of wind speed over large areas for the past 50 winters (1949-1999) using NCEP-NCAR re-analyses, even if the total number of storms is decreasing. However, some of the detected trends in the NCEP-NCAR re-analysis data could be due to improved data quality in the more recent years. It is interesting to note that even if there are considerable differences in the results from future climate projections, some features are common between the trends of the past 40 to 50 years and the predicted trends for the future from most studies. Even if the total number of cyclones decreased

and will further decrease over most parts of the North Atlantic, the intensity of cyclones increased and will further increase according to the majority of the previous studies.

A plausible explanation is that a decreased meridional temperature gradient and the associated reduced baroclinicity in the future climate could be responsible for the decrease in the total number of cyclones, whereas the higher moisture supply, due to a generally higher SST and related increased latent heat fluxes, could trigger the increase in intensity of the cyclones.

However, Geng and Sugi (2001), investigating the connection between cyclone density and SST over the North Atlantic, do not find a direct influence of the meridional SST gradient on the cyclone activity, even if trend and decadal variability of the cyclone density and the SST gradient show a relationship. They find that the SST gradient variations lag behind the cyclone density variations by 1 to 2 years, i.e. a high cyclone density will lead to a strong SST gradient but not vice versa. Two years later, the same authors, using a high-resolution AGCM, revise their opinion about the influence of the meridional temperature gradient on the cyclone frequency (Geng and Sugi, 2003), suggesting that a weaker meridional temperature gradient does lead to a smaller cyclone density.

Because of the uncertainties regarding the reasons for the observed and simulated changes in cyclone intensities and frequencies, single influences must be distinguished and further investigated. Our study contributes to this in looking at the pure influence of an increased sea surface temperature and therefore increased latent heat fluxes, while maintaining the meridional temperature gradient and the large scale circulation. This is done by using a high resolution regional climate model, which is forced at the lateral boundaries with re-analysis data to ensure that the large scale circulation is maintained, and at the lower boundaries with two different sets of sea surface temperatures, both having the same meridional gradient. The main focus is on looking at the frequency and intensity of cyclones. Other associated parameters such as sea level pressure, wind speed and precipitation are investigated in terms of mean values and extreme events as well.

The remaining sections of this article are organised as following. In section 8.2 the design of the performed regional climate model experiments as well as the methods of evaluation, particularly the cyclone counting and tracking algorithm, are described. Section 8.3 shows the mean sea level pressure field to demonstrate that the large scale circulation is maintained in our study. Section 8.4 is the core section dealing with the influence of the SST on the frequency and location of cyclones with different intensities. Changes in the wind speed, which are directly connected with cyclone frequencies and intensities, are discussed in section 8.5. Finally, section 8.6 provides a summary and discussion of the results.

8.2 Model setup and methods of evaluation

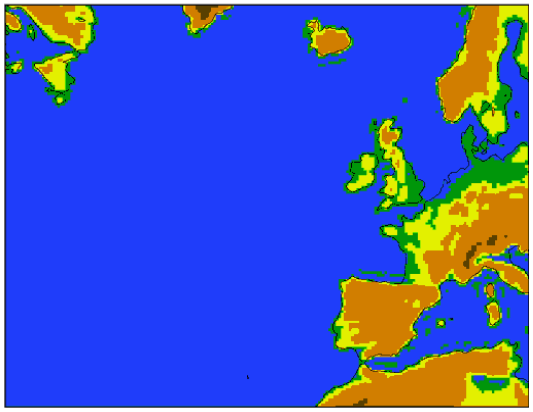

Figure 8.1: Simulation domain

In this study the regional climate model RCA (Rossby Centre regional Atmospheric Climate model version 2) (Jones, 2001; Rummukainen *et al.*, 2001) is used on a model domain including large parts of the North Atlantic to allow the increased SST to have an impact on the development of cyclones. Furthermore, Western Europe is included in the east of the model domain with Ireland and the UK well away from the lateral boundaries (Figure 8.1). To drive the model at the lateral and lower boundaries the 40-year re-analysis data from ECMWF (ERA-40) are used. This is a consistent dataset produced by an earlier version of the ECMWF operational analysis and forecast system, in which a wide range of terrestrial and satellite based observational data are assimilated. The temperature, wind, moisture, liquid water and pressure fields, which are used to drive RCA at the lateral boundaries, should be of high quality, even though the observation density over the North Atlantic is not as good as over the European continent. The RCA simulation period extends from 1985 to 2000. The model has been run with a horizontal resolution of 0.24° (around 27 km) with 40 non-equally spaced vertical levels on a rotated latitude/longitude grid. Two simulations have been performed: one using the original SST from ERA-40 (standard experiment) as lower boundary values and one with an SST increased by 1 K (sensitivity experiment). Results were saved every 3 hours.

The main focus in this study is to investigate the influence of the SST on the frequency and intensity of cyclones. To identify and categorize these features, and to track them over their lifetime, the following algorithm was applied. The centre of a cyclone is defined to be a local sea level pressure minimum of less than 1000 hPa within a radius of 5° or around 560 km, which reflects the typical size of a low pressure system. As a measure of the intensity the maximum pressure gradient within this radius is used rather than the sea level pressure minimum. If the latter is used the cyclones in northern latitudes would be favoured because of the systematically lower sea level pressure in these areas. This approach could also lead to an artificial bias if a systematic difference in the sea level pressure is found between our standard and sensitivity experiment. Sinclair and Watterson (1999) report the same problem for experiments with standard and doubled CO_2 concentrations. The maximum pressure gradient has been chosen, because this is an immediate measure of the related wind speeds, which are of special interest in terms of possible storm damages over land or wind induced flooding in coastal areas.

To track the cyclones over their lifetime successive mean sea level pressure fields from the simulation are compared. Two low centres are considered to be associated with the same cyclone if their lateral separation is consistent with the cyclone moving with a speed of less than 30 m/s. For an output interval of 3 hours this implies that the maximum separation distance should be less than about 320 kms. The relatively high temporal resolution of the fields ensures that we can identify the cyclone tracks with a high reliability (Blender and Schubert, 2000). The tracking between successive output fields is repeated over the whole simulation.

8.3 Mean sea level pressure

Figure 8.2 shows the mean sea level pressure averaged over the whole period from the standard experiment (a), the sensitivity experiment (b) and from ERA-40 (c). Although both RCA experiments show the pressure minimum shifted to the east compared to ERA-40, the overall structure of the pressure distribution and the pressure gradient are similar. While this is to be expected (because the RCA is driven with ERA-40 at the lateral boundaries) it is also essential for the integrity of the experiments as we want to ensure that the circulation characteristics are essentially unchanged by RCA. Also the differences between both RCA experiments are small. In the interior of the model domain the sea level pressure is slightly lower by up to 1 hPa in the sensitivity experiment compared to the standard experiment. Climatological seasonal averages do not show pronounced differences between the standard and the sensitivity experiment in the large scale circulation either (not shown). Thus it is indeed possible to separate the impacts of the increased SST from other impacts such as a changed circulation or changed greenhouse gas concentrations.

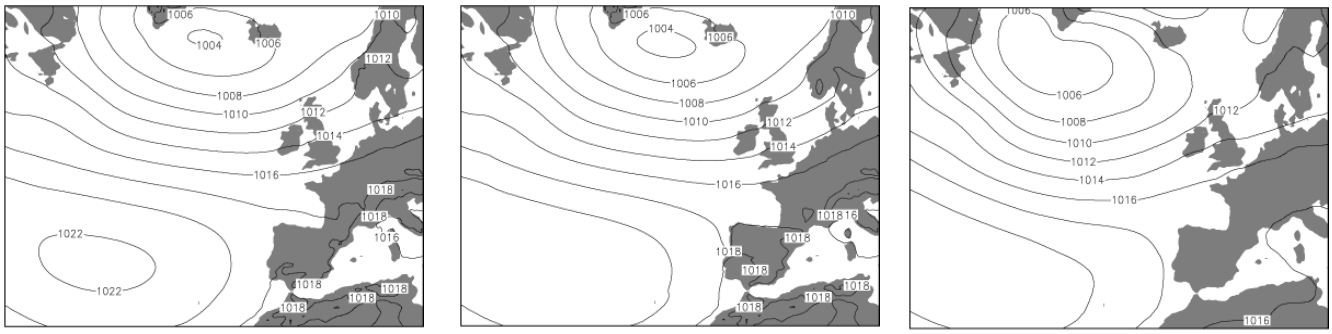

(a) *(b)* *(c)*

Figure 8.2: Mean sea level pressure averaged over the simulation period 1985-2000 (a) from the standard experiment (observed SST), (b) from the sensitivity experiment (increased SST) and (c) from the 40 year ECMWF re-analysis.

8.4 Cyclone statistics

This section is divided up into 3 subsections. The first deals with the frequency of cyclones of different intensities; the second looks at the tracks of very intense cyclones; the third describes hurricane-like cyclones, which only occur in the sensitivity experiment with the increased SST.

8.4.1 Cyclone frequency

Table 8.1 shows the number of cyclones over the full 16-year period in the ERA-40 data, in the standard and sensitivity experiments, and the relative differences between the two experiments for different threshold values of the pressure gradient. All cyclones in the whole model domain are counted for each 3-hour output interval. This means that if a cyclone has a lifetime, for example, of 24 hours, it will be counted 8 times in these statistics. This weighting essentially acknowledges the greater potential impact of deep cyclones with a long lifetime compared to those with a short lifetime. However, as the

ERA-40 data are only available every 6 hours the numbers are multiplied by 2 for compatibility with RCA. This is regarded as a reliable approach with a long sequence of data (16 years). A test using every second output interval of the RCA simulation and multiplying the cyclone numbers by 2 showed that the errors in the numbers are well below 1% for pressure gradients up to 10 hPa per 100 km and that the errors are random, if viewed across all pressure gradients. If we compare the ERA-40 data with the standard experiment (Table 8.1), the numbers are similar only for the total number of cyclones with a pressure gradient of more than 2 hPa per 100 km. The stronger the pressure gradient, the larger the differences between ERA-40 and the standard experiment. This is most probably connected to the coarse horizontal resolution of the ERA-40 data (1.125º or about 125 km), which does not allow the development of strong pressure gradients. However, it is encouraging that both the pressure distribution and the total number of cyclones with a pressure gradient of more than 2 hPa per 100 km, are very similar between ERA-40 and the RCA standard experiment.

More cyclones are counted in the sensitivity experiment compared to the standard experiment with the most remarkable differences occurring with the cyclones with strong pressure gradients (Table 8.1). It is interesting to note, that even the total number of cyclones with a pressure gradient of more than 2 hPa per 100 km is increased in the sensitivity experiment compared to the standard experiment by nearly 10%. The majority of previous studies (discussed in section 8.1), that include other changes apart from the SST, show decreasing total numbers of cyclones during the past 40 to 50 years over the North Atlantic and predict a similar trend for the future. The differences in the number of intense cyclones with pressure gradients of more than 20 hPa per 100 km are striking. The number of such intense cyclones is increased by a factor of more than 6 in the sensitivity study compared to the standard experiment. The maximum pressure gradient recorded over the whole 16 years is 23 hPa per 100 km in the standard experiment and 50 hPa per 100 km in the sensitivity experiment. Such striking differences are not reported in any of the previous studies that include other changes apart from the SST.

Some of the differences in the number of cyclones could be due to the model setup, which may favour the development of cyclones. Only the SST values, and not the atmospheric temperatures in the lateral boundaries, are increased by 1 K, which leads to a more unstable stratification in the sensitivity experiment compared to the standard experiment. This increases the baroclinicity and therefore the number of cyclones. However, the number of strong cyclones is not necessarily connected with the baroclinicity. In a study over East Asia Geng and Sugi (2003) found that, even if stability increases and baroclinicity decreases and the total number of cyclones decreases, the number of strong cyclones increases. Thus the strong increase in the number of intense cyclones in our study is not necessarily due to a decreased static stability.

Table 8.1: Total number of cyclones from 1985 to 2000 in the standard and the sensitivity experiment for different values of the pressure gradient

Pressure gradient [hPa/100km]	***Number of cyclones in ERA-40***	***Number of cyclones in standard experiment***	***Number of cyclones in sensitivity experiment***	***Change sensitivity experiment compared to standard experiment [%]***
>2	39848	38078	41548	9.1
>4	22828	27488	30940	12.6
>6	6000	11304	13582	20.2
>8	1250	4518	5660	25.3
>10	210	1811	2302	27.1
>12	22	681	901	32.3
>14	6	267	409	53.2
>16	0	96	189	96.9
>18	0	31	94	203.2
>20	0	9	64	611.1
>22	0	3	47	1566.7
>25	0	0	34	-

8.4.2 Tracks of very intense cyclones

Figure 8.3 shows the tracks of the very intense cyclones with a pressure gradient of more than 20 hPa per 100 km for both the standard and the sensitivity experiment for the complete simulation period 1985-2000. In the northern North Atlantic we find 3 cyclone tracks in the standard and in the sensitivity experiment. In the sensitivity experiment they have a lifetime of up to 9 hours (three 3-hour output periods) compared to 6 hours (two 3-hourly time steps) in the standard experiment. Further towards the south (30° N to 35° N) we find 3 tracks of very intense cyclones with long lifetimes in the sensitivity experiment, which are not present at all in the standard experiment. A closer look reveals that these are hurricanes which appear in the same month (September) in 1991, 1992 and 1999. These are the cyclones with the strongest pressure gradients - up to 50 hPa per 100 km. They are connected with wind speeds up to 42 m/s and substantial amounts of rain (up to 50 mm/h). According to the wind speed related Saffir-Simpson Hurricane Scale from the National Hurricane Center (2005) all of these cyclones are hurricanes of the lowest category (1 of 5). It is interesting to have a closer look at the structure of those simulated hurricanes, one of which even moved towards Ireland after weakening and converting to an extratropical cyclone.

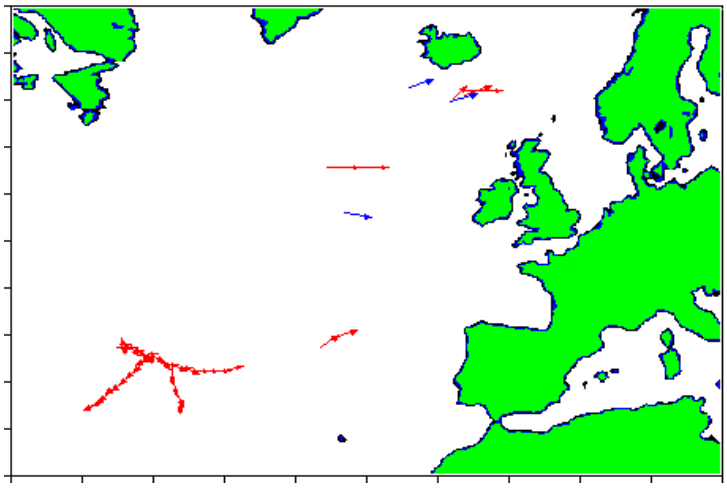

Figure 8.3: Simulated tracks of cyclones with a pressure gradient of more than 20 hPa / 100 km for the time period 1985-2000 from the standard experiment using the observed SST (blue arrows) and from the sensitivity experiment using the SST increased by 1 K (red arrows)

8.4.3 Hurricanes in the sensitivity experiment

The strongest hurricane simulated in the increased SST experiment appears on 13 and 14 September 1999. It originates at 34° N and travels slowly southwards reaching its maximum pressure gradient of 50 hPa per 100 km on 14 September 1999, at 0000 UTC. At this stage the hurricane produces wind speeds up to 42 m/s and therefore close to category 2 on the Saffir-Simpson Hurricane Scale. Figure 8.4 shows the sea level pressure, precipitation, 10-metre wind speed and latent heat flux on 14 September 1999, at 0000 UTC. The eye of the hurricane can clearly be seen with less intense precipitation, weaker winds and latent heat fluxes compared to the adjacent regions. While the hurricane on 13 and 14 September 1999 does not exist at all in the standard experiment, between 26 and 29 September 1992 the hurricane in the sensitivity experiment has a weak cyclone as a counterpart in the standard experiment. The hurricane moves towards Ireland while weakening, transforming into an ordinary cyclone and merging with a low pressure system in the northwest (Figure 8.5). Even if the storm has weakened during its journey to Ireland, it still yields considerable amounts of rain (up to 5 mm/h) over the southwest of Ireland and wind speeds up to 26 m/s south of the country. It suggests that hurricanes evolving further northwards due to higher SSTs compared to present day climate might influence parts of Europe.

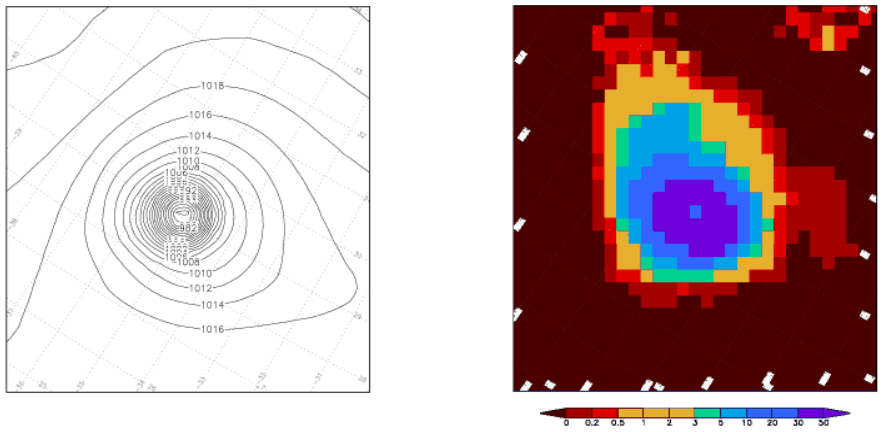

(a) *(b)*

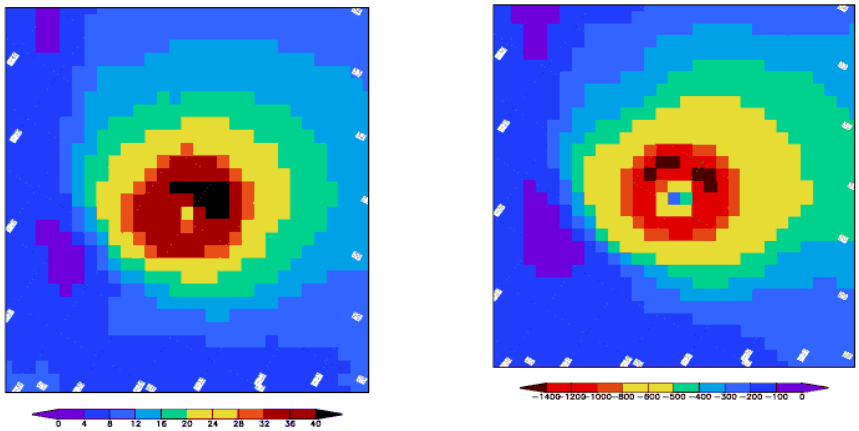

(c) *(d)*

Figure 8.4: Simulated hurricane in the sensitivity experiment on 14 September 1999, 00 UTC. (a) Mean sea level pressure [hPa], (b) precipitation [mm/h], (c) 10 m wind speed [m/s], (d) 30 m latent heat flux [W/m^2]. The dotted lines indicate the geographical latitudes and longitudes.

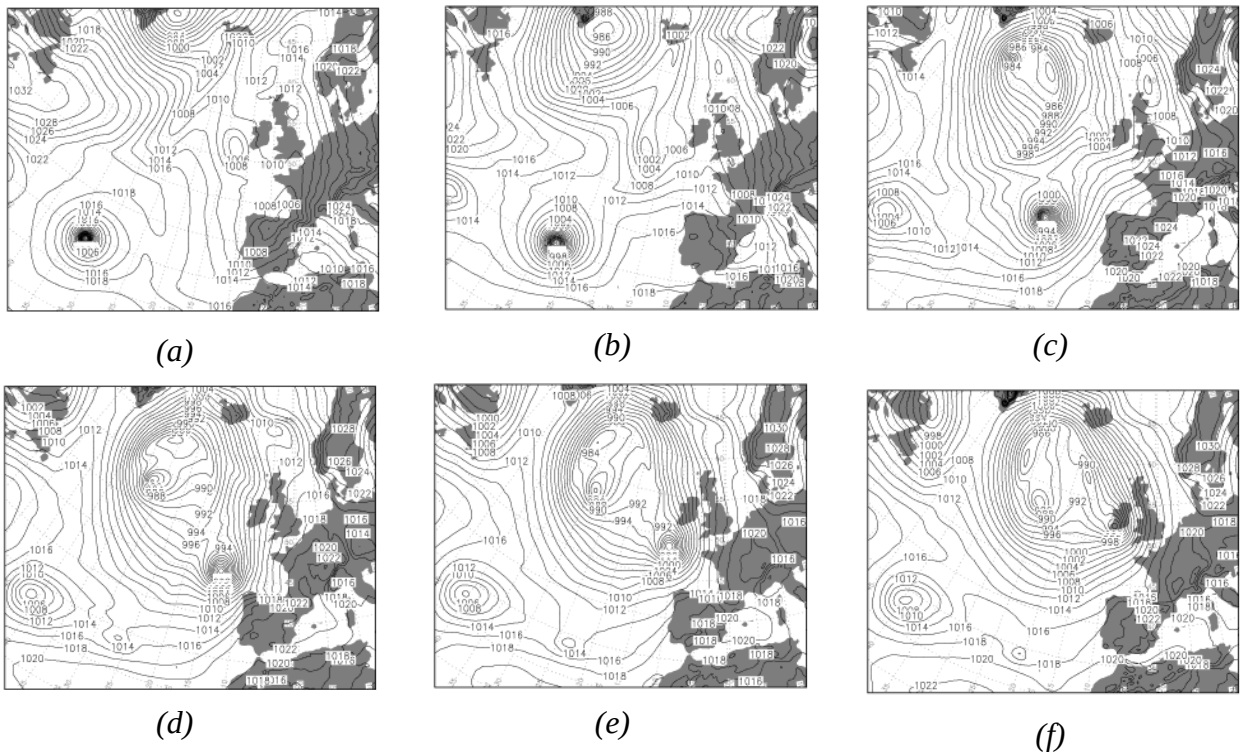

Figure 8.5: Simulated hurricane/cyclone in the sensitivity experiment on (a) 26 September 1999, 00 UTC, (b) 27 September 1999, 00 UTC, (c) 28 September 1999, 00 UTC, (d) 28 September 1999, 12 UTC, (e) 28 September 1999, 18 UTC, (f) 29 September 1999, 00 UTC.

8.5 Wind speed

It is to be expected that an increase in the frequency and intensity of cyclones will also affect the wind speed. Figure 8.6 shows the wind speed averaged over the full simulation period (1985-2000) for both the standard and sensitivity experiment and also includes a plot of the speed ratio. The spatial distribution of strong and weak wind speeds does not seem to be affected by the increased SST. The maximum wind speeds still occur south of Greenland and Iceland, whereas the wind speeds over land are clearly lower than over sea, which is what we expect. Except for the boundary relaxation zone of the model, which extends over 16 grid points into the domain i.e. a distance of about 427 km, there are slight increases in the mean wind speed of up to 3% in the sensitivity experiment compared to the standard experiment (Figure 8.6c). Over land the increases are generally lower and mostly remain below 2%. Whereas the SST is fixed to be 1 K higher in the sensitivity experiment compared to the standard experiment, the increases in surface temperature over land, which are induced by warmer air coming from sea regions, are generally less than 1 K. This could be a reason for the lower increases in the mean wind speed.

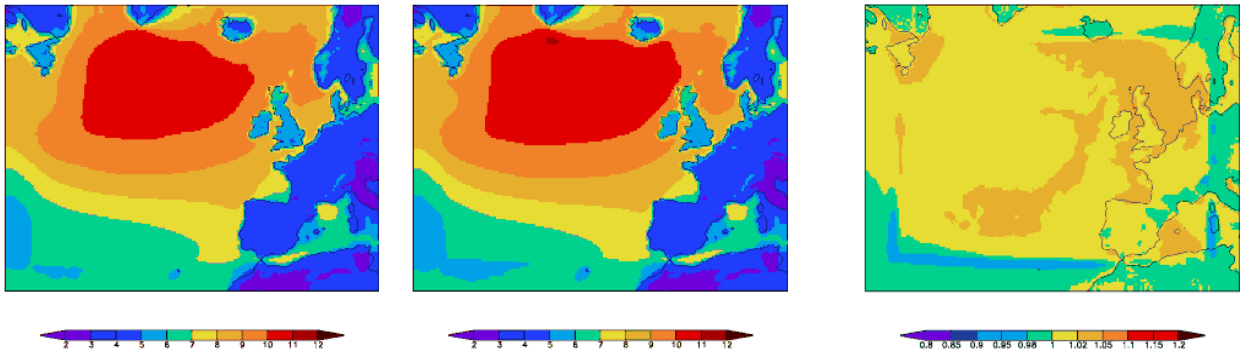

(a) *(b)* *(c)*

Figure 8.6: Mean wind speed [m/s] over the simulation period 1985-2000 from (a) the standard experiment, (b) the sensitivity experiment and (c) ratio sensitivity experiment over standard experiment

If we examine the maximum wind speed recorded over the whole simulation period (Figure 8.7) it is possible to distinguish the tracks of single cyclones that caused the strong winds. In particular the 3 simulated hurricanes in the sensitivity experiment (Figure 8.7b) can be recognized by high maximum wind speeds in the south-west of the model domain. The track of the hurricane in September 1992 (discussed in section 8.4.3), which traveled northeastwards and finally reached Ireland after weakening and transforming into an ordinary cyclone, can be recognized. As expected, the plots do not look as smooth as for the mean wind speed. The ratio plot shows some regions with stronger winds in the sensitivity experiment compared to the standard experiment and other regions with weaker winds. However, the regions with stronger winds prevail, suggesting that an increased SST will not only lead to stronger mean wind speeds but also to more intense wind storms.

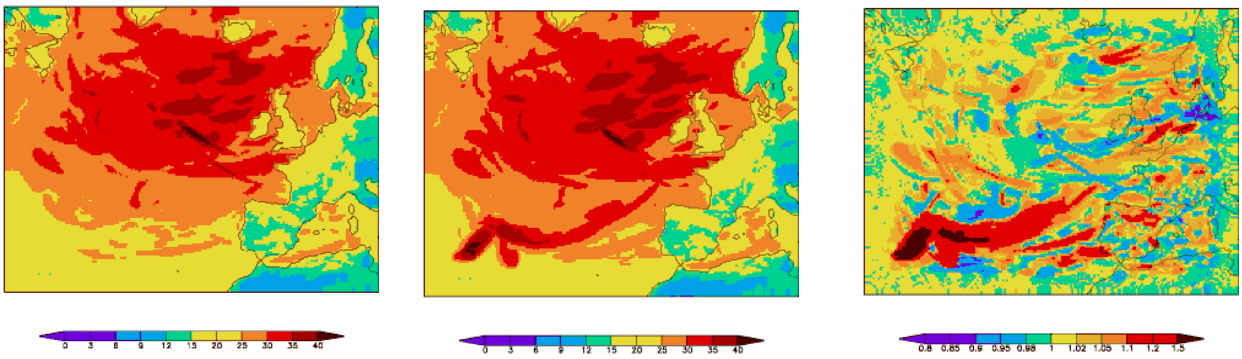

(a) *(b)* *(c)*

Figure 8.7: Maximum wind speed [m/s] over the whole simulation period 1985-2000 from (a) the standard experiment, (b) the sensitivity experiment and (c) ratio sensitivity experiment over standard experiment

8.6 Conclusions

In this study it has been shown, that the North Atlantic SST has a clear influence on the number of cyclones. Two experiments with the Rossby Centre regional Atmospheric climate model, RCA, one using the SST from ERA-40 and the other using the same SST increased by 1 K, have shown that the total number of cyclones with pressure gradients of more than 2 hPa per 100 km is 9.1% higher in the sensitivity experiment compared to the standard experiment. In particular, the number of intense cyclones with pressure gradients of more than 20 hPa per 100 km in the standard experiment is increased by a factor of more than 6 in the sensitivity experiment. This is a very large increase and has not been reported in previous studies that include other changes apart from the SST, such as in the circulation and the meridional temperature gradient. The reason for this very large increase is related to the development of 3 hurricanes in the sensitivity experiment. These develop in the south-west of the model domain between 30 and 35° N in same month, September, in the years 1991, 1992 and 1999. The hurricanes remain very strong over several days resulting in major amounts of rain (up to 50 mm/h) and very strong wind speeds (up to 42 m/s). Interestingly, one of the hurricanes even reaches Ireland after weakening considerably and transforming into an extratropical cyclone. Even at this stage it still leads to heavy precipitation (up to 5 mm/h) and strong wind speeds (up to 26 m/s) suggesting, that the remnants of hurricanes could influence European coastal areas in a world with a warmer SST.

However, the results concerning the intense cyclones should be treated with caution. Even if the total number of cyclones and the pressure distribution are very similar between the ERA-40 re-analysis data and the standard experiment, giving us confidence in our simulation, the number of very intense cyclones is a lot higher in the standard experiment compared to the ERA-40 data. One explanation for this is that the relatively low resolution of the ERA-40 re-analysis fields does not allow the development of very strong pressure gradients. Nevertheless it is difficult to assess whether the simulation of the strong pressure gradients is realistic. However, we know that such strong pressure gradients do occur in the real atmosphere and that hurricane developments in situations with high SSTs close to 27° C are plausible.

It is possible that the model setup in the sensitivity experiment may favour the development of cyclones, because only the SST, and not the atmospheric temperatures in the lateral boundaries, are changed, which leads to a more unstable stratification in the sensitivity experiment compared to the standard experiment. According to Geng and Sugi (2003) this influences the baroclinicity and therefore the number of cyclones. However, the influence of baroclinicity on the number of very strong cyclones is not as clear. Thus in terms of the development of the very strong cyclones our sensitivity experiment is not necessarily affected by the decreased static stability. Probably increased water vapour availability and related stronger latent heat fluxes are more important for the number of very strong cyclones.

The fact that the number of intense cyclones increases more than the total number of cyclones is somewhat consistent with changes observed in the present day climate and in simulations of the future climate based on increasing greenhouse gas concentrations. In the latter case, the number of intense cyclones increases and the total number of cyclones decreases in the majority of the studies discussed in detail in section 8.1. In these studies not only is the SST increasing but there are also changes in the meridional temperature gradient and the general circulation. The results of our study, combined with the results of studies that include other changes apart from an increasing SST, suggest that a decreasing total number of cyclones would be connected with a decreasing meridional temperature gradient and a

decreasing baroclinicity, while an increasing number of intense cyclones would be connected to a higher SST. The increased SST leads to a higher water vapour concentration (3% higher in our sensitivity experiment compared to the standard experiment averaged over the whole model domain) and stronger surface latent heat fluxes (16% stronger in our sensitivity experiment compared to the standard experiment). But to confirm this, further investigations would be needed. A sensitivity study with increased SST plus increased atmospheric temperatures at the lateral boundaries to avoid an increase of unstable situations, as well as a sensitivity study with a changed meridional temperature gradient, would be desirable to further distinguish between the different influences on cyclone development.

References

Blender R, Schubert M. 2000. Cyclone tracking in different spatial and temporal resolutions. *Monthly Weather Review,* **128**: 377-384.

Chan JCL, Duan Y, Shay LK. 2001. Tropical Cyclone Intensity Change from a Simple Ocean-Atmosphere Coupled Model. *Journal of the Atmospheric Sciences,* **58**: 154-172.

Chen S-J, Kuo Y-H, Zhang P-Z, Bai Q-F. 1992. Climatology of explosive cyclones off the east Asian coast. *Monthly Weather Review,* **120:** 3029-3035.

Davis C, Bosart LF. 2002. Numerical simulations of the genesis of hurricane Diana (1984). Part II: Sensitivity of Track and Intensity Prediction. *Monthly Weather Review,* **130:** 1100-1124.

De Maria M, Kaplan J. 1994. Sea surface temperature and the maximum intensity of Atlantic tropical cyclones. *Journal of Climate*, **7**: 1324-1334.

Geng Q, Sugi M. 2001. Variability of the North Atlantic Cyclone Activity in Winter Analyzed from NCEP-NCAR Re-analysis Data. *Journal of Climate,* **14**: 3863-3873.

Geng Q, Sugi M. 2003. Possible change of extratropical cyclone activity due to enhanced greenhouse gases and sulfate aerosols – study with a high-resolution AGCM. *Journal of Climate,* **16**: 2262-2274.

Gyakum JR, Danielson RE. 2000. Analysis of Meteorological Precursors to Ordinary and Explosive Cyclogenesis in the Western North Pacific. *Monthly Weather Review*, **128**: 851-863.

Hall NMJ, Hoskins BJ, Valdes PJ, Senior CA. 1994. Storm tracks in a high-resolution GCM with doubled carbon dioxide. *Quarterly Journal of the Royal Meteorological Society,* **120**: 1209-1230.

Hobgood JS. 2003. Maximum Potential Intensities of Tropical Cyclones near Isla Socorro, Mexico. *Weather and Forecasting*, **18:** 1129-1139

Jones C. 2001. A brief description of RCA2. *SWECLIM Newsletter,* **11**: 9-14.

König W, Sausen R, Sielmann F. 1993. Objective Identification of Cyclones in GCM Simulations. *Journal of Climate,* **6**: 2217-2231

Lambert SJ. 1995. The effect of enhanced greenhouse warming on winter cyclone frequencies and strengths. *Journal of Climate,* **8**: 1447-1452.

McCabe GJ, Clark MP, Serreze MC. 2001. Trends in Northern Hemisphere Surface Cyclone Frequency and Intensity. *Journal of Climate,* **14**: 2763-2768.

National Hurricane Center, cited 2005. [Available online at http://www.nhc.noaa.gov/aboutsshs.shtml]

Paciorek CJ, Risbey JS, Ventura V, Rosen RD. 2002. Multiple Indices of Northern Hemisphere Cyclone Activity, Winters 1949-99. *Journal of Climate,* **15**: 1573-1590.

Pavan V, Hall N, Valdes P, Blackburn M. 1999. The importance of moisture distribution for the growth and energetics of mid-latitude systems. *Ann. Geophys.,* **17**: 242-256.

Rummukainen M, Raisanen J, Bringfelt B, Ullerstig A, Omstedt A, Willen U, Hansson U, Jones C. 2001. A regional climate model for Northern Europe: Model description and results from the downscaling of two GCM control simulations. *Climate Dynamics,* **17**: 339-359.

Sinclair MR, Watterson IG. 1999. Objective Assessment of Extratropical Weather Systems in Simulated Climates. *Journal of Climate,* **12**: 3467-3485.

Zhang Y, Wang W-C. 1997. Model-Simulated Northern Winter Cyclone and Anticyclone Activity under a Greenhouse Warming Scenario. *Journal of Climate,* **10**: 1616-1634.

9 Sensitivity of the downscaling to boundary data resolution

A test experiment was run with the RCA climate model to investigate the effect of lowering the resolution of the driving boundary data from T159, the resolution of the ERA-40 data used in the validation of the model, to T42, the resolution of the ECHAM4 data used to drive future simulations. Simulations were run with both sets of data for one year on a large domain. With the exception of precipitation both simulations showed good agreement with observed weather parameters over the period. In the case of precipitation, agreement was less good, the model producing too many light precipitation events and lacking sufficient seasonal variability. More importantly, there were also differences between the two simulations, most noticeably in summer when the simulation driven by lower resolution boundary data showed a greater over-prediction of precipitation compared to the simulation driven by the higher resolution boundary data.

9.1 Introduction

For regional climate modelling to be effective the large scale features of the driving GCM data must be left largely unchanged by the regional simulation. Experiments with the RCA model driven with ERA-40 and ECHAM4 GCM data showed that this was essentially the case when the integration area is relatively small (sections 3 and 5) but it is not clear whether the same applies for larger domains, particularly when there is a large mismatch between the resolutions of the models. With an RCA horizontal grid resolution of 0.12 degrees the resolution ratio is approximately 9:1 for ERA-40 driving data but this increases to approximately 24:1 for the coarser ECHAM4 data. Is such a large ratio detrimental to the downscaling?

In this experiment the sensitivity of the downscaling to the resolution of the driving data was tested using two sets of ERA-40 driving data: a reference set retrieved with the "native" resolution, T159, and a coarse set filtered to T42 resolution. The filtering is done on the global fields by truncating the summation of the spherical harmonic components; this simplifies the design of the experiment.

9.2 Experiment design

The area used, and the surface geopotential at the two resolutions, is shown in Figure 9.1. At a resolution of T42 Ireland and the UK are represented in very coarse detail while the sea areas show marked undulations in height that arise from the spectral representation of the orography. Improvements can be seen with the move to T159, with Ireland and the UK now showing distinct contours, and the changes in height over the sea are greatly reduced. The RCA model, with a 0.12 degree resolution, shows a much more realistic representation of the land areas and the sea is flat, as the RCA is a grid-point model and the orography is not spectral.

Test simulations with the RCA model were run for one year (1993) using boundary data retrieved from the ECMWF MARS archive at the native resolution of T159, and at a resolution of T42.

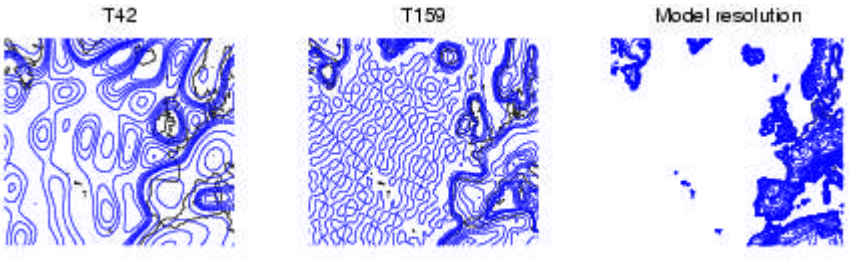

Figure 9.1: ERA-40 surface geopotential for T42 and T159 resolutions compared with the RCA surface geopotential (0.12 degrees resolution).

The different spectral orographies have an initial impact on the output parameters as the driving data are used to initialise the full area at the start of a simulation. Differences are noticeable up to about 3 hours after startup in the mean sea level pressure (MSLP) field, a little longer in other fields (e.g. relative humidity at 1000 hPa), but are no longer noticeable in any field after about 9 hours.

9.3 Comparison of MSLP for RCA-T42 and RCA-T159

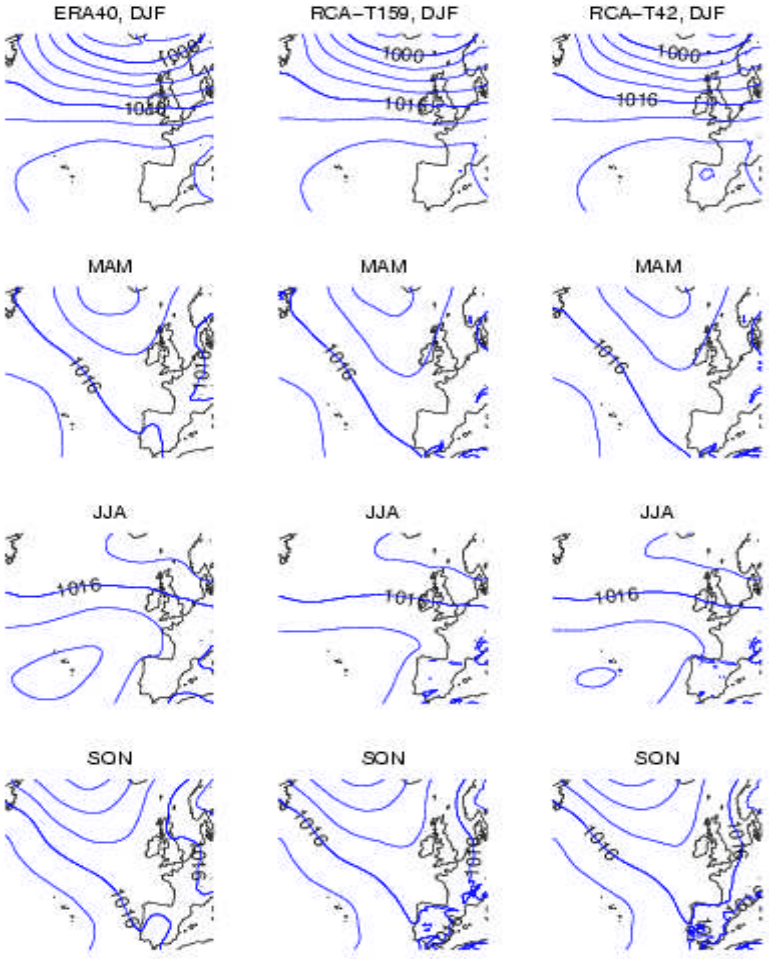

Figure 9.2: Mean Seasonal MSLP RCA-T42, ERA-40 and RCA-T159

The MSLP outputs of the RCA simulations driven by ERA-40 data at T159 and T42, hereafter called RCA-T159 and RCA-T42, were compared against ERA-40 MSLP data (at the native resolution, T159). The plots of mean seasonal MSLPs are shown in Figure 9.2. There is good agreement between the ERA-40 MSLP and the model output, for both RCA-T42 and RCA-T159. The model has a positive bias over the domain for winter (DJF), and a negative bias for spring (MAM) and summer (JJA). The lower-resolution RCA-T42 seasonal MSLP matches the ERA-40 data better than RCA-T159 for all seasons except DJF, but the differences are quite small.

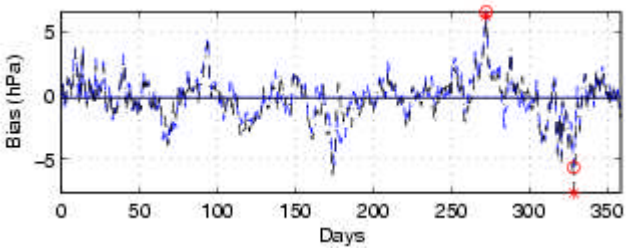

(a) Bias, RCA-T42 (blue), RCA-T159 (black)

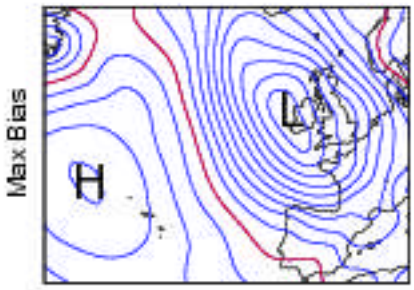

(b) ERA-40

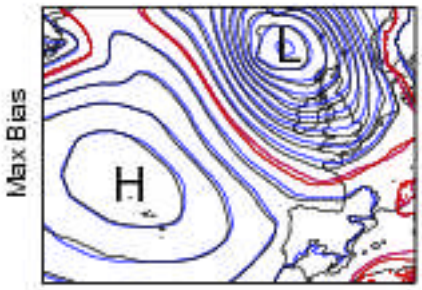

(c) RCA-T42 (blue), RCA-T159 (black)

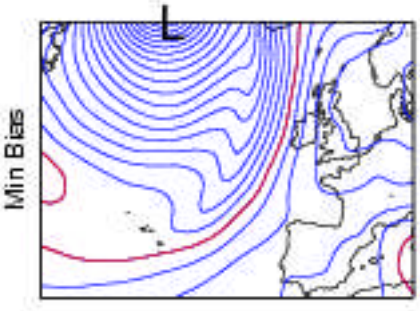

(d) ERA-40

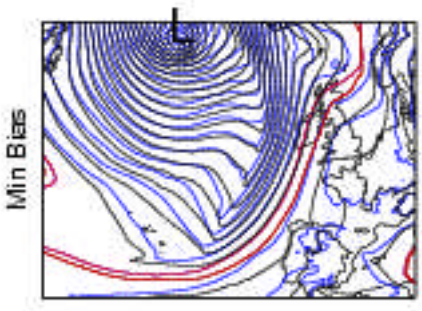

(e) RCA-T42 (blue), RCA-T159 (black)

Figure 9.3: (a) MSLP bias for RCA-T42 and RCA-T159, red star indicates extreme RCA-T159 bias, red circles the extreme RCA-T42 bias, (b) ERA-40 MSLP at time of bias maximum, (c) RCA-T42 and RCA-T159 at time of maximum bias, (d) ERA-40 MSLP at time of minimum bias, (d) RCA-T42 and RCA-T159 at time of minimum bias. The 1016 hPa contour is shown in red to aid comparison

A better idea of the behavior of the MSLP output of the two models is given by considering the bias calculated over the domain, shown in Figure 9.3(a). Both the RCA- 42 bias (blue) and the RCA-T159 bias (black) follow a very similar trend, deviating from the ERA-40 values during the same events. The mean bias for both models is small, with RCA-T42 slightly smaller: -0.1 hPa compared to RCA-T159's -0.3 hPa. The dates corresponding to the largest positive and negative bias were also the same for both models. Figure 9.3(b) shows the ERA-40 MSLP at the time of maximum bias, while Figure 9.3(c) shows the MSLP of RCA-42 and RCA-T159 at this time. It can be seen that both simulations have deviated from the ERA-40 in the same manner. Figures 9.1.2(d) and 9.1.2(e) show a similar result for the date of the largest negative bias.

To examine the spatial pattern differences between the experiments a spatial correlation coefficient is used. This is defined as

$$CorrX = \frac{\sum_i \sum_j (a_{ij}^m - \overline{a_{ij}^m})(a_{ij}^o - \overline{a_{ij}^o})}{\left[\sum_i \sum_j (a_{ij}^m - \overline{a_{ij}^m})^2 \sum_i \sum_j (a_{ij}^o - \overline{a_{ij}^o})^2\right]^{\frac{1}{2}}}$$

where *a* is the parameter being investigated, subscripts *i, j* are the grid-point indices, superscripts *m, o* are the model data and observed data respectively, and the overbar denotes spatial averaging.

The spatial correlation coefficient for the MSLP is shown in Figure 9.4(a). On average, agreement between the model and ERA-40 data is good. Furthermore, when the simulations do deviate from the ERA-40 data, they appear to do so in the same manner, suggesting that the resolution of the driving data does not have a strong influence on these events. There are, however, two events during which the model significantly deviates from the ERA-40 data. The ERA-40 MSLP plot for the first of these events is shown in Figure 9.4(b), with isobars below 1016 hPa shown in red to aid in the visual comparison of the figures. A high pressure ridge runs from Ireland across the domain in a southwesterly direction. Figures 9.1.3(c) and 9.1.3(d) show the same event for RCA-T159 and RCA-T42 respectively. The high pressure ridge is missed in the model simulations. The depression in the north- west has instead split and moved towards the centre of the domain. Figures 9.1.3(e), (f) and (g) similarly show the second event with a poor spatial correlation. In this case both simulations are very similar but differ substantially from the ERA-40 pattern.

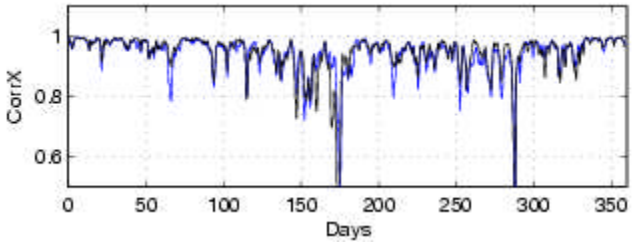

(a) Spatial Correlation Coefficient, RCA-T42 (blue), RCA-T159 (black)

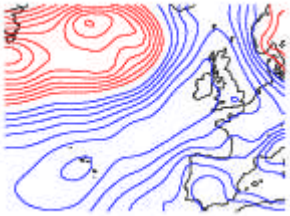

(b) ERA-40

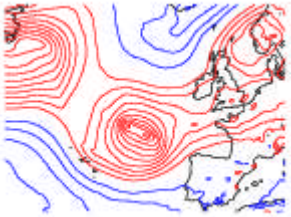

(c) RCA-T159

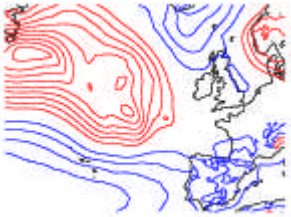

(d) RCA-T42

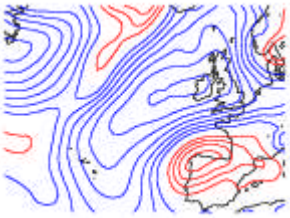

(e) ERA-40

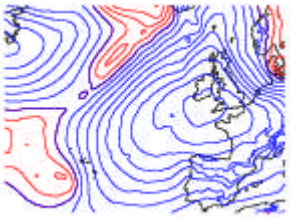

(f) RCA-T159

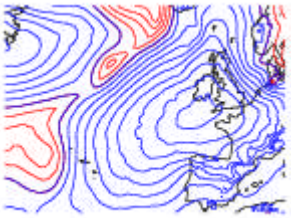

(g) RCA-T42

Figure 9.4: (a) Spatial Correlation Coefficient for RCA-T42 and RCA-T159, (b) ERA-40, (c) RCA-T159, (d) RCA-T42 MSLP for first low correlation event, (e) ERA-40, (f) RCA-T159, (g) RCA-T42 MSLP for second low correlation event. Contour spacing is 4 hPa, and contours < 1016 hPa are red to aid comparison

Cyclone statistics for the year are shown in Figure 9.5: ERA-40 data are shown in red, RCA-T42 data in blue, and RCA-T159 data in black. There is good agreement between the simulations and ERA-40 for the numbers of cyclones with core pressures less than 1000 hPa (Figure 9.5(a)) and the seasonal dependence of the numbers (Figure 9.5(b)). In the latter case RCA-T159 slows slightly better agreement with the ERA-40 data compared with RCA-T42.

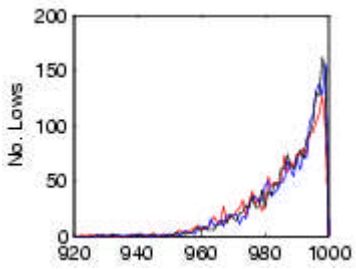

(a)

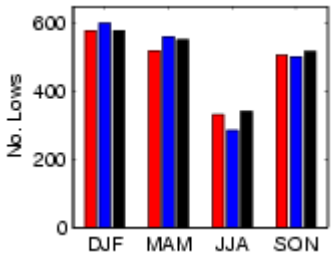

(b))

Figure 9.5: Cyclone statistics, (a) number of cyclones at different core pressures, (b) number of cyclones < 1000 hPa by season. ERA-40 (red), RCA-T159 (black), RCA-T42 (blue)

9.4 Comparison of 2-metre temperature

The mean RCA-T42 and RCA-T159 simulated 2-metre temperatures, stratified by season (1 year only), are shown in Figure 9.6 together with observed temperatures based on UKCIP data. Both of the simulations produce output that is in good agreement with the UKCIP data; the spatial pattern and local values are reasonably well reproduced. Compared with RCA-T42, RCA-T159 temperatures are perhaps in slightly better agreement with the UKCIP data in winter, spring and autumn.

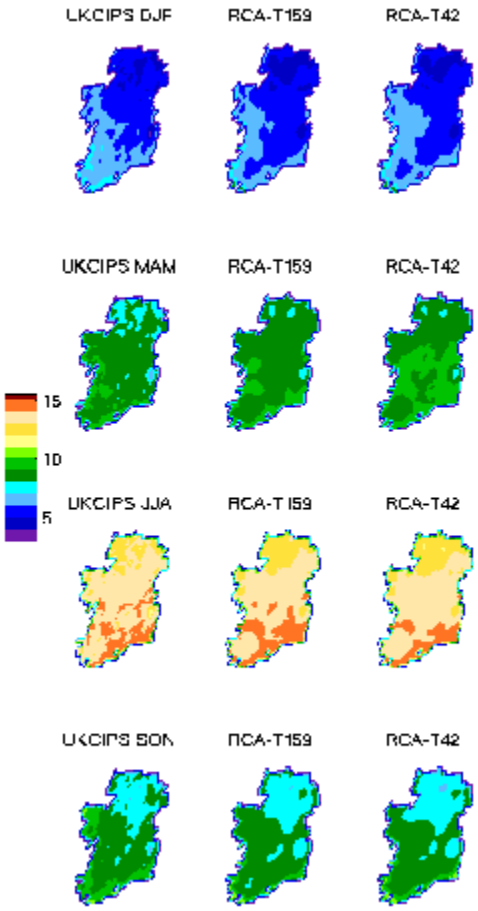

Figure 9.6: Seasonal 2-metre Temperature

9.5 Comparison of precipitation

Precipitation data stratified by season for both simulations and for the UKCIP data are shown in Figure 9.7. For winter, the rainfall spatial patterns and the mean rainfall (averaged over Ireland) for both simulations are close to those observed, but the simulations over-predict the mean values for the other seasons. Thus the seasonal variability of the mean precipitation is under-predicted by the model. Mean rainfall amounts produced by the two simulations agreed well with each other except during the summer, when the lower resolution boundary run (RCA-T42) produced more rainfall than RCA-T159, giving quite poor agreement with the UKCIP data.

Rainfall amounts in the 95th percentile were lower than those observed in winter, and higher in summer. Again, model seasonal variability was too low, and RCA-T42 values were too high in summer. Looking at the other end of the rainfall scale, amounts in the 5th percentile are too high for all seasons, with values twice as high as observed. This is consistent with previous findings of the model producing too much rainfall for low rainfall events.

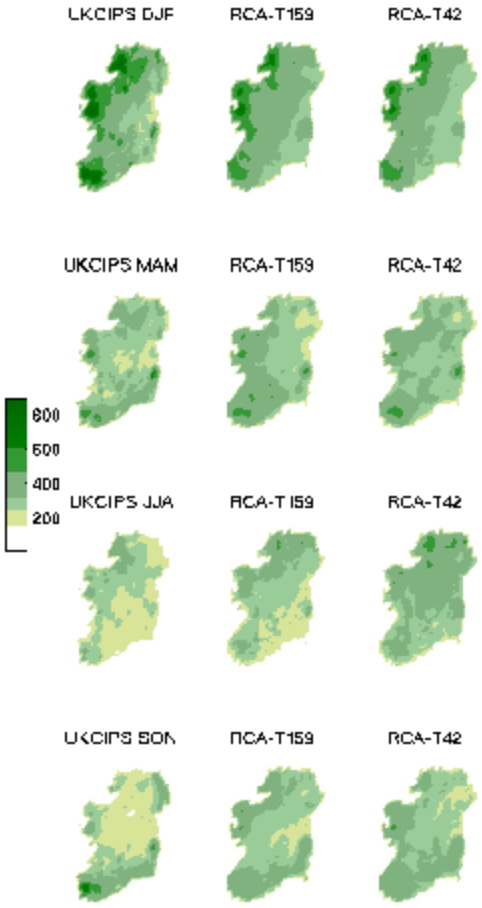

Figure 9.7: Seasonal precipitation

9.6 Conclusions

Simulations were run over a large area, and at a high resolution, to investigate the effect of different boundary data resolutions on the output. In general, agreement between the model output and ERA-40/UKCIP data was found to be quite good. For the MSLP fields, large departures relative to the ERA-40 reference data occasionally occur but both simulations tend to show the same error. Overall, the resolution difference appears to have a mostly neutral impact on the MSLP fields.

Statistical data on the number of lows produced over the whole year showed that the seasonal differences were well captured.

Data for the 2-metre temperature also showed good agreement between the simulations and observed data with no apparent advantage of one simulation over the other.

The precipitation statistics showed larger differences. The model did not produce the same seasonal variability as seen in the observations, and tended to produce too many small precipitation events. More importantly, there were also differences between the two simulations, most noticeably in summer when the simulation driven by lower resolution boundary data showed an even stronger over-prediction of precipitation compared to the simulation driven by the higher resolution boundary data.

This difference between the simulations could be sensitive to the domain size and needs to be explored further, particularly for dry or very wet periods. The vertical resolution is also an issue that needs to be investigated. The ECHAM4 T42 data, for example, are on 19 vertical levels whereas the ERA-40 data are on 60. Running the same experiments with a reduced number of vertical levels in the ERA-40 driving data should shed some light on the sensitivity of the RCA downscaling to vertical resolution.

10 Spatial and temporal errors in stratospheric radiosonde data: implications for climate change detection[2]

Radiosonde data are a valuable resource in the detection of climate change in the upper atmosphere. Long time series of stratospheric temperature data, carefully screened and corrected to remove errors, are available for this purpose. Normal reporting practice usually ascribes a fixed time and position (the station location) to all data reported in the ascent. This report examines the magnitude of the errors associated with this practice using simulated radiosonde data generated from the ECMWF re-analysis archive. The results suggest that the temperature errors, while generally small in the troposphere, are significant in the upper stratosphere, particularly in the jet stream areas, and may mask genuine data trends associated with climate change. Errors in the wind and humidity data are also examined.

10.1 Introduction

While the upper-air observing stations were primarily established to support operational weather forecasting, the sounding data they provide are a valuable resource for studying changes in the climate. However, the nature of the observations and the supporting station practices are not conducive to securing a homogeneous sequence of data extending over many years. Changes in the sonde type, inappropriate corrections for radiative heating or cooling of the temperature sensors, or changes in the reporting practice, make it a challenging task to identify genuine climate change signals in a sequence of observations. The situation is particularly acute in the stratosphere where the low air density may lead to inadequate sensor ventilation and spuriously high temperatures arising from solar heating. In spite of this, considerable effort has been devoted to identifying and correcting the errors and to make a homogeneous dataset acceptable for climate investigations. The Comprehensive Aerological Reference Data Set (CARDS) Project (Eskridge et al. 1995), for example, has led to the creation of a database of observations, screened with state-of-the-art quality control procedures, together with metadata describing any relevant changes in equipment or station practices. Even with such initiatives it is difficult to eliminate spurious signals associated with radiative errors or changes in station practices (Zhai and Eskridge 1996; Luers and Eskridge 1998; Angell 2003; Lanzante et al. 2003). It is noteworthy that only recently Redder et al. (2004) discovered a temporal coding error in the radiation bias correction scheme for U.S. Vaisala sondes, significantly reducing a systematic difference between the 0000 and 1200 UTC temperature and height measurements at some stations. Comparisons between temperature datasets derived from radiosondes and the satellites based Microwave Sounding Units (MSU) and Advanced MSU (AMSU) instruments show reasonable agreement when averaged globally or over the NH, SH and Tropics (TR) (Seidal et. al 2004) but it is doubtful whether the radiosonde data from a single station are suitable for addressing issues on local climate change in the upper atmosphere.

Here, the practice of treating each radiosonde ascent as fixed in space and time – an interpretative error – is examined to assess its impact on the detection of climate change. The remainder of this report is organized as follows: in section 10.2 the scope of the problem is addressed; section 10.3 describes the

[2] NOTE: this is a preview of an article submitted for publication.

generation of simulated radiosonde data to evaluate the errors; sections 10.4-10.6 provide estimates of the temperature error for sample stations and climate averages for geographical regions; section 10.7 examines the associated wind and humidity errors followed by a discussion and concluding remarks in section 10.8.

10.2 Drift error – coding practices for radiosonde data

The data routinely available to researchers are usually based on the products disseminated internationally for Numerical Weather Prediction (NWP). The original station data will normally contain information at significantly more levels in the vertical compared with the disseminated product and will also record the position and time of the balloon at each level. The disseminated subset is usually coded using the World Meteorological Organization (WMO) alphanumeric TEMP code (WMO 1995) and may be unpacked and repacked in the binary BUFR code (WMO 2001) by the National Weather Services for use in NWP or re-analysis projects. For land based stations the alphanumerically coded product does not include any position information; the user must match a coded station identifier with the entry in a WMO station catalogue (WMO 2004) to determine the elevation and position. The launch time of the balloon, in hours and minutes, is available in the coded data but an additional time, rounded to the nearest hour in the report, is traditionally taken to be the official observation time. To facilitate NWP the balloon may be launched approximately 1 hour ahead of the main synoptic hours (0000, 0600, 1200 and 1800 UTC) so that the mid point of the ascent matches the NWP analysis time. However, for some stations one suspects that the official observation time corresponds with the main hours and not with the balloon release time. Regardless of local practices even if the raw data are available it is clear that ascribing a fixed time to the entire ascent introduces a temporal error at best around 45 minutes and possibly as much as 90 minutes over a portion of the ascent. Note, however, that this does not affect radiative corrections performed on the data at the station. Note also that the coding practice for the balloon release time was changed in 2000.

The current TEMP and BUFR codes do not provide positional information for the horizontal movement of the sonde. Although the spatial drift may be over 200 km in the stratosphere, for many applications the drift is simply ignored.

Before the advent of high resolution NWP models the temporal and spatial errors were deemed to be small and tolerable, particularly as the horizontal grid spacings were usually much larger than the typical spatial drift. However, with the move to finer numerical grids the issue has received more attention. The NCEP mesoscale ETA model assimilation system, for example, allows for drift by assuming the sonde balloon rises at 5 ms^{-1}, using the observed winds to calculate the horizontal displacement (Manikin 2000). For climate studies it is generally assumed that the drift errors are small and do not impact on the statistical means and trends over long periods. However, this is not necessarily true: if the mean flow pattern changes, the reported data may show a spurious time trend associated with a slow change in the mean drift direction.

Recently, WMO have recognised the need for a more accurate coding of upper-air data and plan to introduce a new BUFR code format that will allow the full set of data to be transmitted on the Global Telecommunication System (WMO 2003).

10.3 Simulated radiosonde observations

10.3.1 Rationale and data generation

Even if the original station data are available it is not possible without further information to estimate the data that would have been recorded if the balloon ascent were instantaneous (time t_{ref}) and without horizontal displacement. One approach would be to match the observed data with high quality NWP analyses valid for t_{ref} and examine the differences, hereafter refer to as drift error. However, the drift error will be susceptible to errors in the observations and errors in the analyses and therefore difficult to assess particularly when looking for trends over several years of data.

Here, a different approach is used. Simulated radiosonde data are generated using ERA-40 re-analysis data generated by the European Centre for Medium-Range Weather Forecasts (ECMWF) (Simmons and Gibson 2000). For selected locations a fictional balloon is allowed to rise at 5 ms^{-1} through the atmosphere, starting at time t_{ref}, and the temperature (T), wind (components U and V) and specific humidity (Q) are computed at intervals of 30 seconds using interpolated re-analysis fields. Standard pressure level data are computed from the complete ascent. The original model level data are used to benefit from the full vertical and horizontal resolution of the model. Further details are listed in the appendix. Note that actual ascent data are usually recorded at a higher sampling frequency and normally only a selection of the original level data are disseminated. The 30 second sampling interval, producing around 200 points for an ascent to 10 hPa, was chosen to ensure reasonable accuracy in the interpolation of the data to standard levels; tests with a finer sampling interval did not produce significantly different results.

To mimic real station data, simulations were generated twice per day at the main synoptic hours i.e. t_{ref} equal to 0000 and 1200 UTC. Three types of simulated observations were generated.

(a) Full drift simulations: spatial and temporal drift allowed; position and time at each "level" are also recorded.

(b) Static simulations: no spatial or temporal drift allowed; the data are simply the vertically interpolated NWP fields valid at t_{ref} for the (fixed) location.

(c) Static offset simulations: same as (b) but data are for t_{ref} +1 hour.

Differences between matching (a) and (b) simulations and between matching (a) and (c) simulations, hereafter referred to as type I and type II data, give a measure of the drift error for actual radiosonde measurements.

Type II data are a gesture to local practices where the radiosondes are launched approximately 1 hour in advance of the reported time to ensure the mid point of the ascent corresponds approximately with

the coded report time. (A positive offset is used here simply to facilitate the data setup in running the simulations; the mid point of the full drift simulations corresponds approximately to t_{ref} +1 hour.)

Simulated observations were generated for 0000 and 1200 UTC each day for the period 1 January 1960 to 31 July 2002 for the 87 CARDS station positions (Figure 10.1; see also Lanzante et al. 2003, appendix A, for station list and positions). For convenience, individual ascent data will be referred to using the WMO identifier of the physical station. All references are to simulated data.

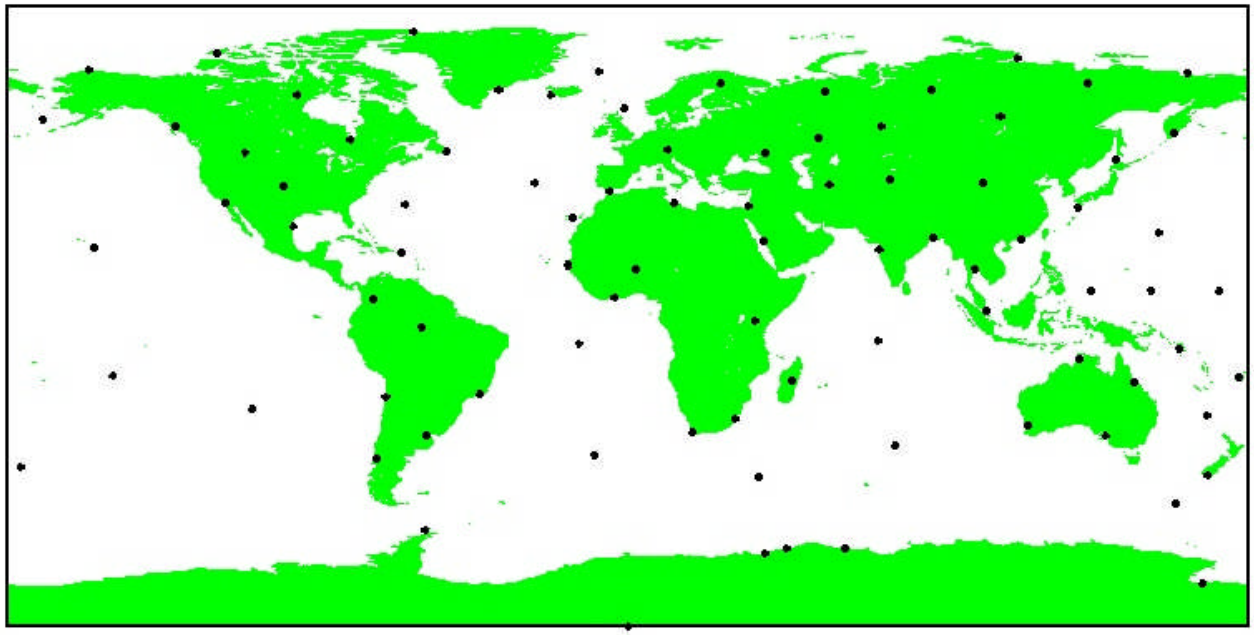

Figure 10.1: Positions of CARDS stations.

With real ascents the radio-telemetry system may lose contact with the sonde if the horizontal displacement is excessive. For example, at Valentia Observatory in Ireland the range is about 250 km although this figure can be exceeded if the atmospheric conditions are favourable. For the simulated observations this range was taken to be the cut-off point for the sounding: if the range exceeded 250 km at any level the higher level data were discarded. All discussions from hereon refer to the simulated observations generated from this dataset. Furthermore, only the differences between the simulations, as discussed above, are used; positive differences for scalar values (e.g. temperature) imply that the conventional treatment of the ascents (no drift) overestimates the value at the station.

10.3.2 Data quality

The simulated observations avoid data quality problems with real observations and as only the differences between the simulated ascents are being used for climate change evaluation the impact of errors in the re-analysis data are minimized. However, the quality of the re-analysis data is a pertinent issue as the fields are based on real observations (from terrestrial and satellite systems) and in the vicinity of upper-air stations, particularly in data-sparse regions, the analyses will be strongly influenced by the local observation and related error. In data-rich areas the impact of the radiosonde

observation errors is less of an issue as the ECMWF NWP variational assimilation system takes a global view in fitting data and will adjust fields locally to maintain physical and dynamical consistency with other data. Note that the ERA-40 assimilation system did not allow for drift in the radiosonde data.

The 1970s were a significant period for the ERA-40 assimilation system: satellite data were unavailable before 1973, prior to which the upper-air analyses are more heavily dependent on radiosonde data, and radiosonde temperatures were bias-corrected after 1979 (Andrae et al. 2004). As pointed out by Bengtsson et al. (2004) the large increase in the number of observations in the late 1970s has probably lead to an overestimation of the warming trend in the ERA-40 lower troposphere temperatures. The homogeneity of the analyses, particularly in the Southern Hemisphere prior to 1980, is also questionable (Sterl 2004) for similar reasons. The simulated observations are subject to further errors arising from the interpolation of the analysis fields, particularly from the time interpolation as the fields are only available at 6-hour intervals.

In view of the above comments it is clear that the simulated observations per se are not suitable for investigating climate change. However, we believe that the differences between the simulated datasets, as defined above, are capable of shedding light on the drift error in radiosonde observations in data-rich areas. The similarity of results from nearby stations (see 10.5) provides a measure of support for this approach. In data-sparse areas the results need to be treated more cautiously.

10.4 Drift error – general considerations

The relationship between the drift error and the atmospheric state is not intuitive. As pointed out by Macpherson (1995) in an idealised flow with advection dominant and the wind independent of height there is a cancellation between the temporal and spatial errors in the evaluation of the wind relative to a model background field. However, for other parameters (e.g. temperature) the situation is more complex and in the real atmosphere wind errors associated with the drift can also be expected. Figure 10.2 shows the temperature differences at 50 hPa for type I and type II data compared with the horizontal spatial drift for station 04018 (Keflavik). In general the largest errors are associated with extreme horizontal drift when the ascent takes place in the vicinity of jet streams. Note however that even for modest horizontal drift (<50 km) the drift error is occasionally of the order of 1 K. Analysis of data from other sites show similar patterns: the drift errors are largest in meteorologically active regions and generally low in regions with relatively light winds. To investigate the impact of the drift error on climate averages the simulated data are stratified by season (winter: December-February; spring: March-May; summer: June-August; autumn: September-November) and geographical region NH, TR and SH.

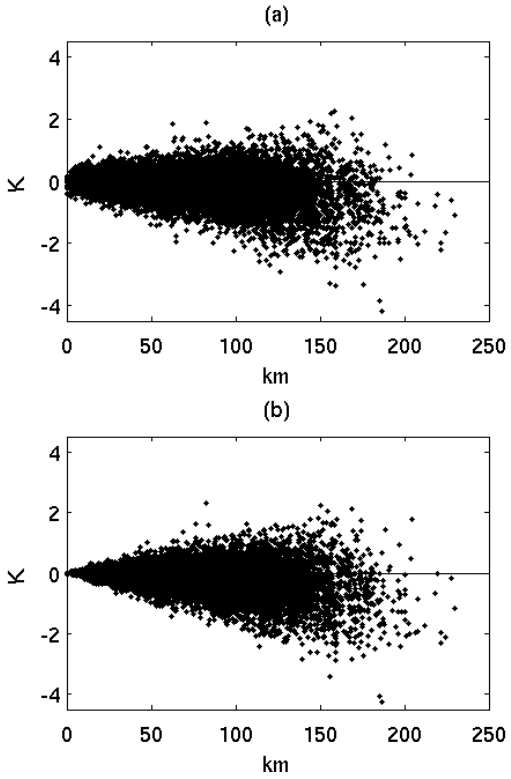

Figure 10.2: Scatter plot of temperature errors at 50 hPa for type I (a) and type II (b) data for station 04018 as a function of the horizontal displacement. Data are for 0000 and 1200 UTC for the period 1960-2002.

10.5 Drift error – climate averages: sample stations

10.5.1 Data-rich regions

Figure 10.3 shows the mean temperature drift error at 50 hPa level stratified by season for sample stations for the temporally offset type II data. For the Icelandic station 04018 (Figure 10.3a) there is a marked negative bias in the winter data, when the atmospheric flow is most active, with smaller biases in the other seasons. The pattern for the Greenland station 04360 (Angmagssalik) – located about 700 km west of 04018 – is very similar (Figure 10.3b) with mean winter biases of around -0.25 K for both stations, suggesting that the bias is a genuine regional feature. In both cases there is some evidence of a small negative trend in the bias: a linear fit of the data shows a decrease of around 0.08 K over the whole period. For station 30230 (Kirensk) the bias is positive (Figure 10.3c) with a mean value of around 0.40 K. Note that for station 08495 (North Front) the mean drift errors are very small (Figure 10.3d), reflecting the weaker wind flow regime in this area compared with stations in the higher latitudes. For type I data the mean drift errors are in all cases slightly larger (not shown). The drift errors for 04018, 04360 and 30230 are the largest in the CARDS set.

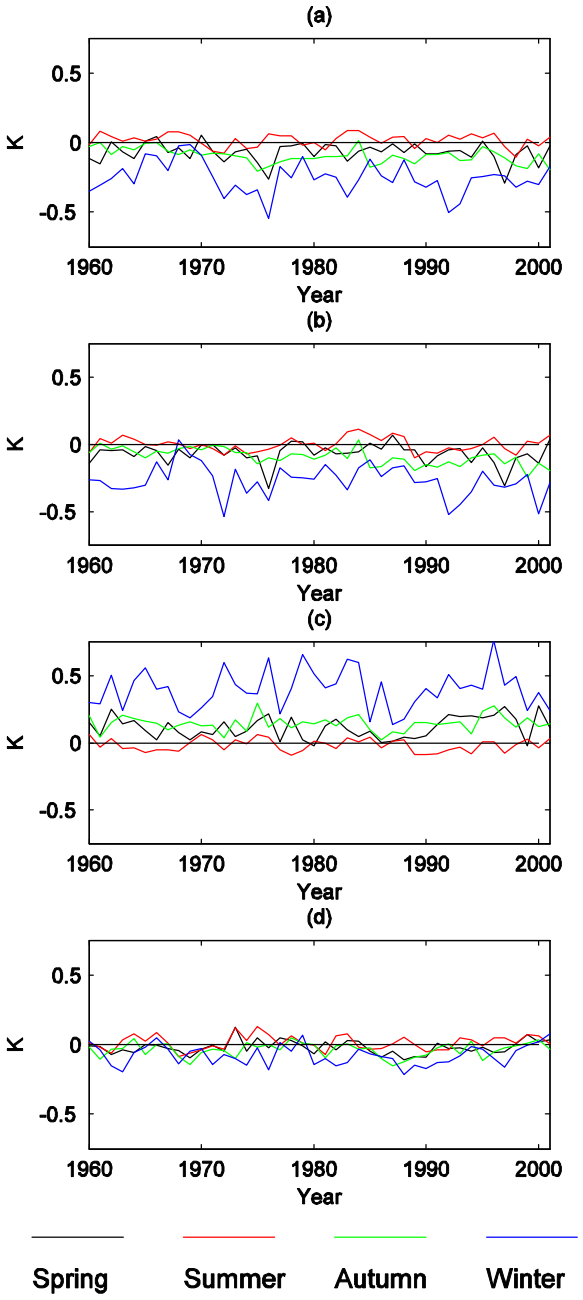

Figure 10.3: Mean seasonal temperature errors at 50 hPa for type II data for station 04018 (a), 04360 (b), 30230 (c) and 08495 (d). Data are for 0000 and 1200 UTC for the period 1960-2002 stratified by season. Winter: December-February; spring: March-May; summer: June-August; autumn: September-November.

Figure 10.4a shows the vertical profile of the mean winter bias and root-mean-square (rms) error for 04018 for type I and type II data. For both sets of data the bias is of the order of -0.1 K around 100 hPa, increasing to around -0.3 K at 10 hPa. The type II drift error has a much larger rms error in the lower atmosphere but is approximately the same, or slightly lower than, the type I rms error above 100 hPa when the measurements are temporally closer to the reference data. Note that the type II data show a small (< 0.05 K) positive bias in the lower levels but have a slighter smaller bias and rms error above

100 hPa. The extreme drift errors are smaller in the type II data (not shown). Figure 10.4b shows the same plot for station 30230 data. The maximum (positive) bias occurs around 30 hPa. Again, the type II data produce slightly reduced bias and rms error statistics above 100 hPa but both types show small negative biases below 300 hPa.

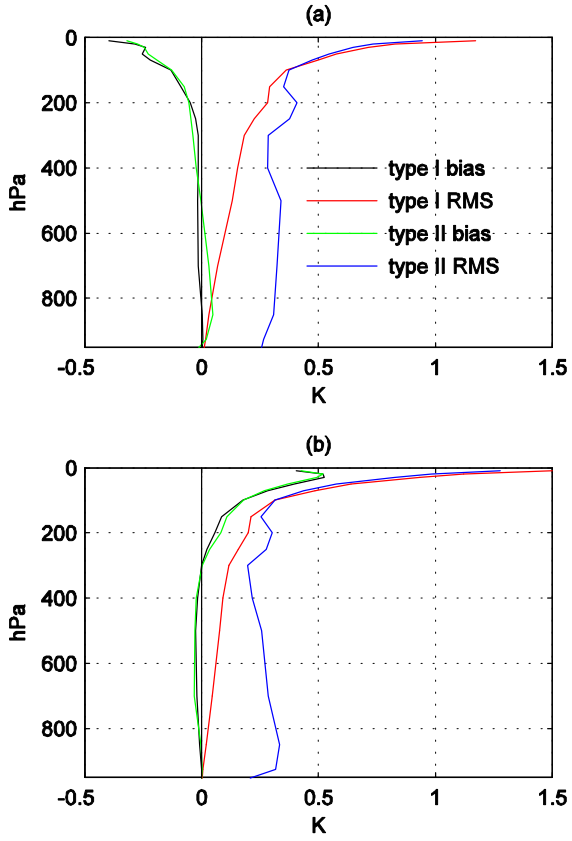

Figure 10.4: Vertical profile of the winter mean drift error for temperature for station 04018 (a) and 30230 (b). Bias and rms error are shown for type I and type II simulated observations.

It is difficult to find independent evidence for the temperature biases suggested by the simulated observations. Modern analysis systems provide feedback on the differences between the observed radiosonde data and a background NWP field; averaged over time these differences are often used to identify systematic errors in the observations. However, the presence of other errors (related to the sensors and model) makes it difficult to identify the effects due to radiosonde drift, particularly in the stratosphere. For example, mean differences (observed-background) for station 04018 for the period December 2004 to February 2005 from the ECMWF operational forecast system show a positive temperature bias of around 1 K at 50 hPa but it is not clear whether this is a genuine observation error or a reflection on the NWP model (ECMWF, personal communication).

10.5.2 Data-sparse regions

Time series plots of the temperature bias at 30 hPa for two Antarctic stations are shown in Figure 10.5.

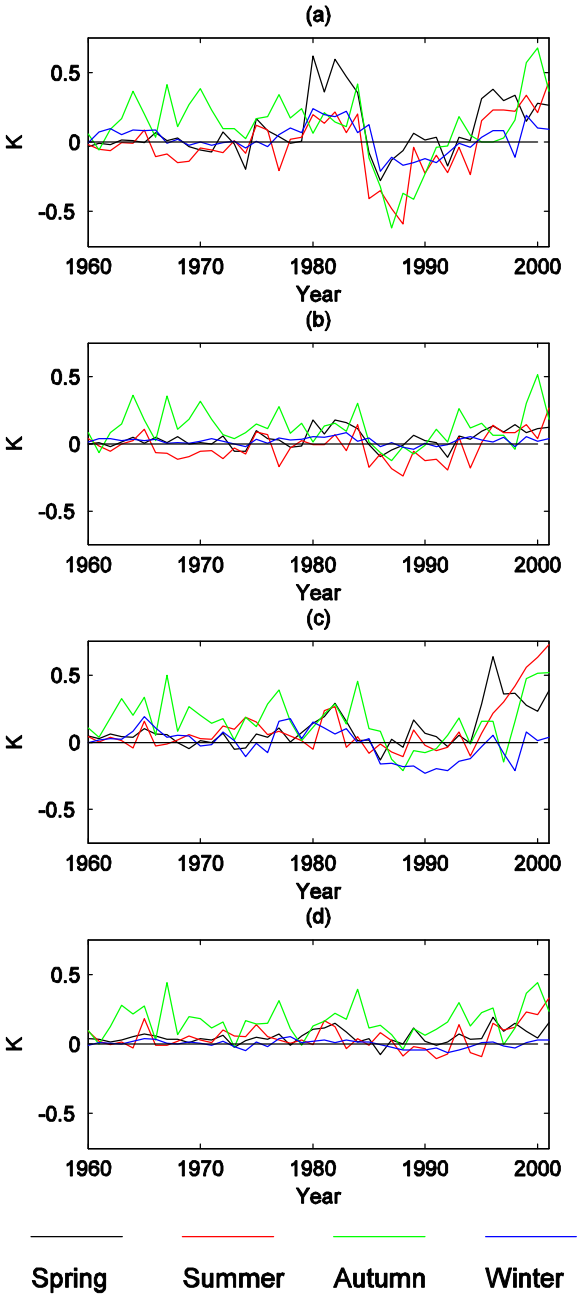

Figure 10.5: Seasonal mean drift errors for temperature at 30 hPa based on simulated observations from station 89542 for type I (a) and type II (b) data. The equivalent data for station 89564 are shown in (c) and (d). Data are for 0000 and 1200 UTC for the period 1960-2002 stratified by season. Winter: December-February; spring: March-May; summer: June-August; autumn: September-November.

Station 89542 (Molodezhnaya) shows a rise of about 1 K in the autumn bias (type I) from 1997-2001 (Figure 10.5a) but the trend is much reduced in the type II data (Figure 10.5b) and the seasonal biases are also significantly reduced. For station 89564 (Mawson) the bias pattern near the end of the century

(Figure 10.5c) and the reduction in the bias for type II data (Figure 10.5d) are similar to those from station 89542.

10.6 Drift error – climate averages: global impact

Figure 10.6 shows the vertical pattern of the bias and rms of the drift error for the combined CARDS stations in the NH.

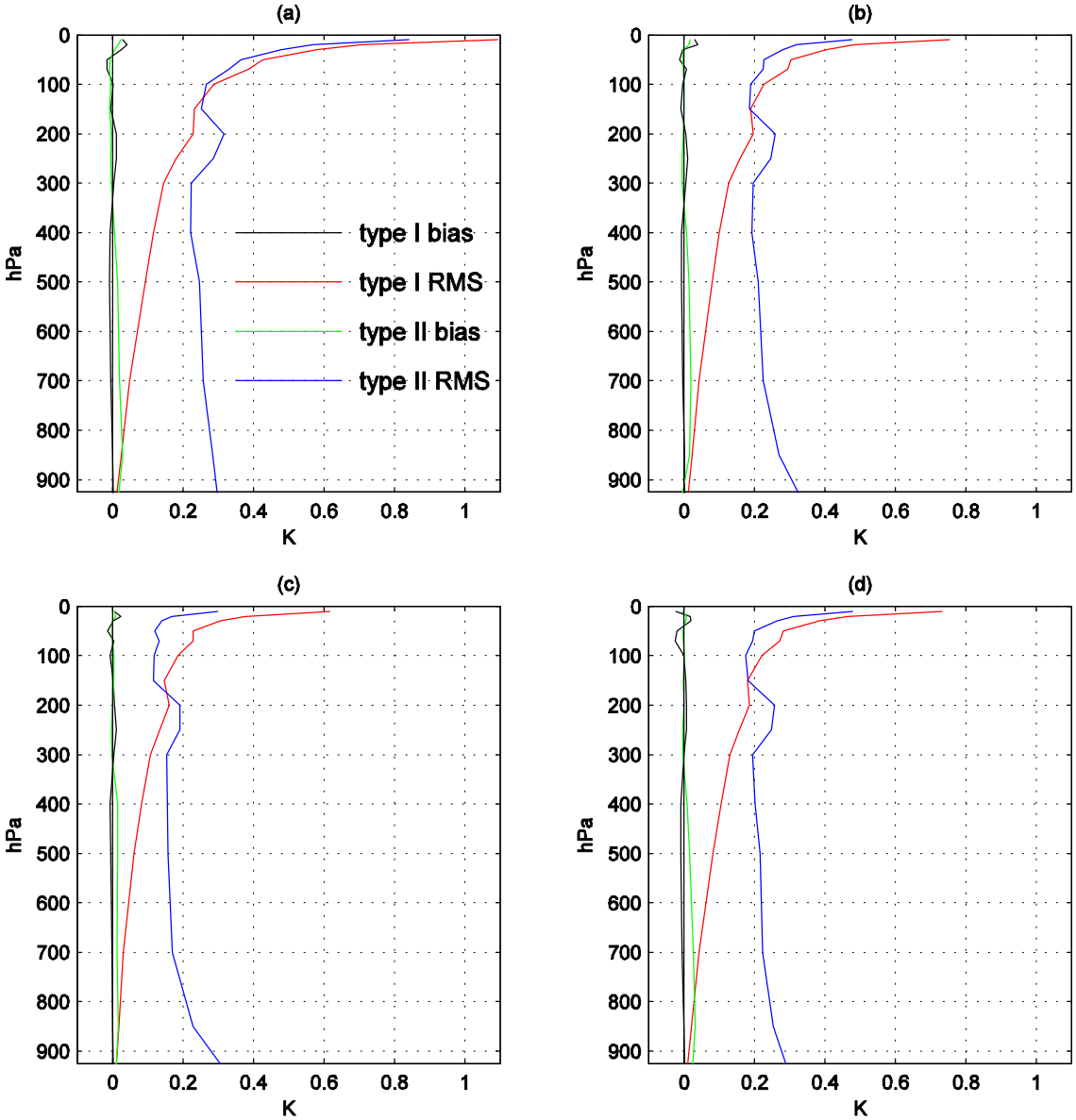

Figure 10.6: Vertical profiles of the mean seasonal temperature drift error for simulated observations (type I and type II data) in the NH (CARDS list): winter (a), spring (b), summer (c) and autumn (d).

In general the bias is very small and less than 0.05 K throughout the ascent. Note that the sign of the bias is positive for the temporally offset type II data up to about 300 hPa and that the corresponding rms errors are larger relative to the type I data. Above about 150 hPa the rms errors are generally smaller for type II data, particularly in summer. For the SH (Figure 10.7) and the TR (not shown) the patterns are very similar to those in the NH apart from a seasonal dependence in the magnitude of the rms error; the stratospheric temperature errors are a little larger but less than 0.1 K.

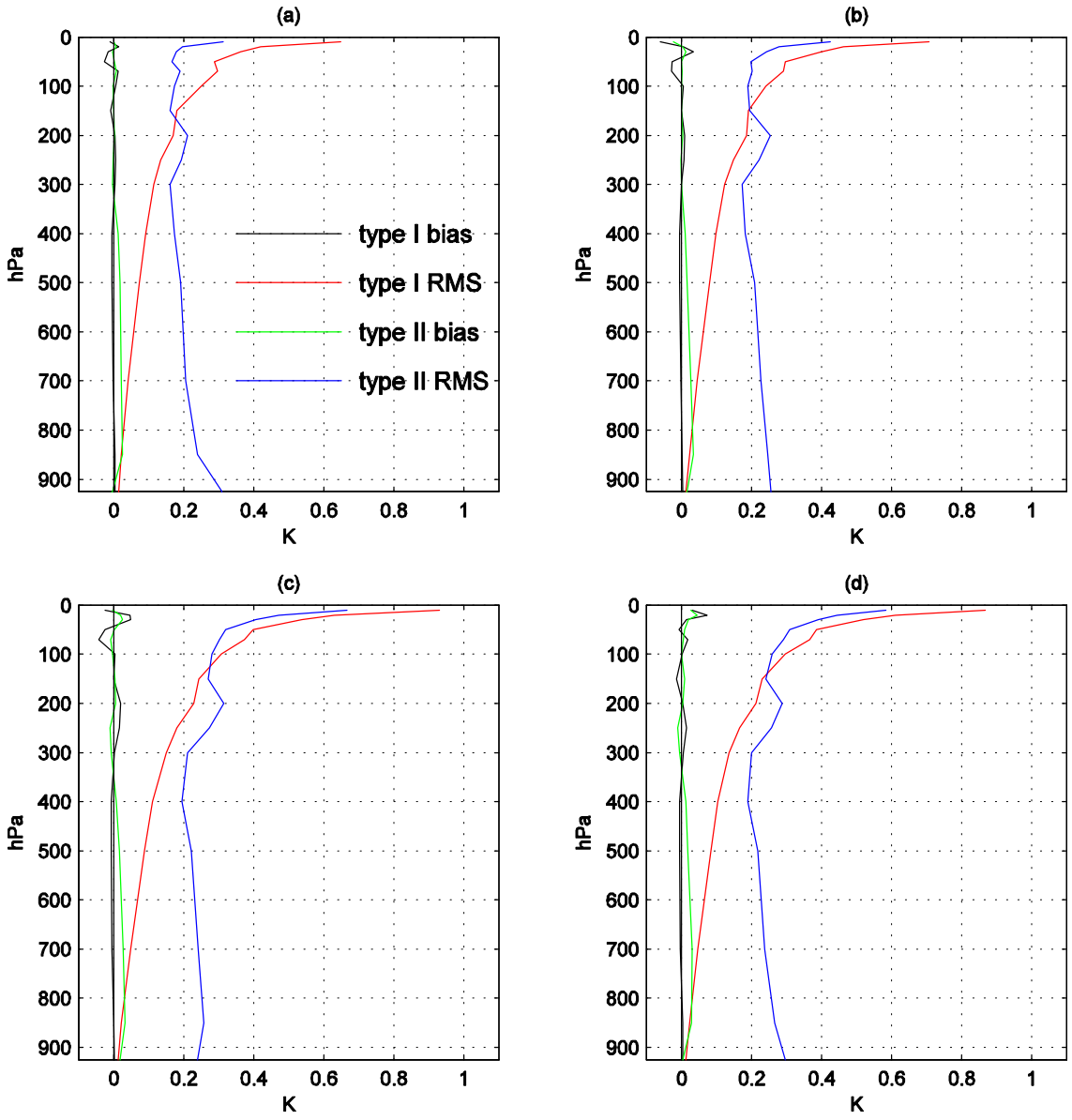

Figure 10.7: Vertical profiles of the temperature drift error for simulated observations (type I and type II data) in the SH (CARDS list): winter (a), spring (b), summer (c) and autumn (d).

10.7 Drift error: wind and humidity

In general the drift errors follow a similar pattern to those for temperature and are relatively small and comparable to instrument error but are more pronounced in regions with a strong upper-air flow. As an example, Figure 10.8 shows the mean and rms error in the vertical for the vector wind differences and relative humidity for winter months for station 04018. For the wind data the type II data show larger errors up to about 150 hPa; at 300 hPa the maximum rms (vector wind) errors are 8.5 and 11.5 ms^{-1} for type I and type II data respectively. The stratospheric wind error shows a strong seasonal bias (not shown). The humidity error is difficult to evaluate above 400 hPa due to the lack of moisture in the atmosphere but in the lower troposphere errors are generally less than 1% for type I and type II data. At 700 hPa the extreme absolute errors are around 5 and 15% respectively for this station.

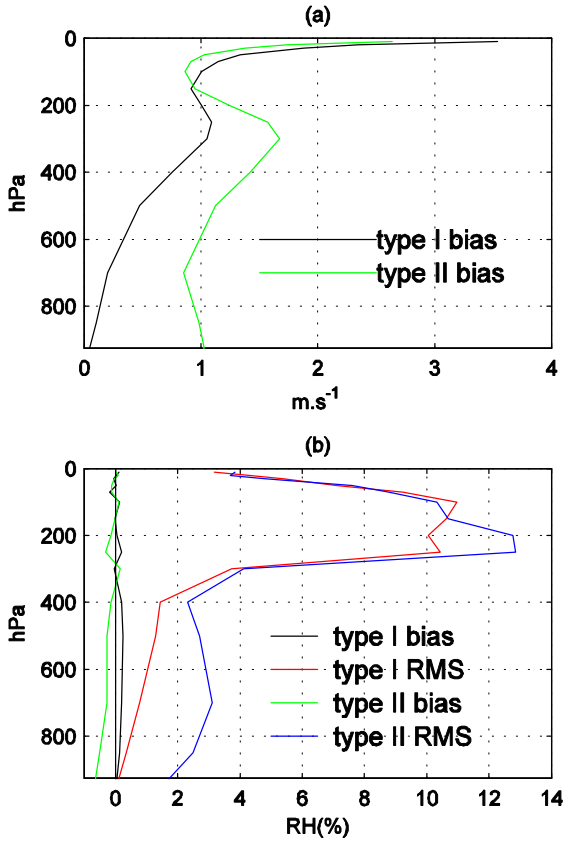

Figure 10.8: Vertical profile of drift error for type I and type II simulated observations for station 04018: vector wind (a), relative humidity (b). Data are 0000 and 1200 UTC for the period 1960-2002.

10.8 Discussion and concluding remarks

This study focuses on the impact of ignoring the spatial and temporal spread of data, inherent in radiosonde observations, for evaluating the climate of the upper atmosphere. The usual practice is simply to ignore the drift and to credit the data from each ascent as representative of the instantaneous

vertical profile of the atmospheric state directly above the radiosonde launch point. It is difficult to obtain precise estimates of the errors without access to the original sounding data as current coding standards do not contain provision for the inclusion of detailed information on the time and position of each measurement. While the launch time of the ascent is often timed so that the mid part of the ascent coincides with the main synoptic hours, the temporal discrepancy for part of the ascent is around 45 minutes and may be as much as 90 minutes. The horizontal drift can exceed 200 km. For climate work these errors are usually ignored and assumed not to impact on the statistical means and trends of long sequences of observations. The validity of this assumption is addressed by generating simulated radiosonde data using the ERA-40 re-analysis dataset. The simulated data, based on the tracking of an air parcel rising at a fixed rate of 5 ms^{-1} through the atmosphere, were generated for three type of ascents: an ascent with full temporal and spatial drift allowed; an ascent with no spatial or temporal drift i.e. using the analysis data coincident with the station for the launch time; and an ascent with no spatial or temporal drift but with the launch time advanced one hour. Differences between the full drift and reference ascents are used to estimate the drift error of actual ascents. The temporally offset simulated data are aimed at assessing the drift error in situations where the time of the mid point of the ascent is taken to be the official time of the data. Simulated observations were generated for the period 1960-2002 for each of the CARDS stations. The simulated observations are relatively crude compared with actual observations but we believe that the differences between the full drift and reference ascents reflect the real errors associated with radiosonde drift, particularly in data-rich areas.

The results for temperature show that the mean drift error is largest in the stratosphere (30-50 hPa) and seasonally influenced, particularly for stations located where the upper-air flow is strong and the horizontal displacement of the radiosonde is large. For stations 04018 (Iceland) and 04360 (Greenland) the winter bias at 50 hPa is negative and around -0.25 K with evidence of a small negative trend (0.08 K over the whole period); for station 30230 (Russian Federation) the winter bias is positive and around 0.4 K. For other stations in the CARDS list the biases are generally much smaller. Any trends, such as those in the Greenland and Iceland stations, are related solely to the radiosonde drift and not the climate system. For isolated stations (e.g. in Antarctica) there is further evidence of spurious data trends in the stratospheric temperatures but the quality of the simulated observations is questionable in such a data-sparse area. Combining data into geographical regions the maximum temperature bias in the stratosphere is less than 0.05 K for the NH. In the SH and TR the biases are a little larger but less than 0.1 K.

The impact of the temporal adjustment of the data is generally to reduce the drift bias and rms errors in the stratosphere but the rms error is increased in the troposphere.

For wind and humidity the patterns are similar to those for temperature but as these elements are features of the middle and lower atmosphere they are less affected by radiosonde drift and the mean errors are generally small (less than 1% for relative humidity, and typically 1-1.7 ms^{-1} for the wind, for station 04018, for example).

In summary, the errors associated with radiosonde drift are generally small and probably do not impact on climate assessment studies when data are combined for regional average values. However, for individual stations the impact may be important and may be responsible for spurious seasonal biases and trends in the observed stratospheric temperatures. While the mean errors may be small, individual errors may be large and of significance for NWP applications. This issue is not addressed here.

Appendix

The simulated observations were derived using the ERA-40 analysed model level velocities, temperatures and specific humidities, and the surface pressure. For wind components, temperature and surface pressure the full spectral fields, with a triangular truncation at wave number 159, at the 60 hybrid model levels, were used directly in the trajectory calculations to reduce interpolations errors. Fields were interpolated linearly in time and linearly in log pressure in the vertical using a simple predictor-corrector scheme to derive the trajectory arrival points at each time step. For specific humidity, the quasi-regular Gaussian grid fields of the ERA-40 data were interpolated linearly in space and time to derive the moisture data for the ascent. For each of the CARDS station positions the three-dimensional trajectory of an air particle, launched from the surface, under the influence of the horizontal winds and a constant vertical velocity of 5 ms^{-1} was calculated using a 30 second time step. Each ascent was terminated when the trajectory extended beyond the highest model level at 10 hPa. The output data were post-processed to derive data at standard pressure levels by vertically interpolating the wind components and temperature linearly in log pressure, the specific humidity linearly in pressure.

Compared with actual radiosonde ascents the simulated data suffer from several deficiencies. The temporal interpolation scheme, for example, is rather crude as the analysis fields are only available at 6-hour intervals. Also, the rate of rise of the balloon, while typically 5 ms^{-1}, is only approximately constant and varies with height; it is also influenced by the encountered weather conditions and will be slower in heavy precipitation. It is also assumed that the balloon follows the ambient air velocity without any drag effects. For long flight times these are serious issues that will degrade accuracy (Dvorkin et al. 2001) but in these experiments the flight time is typically under 2 hours and we do not consider the errors to be significant when only the differences between simulations are being used to calculate climate averages.

References

Andræ, U., N. Sokka and K. Onogi (2004): The radiosonde temperature bias corrections used in ERA-40. ERA-40 Project Report Series No. 15, 34 pp.

Angell, J. K., 2003: Effect of Exclusion of Anomalous Tropical Stations on Temperature Trends from a 63-Station Radiosonde Network, and Comparison with Other Analyses. *Journal of Climate*, **16**: 2288–2295.

Bengtsson L., S. Hagemann and K. I. Hodges (2004): Can climate trends be calculated from reanalysis data? *J. Geophys. Res.*, **109**: D11111.

Dvorkin, Y., N. Paldor, and C. Basdevant, 2001: Reconstructing balloon trajectories in the tropical stratosphere with a hybrid model using analysed fields. *Quart. J. Roy. Meteor. Soc.*, **127**: 975-988.

Eskridge, R. E., O. A. Alduchov, I. V. Chernykh, Z. Panmao, A. C. Polansky, and S. R. Doty, 1995: A Comprehensive Aerological Reference Data Set (CARDS): Rough and Systematic Errors. *Bulletin of the American Meteorological Society*, **76**: 1759–1776.

----, J. K. Luers, and C. R. Redder, 2003: Unexplained Discontinuity in the U.S. Radiosonde Temperature Data. Part I: Troposphere. *Journal of Climate,* **16**: 2385–2395.

Gaffen, D. J., M. A. Sargent, R. E. Habermann, and J. R. Lanzante, 2000: Sensitivity of Tropospheric and Stratospheric Temperature Trends to Radiosonde Data Quality. *Journal of Climate*, **13**: 1776–1796.

Lanzante, J. R., S. A. Klein and D. J. Seidel, 2003: Temporal Homogenization of Monthly Radiosonde Temperature Data. Part I: Methodology. *Journal of Climate,* **16**: 224–240.

Macpherson, B., 1995: Radiosonde balloon drift – does it matter for data assimilation? *Meteorol. Appl.,* **2**: 301–305.

Manikin, G., M. Baldwin, W. Collins, J. Gerrity, D. Keyser, Y. Lin, K. Mitchell, and E. Rogers, 2000: Changes to the NCEP Meso Eta Runs: Extended range, added input, added output, convective changes. NOAA Technical Procedures Bulletin No. 465: 84 pp.

Redder, C. R., J. K. Luers, and R. E. Eskridge, 2004: Unexplained Discontinuity in the U.S. Radiosonde Temperature Data. Part II: Stratosphere. *Journal of Atmospheric and Oceanic Technology,* **21**: 1133–1144.

Simmons, A. J., and J. K. Gibson, Eds., 2000: The ERA-40 Project Plan. ERA-40 Project Report Series No. 1, ECMWF, 62 pp.

Sterl, A., 2004: On the (In)Homogenity of Reanalysis Products. *Journal of Climate,* **17**: 3866-3873.

WMO, 1995: *Manual on Codes*. Volume I.1 Part A: Alphanumeric Codes. WMO Publ. 306, World Meteorological Organization, Geneva.

---, 2001: *Manual on Codes*. Volume I.2 Part B: Binary Codes. WMO Publ. 306, World Meteorological Organization, Geneva.

---, 2004: *Observing Stations*. WMO Publication No. 9, Volume A. World Meteorological Organization, Geneva.

---, 2003: *Meeting of the Expert Team on Data Representation and Codes: Final Report.* Commission for Basic Systems, World Meteorological Organization, Geneva: 66 pp.

11 Grid Computing

11.1 Introduction

To quantify the uncertainty in the projections for the future Irish climate it will be necessary to run ensemble-type simulations with a regional climate model. This will require considerable computing power. Grid computing initiatives such CosmoGrid have huge potential in this area but the complexity of the systems requires that a considerable amount of testing must be done before the resource can be fully used.

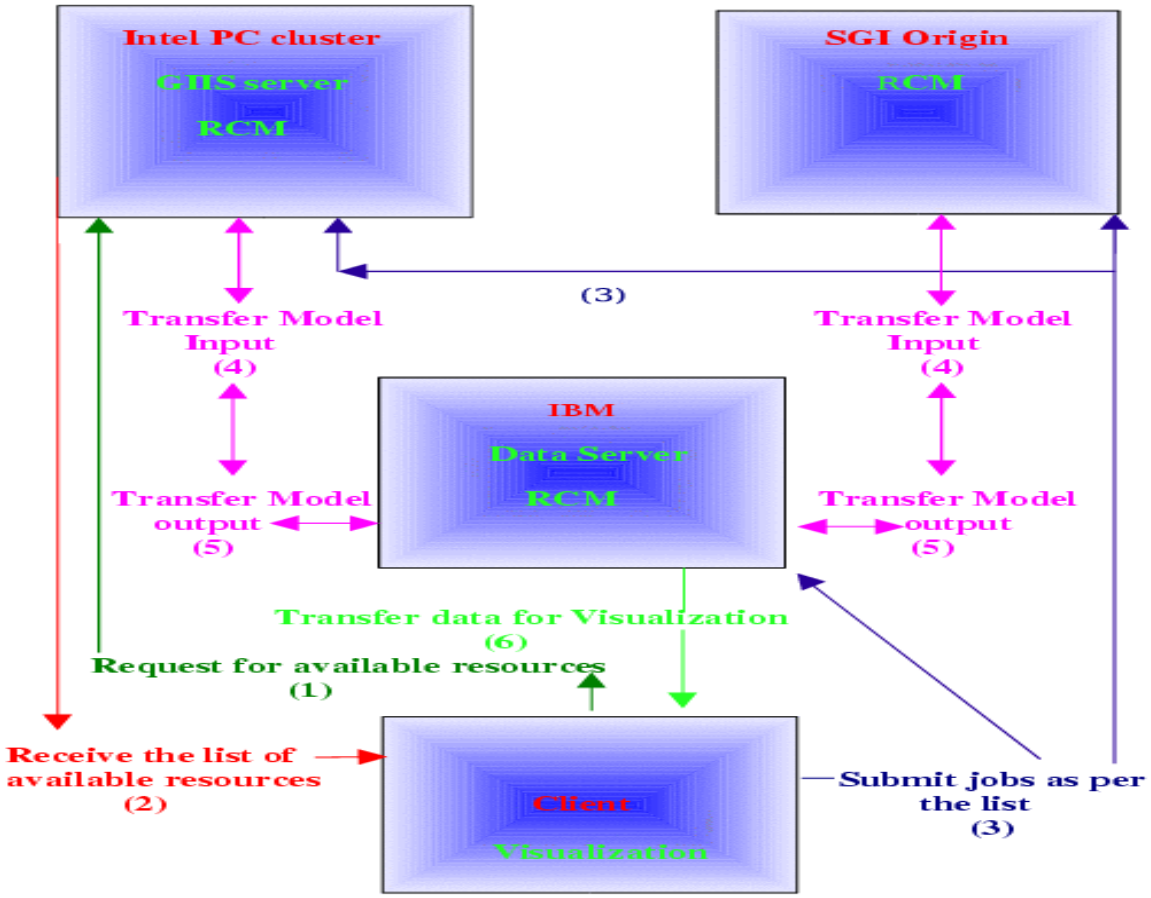

Figure 11. 1: Test grid setup. Asynchronous I/O is used for writing out the simulation results.

In preparation for this work, the following tasks were accomplished.

The RCA code was ported to three heterogeneous computers: a four processor IBM p630, an eight processor SGI Origin 2000 and a cluster of Intel PCs. Using Globus 2.4 and mpich-g2 a test grid with these platforms was then set up and the RCA model run on different machines with different numbers of processors for one month. Ideally the results should be identical. In reality, different compilers and different machines lead to slightly different results. This is acceptable if the differences are small and random but systematic errors are not; they will make it difficult to detect genuine changes in the climate.

11.2 Test simulation

To test the RCA model in a grid environment a 1-year simulation was performed on the three platforms described above.

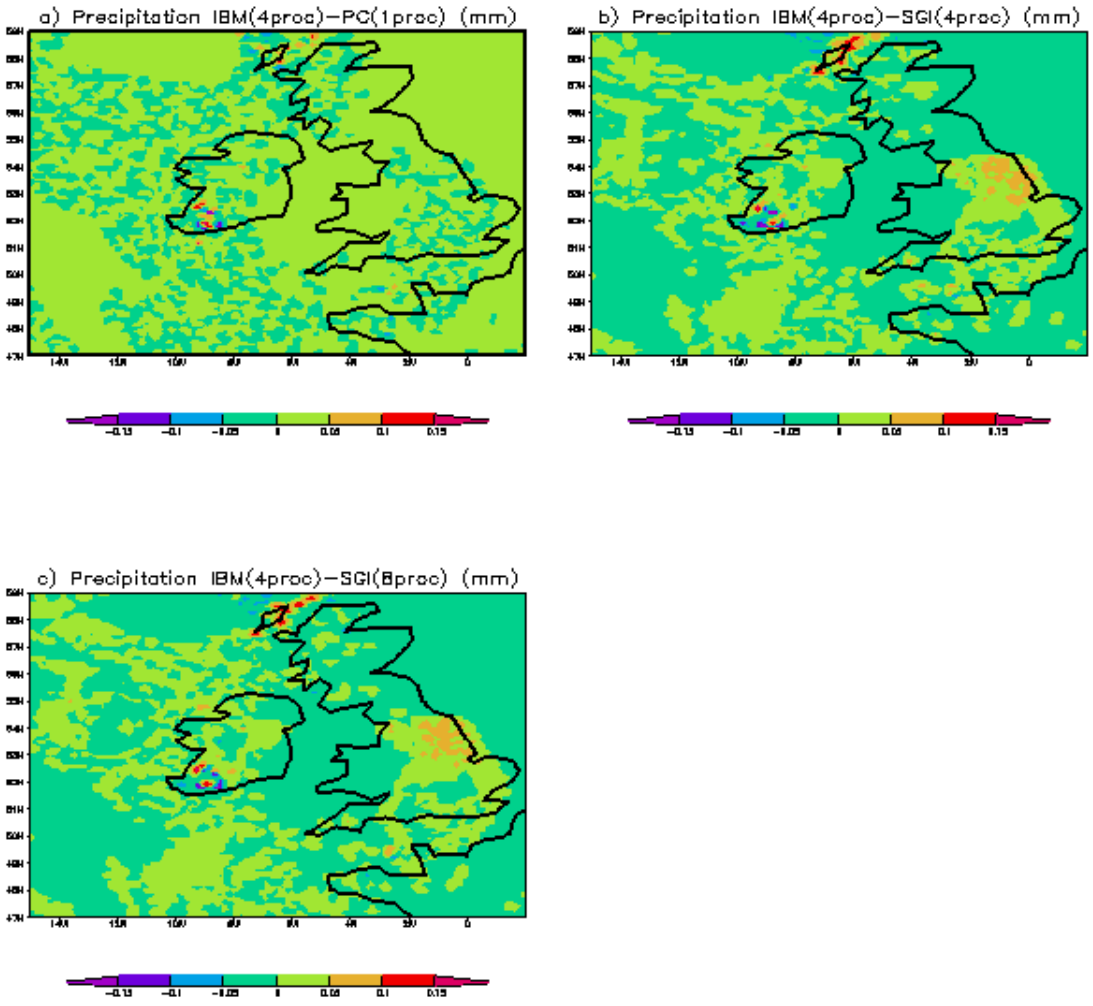

Figure11.2 Differences of monthly averages of precipitation (mm/3h) from simulations on different machines and with different numbers of processors. (a) IBM 4 processors minus Intel PC 1 processor, (b) IBM 4 processors minus SGI 4 processors and (c) IBM 4 processors minus SGI 8 processors.

Figure 11.2 shows the results for one of the most sensitive parameters, precipitation. Indeed the differences are small (usually below 0.05 mm/3h) and essentially random. Differences for other parameters (not shown) are very small, confirming that the RCA is properly coded in this environment.

11.3 Conclusions

A grid-capable version of the RCA model has been successfully tested on a simulated Grid composed of three different computers. The results from a 1-year simulation on the Grid show that there is a slight dependence on the targeted hardware configuration and system compiler but the differences are small and considered to be acceptable for climate modelling.